Identification of haptic based guidance in low visibility conditions

Dissanayake Mudiyanselage, Anuradha Ranasinghe

Awarding institution:
King's College London

Identification of haptic based guidance in low visibility conditions

Dissanayake Mudiyanselage Anuradha Ranasinghe

Department of Informatics

King's College London

A thesis submitted in partial fulfilment of the requirements for the degree of Doctor of Philosophy in Robotics

September 2015

Dedicate this thesis to my loving parents ...

DECLARATION

I hereby declare that except where specific reference is made to the work of others, the contents of this thesis are original and have not been submitted in whole or in part for consideration for any other degree or qualification in this, or any other University. This thesis is the result of my own work and includes nothing which is the outcome of work done in collaboration, except where specifically indicated in the text. This thesis contains fewer than 65,000 words including appendices, bibliography, footnotes, tables and equations and has fewer than 150 figures.

Dissanayake Mudiyanselage Anuradha Ranasinghe

September 2015

ACKNOWLEDGEMENTS

I would like to express my special appreciation and thanks to my advisor Dr. Thrishantha Nanayakkara, you have been a tremendous mentor for me. I would like to thank you for encouraging my research and for allowing me to grow as a research scientist. Your advice on both research as well as on my career have been priceless. I would also like to thank professor Kaspar Althoefer, and professor Prokar Dasgupta for providing me an opportunity to join as a KCL member. I am very much grateful to the thesis review panel professor Angelo Cangelosi, and professor Etienne Burdet for accepting to be my examiners. I would especially like to thank all Thrish lab members, and CoRE members in KCL. All of you have been there to support me when I need subjects for my experiments and you all participated voluntarily.

I would like to thank the funding sources of my project: UK Engineering and Physical Sciences Research Council (EPSRC) grant no. EP/I028765/1, the Guy's and St Thomas' Charity grant on developing clinician-scientific interfaces in robotic assisted surgery: translating technical innovation into improved clinical care (grant no. R090705), and Vattikuti foundation.

A special thanks to my family. Words cannot express how grateful I am to my mother, father, my sister's family for all of the sacrifices that you've made on my behalf. Your prayer for me was what sustained me thus far. My big thank and gratitude go to all in Amaravathi Buddhist Monastery for showing me how simple life is. I would also like to thank all of my friends in UK who supported me many ways, and incented me to strive towards my goal.

ABSTRACT

This thesis presents identification of abstracted dynamics of haptic based human control policies and human responses in guiding/following using hard reins in low visibility conditions. The extracted haptic based guidance policies can be implemented on a robot to guide a human in low visibility conditions like in indoor fire-fighting, disaster response, and search and rescue.

Firstly, the thesis presents haptic based guidance in Human-human interactions. The control policies were modeled by a simple linear Auto-Regressive model (AR). It was found that the guiding agent's control policy can be modeled as a 3^{rd} order predictive AR system and the human follower can be modeled as a 2^{nd} order reactive AR system. Secondly, the human follower's dynamics were modeled by a time varying virtual damped inertial system to understand how trust in the guider is reflected by physical variables. Experimental results on human trust showed that the coefficient of virtual damping is most sensitive to the follower's trust.

Thirdly, the thesis evaluates human-robot interactions when the control policy identified from human guiders was implemented on a planar 1-DoF robotic arm to perturb the blindfolded subjects' most dominant arm to guide them to a desired position in leftward/rightward directions. Experiments were carried with naive and trained subjects. Humans' behavior in leftward/rightward movements are asymmetric for naive subjects and symmetric for trained subjects. Moreover, it was found that naive subjects elicit a 2^{nd} order reactive behavior similar to human demonstration experiments. However, trained subjects developed a 2^{nd}

order predictive following behavior. Furthermore, naive and trained subjects' arm muscle activation is significantly different in leftward/rightward arm perturbation.

Finally, the thesis presents how humans trained in primitive haptic patterns given using a wearable sleeve, can recognize their shifts and linear combinations.

TABLE OF CONTENTS

LIST OF FIGURES

LIST OF TABLES

CHAPTER 1

INTRODUCTION

Abstract

Haptic perception is a natural solution for humans when the vision is impaired. This thesis presents identification of abstracted dynamics of human control policies and responses to guide/follow using a hard rein in low visibility conditions. These results would give an intuition to identify computational models to explain the structure of motor controllers used by human participants to guide a blindfolded counterpart. The extracted haptic based guidance policies can be implemented on a robot to guide an impaired human in low visibility conditions like in indoor fire-fighting. Moreover, a major pre-condition for successful human-robot interactions in these circumstances is the human trust in the robot. If the robot can detect trust level of the human, it is easy to develop a mutual understanding between the robot and the human in guiding. Therefore, this thesis presents how the trust of a human in following another agent can be estimated by the coefficients of a virtual damped inertial model of the human in real time. Furthermore, the implementation of control policy identified from human guiders on a planar 1-DoF robotic arm is presented to study humans' and robot's behavior, their muscle activation when the arm is perturbed in leftward/rightward directions. Apart from those humans' response on proprioceptive feedback studies, humans'

responses on cutaneous feedback is presented to understand how humans generalize the cutaneous feedback in different scenarios such as shifting and scaling, how they recognize all trained patterns when played randomly, and how they can recognize linear combination of primitive patterns. Those findings would be used to design guidelines for guiding humans in low visibility conditions like in indoor fire-fighters, disaster responders, and search and rescue.

1.1 Introduction

Imagine being in room full of light, that suddenly becomes dark. To go out from the room, you will use touch sensation to understand the immediate environment. The human brain has the remarkable ability to use a reduced number of sensory modalities to accomplish tasks that they used to do without any sensor deprivation as well as the ability to derive complex perceptions by combining different sensory modalities [1]. For instance, in the case of indoor fire-fighting, fire-fighters move inside the buildings under low visibility conditions using only haptic sensation. In the case of indoor fire-fighting, fire-fighters have to work in low visibility conditions due to smoke or dust and high auditory distractions due to their Oxygen masks and other sounds in a typical fire-fighting environment. In such cases, a knowledge about the control policies of the humans and the modified behavioral characteristics due to reduced sensory modalities will help to design external assistive agents like robots to optimally assist human movements.

As social animals, humans use different communication methods. The communication can be verbal, non verbal, written, or based on other medium that stimulate any of five sensors. Very often both parties respond to communicate. When the vision is impaired, haptic is a good alternative communication method between two parties [2], [3], and [4]. It is very important to understand the control policies in haptic-based guidance − that would in turn shed light on optimal robotic guidance of humans in low visibility conditions in a hazard or uncertain environments.

There have been some studies on guiding people with visual and auditory impairments using intelligent agents in cases such as indoor fire-fighting [5] and guiding blind people using guide dogs [2]. Most of the studies did not take into account human response and humans' physical state for guiding to have a proper bi-directional communication between two parties. Therefore, this thesis presents how to model control policies by a simple Auto Re-

gressive model (AR) when a human is guided by another intelligent agent and the human's responses in guiding when the vision is impaired.

Moreover, understanding the humans' psychological state is important to have a good mutual understanding between two parties. Trust is an important psychological factor in these contexts because it directly affects the willingness of people to follow robots' suggestions [6]. Any robotic assistant to a person with limited perception of the environment should monitor the level of mutual trust of the person in the robot for it to be relevant to the psychological context of the person being assisted. Human trust level has been studied qualitatively in [7], [6], [8], [9]. None of the above studies quantify the trust level of the human in real time. However, in a simulated game of fire-fighting, Stormont *et al* [10] showed that the fire-fighters become increasingly dependent upon robotic agents when the fire starts to spread along randomly changing wind directions. However, so far, there has been little discussion about mutual trust measurement in real time in Human-Robot Interactions (HRI). Therefore, the thesis highlights how humans' mutual trust in the robot can be modeled by virtual damped inertial model to indicate trust level by its coefficients in real time. This approach will give us an insight into how virtual coefficients would be used as an indicator to describe a human trust in real time in low visibility conditions.

It is also important to understand factors determining haptic perceptions in low visibility conditions when the human is guided by a robot. Therefore, this thesis presents humans' behavior, perceptions, and arm muscle activation when the control policy identified from human guiders was implemented on a planar 1-DoF robotic arm to perturb the blindfolded subjects' most dominant arm to guide them to a desired position in leftward/rightward directions.

Haptic perception is critical to our physical and mental well being, our social interactions, and our sense of self. In many ways the sense of touch is the central perception system to human life [11]. To make a complete picture of haptic perceptions, not only the

proprioceptive feedback but also cutaneous feedback is studied to understand the humans' responses/perceptions. The combination of proprioceptive and cutaneous feedback will give us a good insight about humans' perceptions when the vision is impaired. The conclusion derived from control policies and humans' perceptions would be used to guide a human in low visibility conditions like in indoor fire-fighters. Therefore, finally, the thesis presents how humans trained in primitive haptic patterns given using a wearable sleeve, can generalize their shifts/scale and combine linear primitive patterns.

1.2 Motivation

Oxford dictionary defines senses as "A faculty by which the body perceives an external stimulus; one of the faculties of sight, smell, hearing, taste, and touch" [12]. Out of all senses, visual and auditory feedback are mostly depended upon to navigate in the environment. Sometimes humans have to depend limited perceptions due to environmental conditions. For example, a smoky and noisy environment like in indoor fire-fighting. In such conditions, humans might not hear properly or they might not see the immediate environment clearly. Such sensor deprivation can cause stress on humans. In such circumstances, haptic perception is a natural solution to understand the environment. If an intelligent agent (man/machine) can have guiding abilities to guide an impaired human, it would be the best solution for safe human robot navigation.

1.2.1 Exploration of haptic space in fire-fighting practice under no visibility

When proceeding into an environment with no or limited visibility, fire-fighters have to rely heavily on their sense of touch. Standing on a rear foot, they use the front foot to stamp ahead in a fan-like pattern in order to feel for obstacles and to test the floor before a real step is made [5]. Meanwhile one hand will be moved up and down in front of the head and

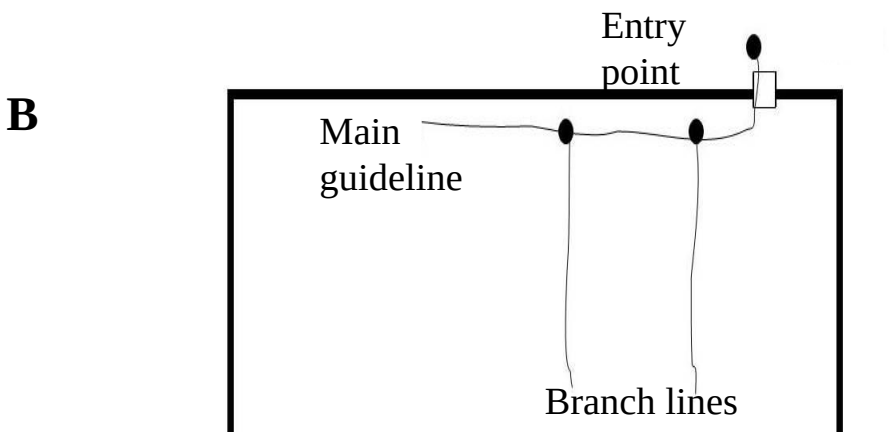

Fig. 1.1 The fire-fighters: A) Searching fire- fighters in a trial with the visor aid; note the arms exploring the haptic space. B) Basic principle for guideline layout in a search operation.

upper body to feel for hanging obstructions and in particular loose hanging wires, as shown in Fig. 1.1A. Exploration of their haptic space is utmost importance for a fire-fighter and this exploration precedes locomotion.

1.2.2 Lifeline in indoor fire-fighting

Fire-fighters use a standard procedure when a team enters a building called "lifeline" which a rope latched on one end to the belt of the exploring fire-fighters and held on the other end by a team leader who is in charge of pulling out the lifeline when requested by the exploring team, to guide them outside the building as shown in Fig. 1.2.

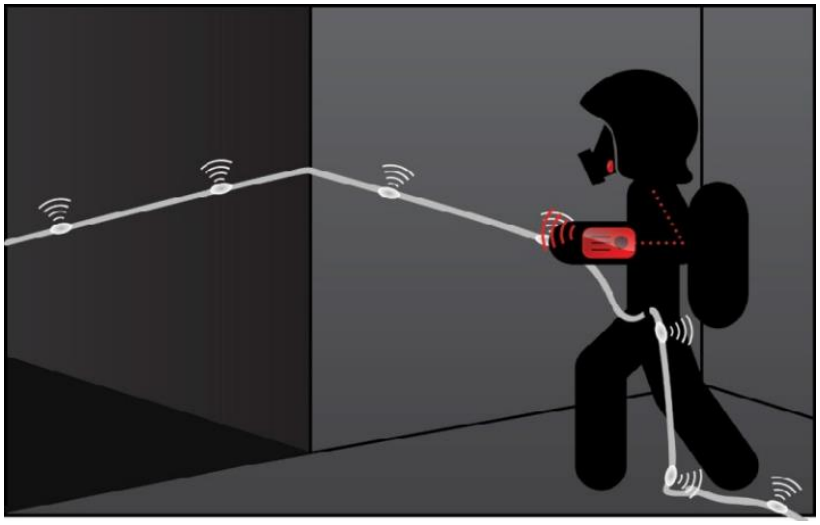

Fig. 1.2 Lifeline in indoor fire-fighting adapted from [13].

To save lives of fire-fighters have to act swiftly as chances for rescues reduce considerably over time and certainly when the situation deteriorates. This implies considerable time pressure for all the crew and their commanders. Nowadays, they depend on touch sensation (haptic) of walls for localizing and ropes or lifeline for finding the direction [5] as shown in Fig. 1.1B and Fig. 1.2 and also humans naturally interact with animals using stiff reins in scenarios such as working with guide dogs and horse riding as shown in Fig. 1.3A and Fig. 1.3B respectively. The blind person or the horse get moving direction and speed when

the rein is stiff. To extend the same practice, this thesis presents experiments which were designed to use a hard rein to guide a blindfolded human in Human-Human Interactions (HHI) and HRI.

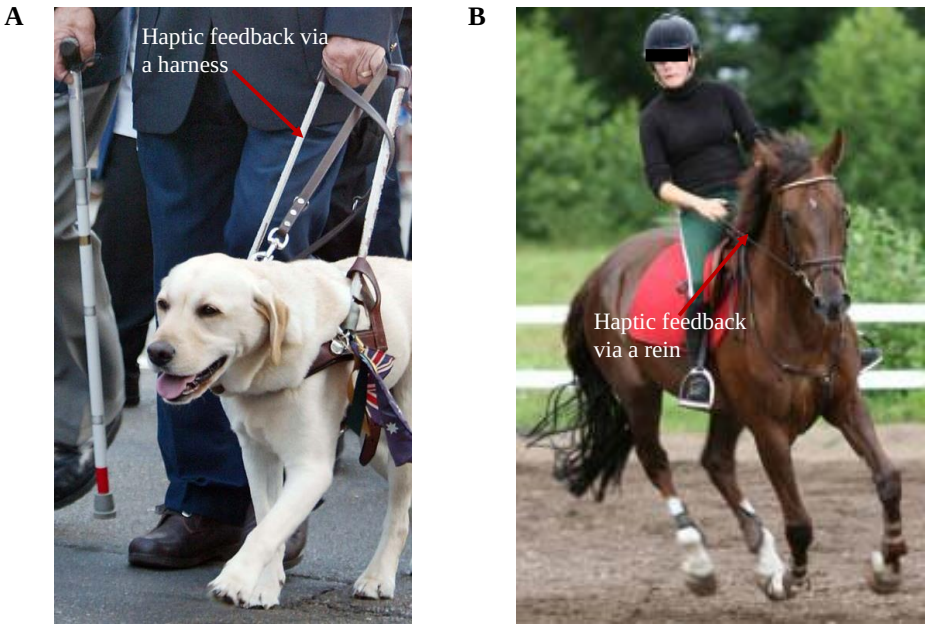

Fig. 1.3 How humans naturally interacts with haptic perceptions: A) Guide dog: The blind person feels haptic feedback via a harness. Adapted from [14], and B) Horse riding: The horse understands the command via a rein. Adapted from [15].

1.3 Aims and objectives

- Aims

The aim of the thesis is to present identification of abstracted dynamics of human control policies and human responses in haptic perceptions when the vision is impaired.

- Scientific objectives

1. To understand the structure of guiding/following control policies when the vision is impaired.

Humans use different strategies and behaviors in guiding and following. By analyzing the experimental data, the guider's and follower's behavior can be modeled by a simple Auto-Regressive model (AR) to understand the structure of the control policies. Then the model order and predictive/reactive nature of the control policies explain the behavior of the duo.

2. To understand how humans' optimize the effort.

   Responsibility assignment for muscle recruitment in guiding is important to understand how the guider optimize the effort in guiding.

3. To study how the guider may modulate the pulling force in response to the trust level of the follower.

   For efficient guiding, an optimal closed loop controller can be constructed by combining the mutual trust and the difference of heading directions of the two parties to generate corrective actions to guide the follower. Therefore, it is important to consider trust of the human on the robotic counterpart in uncertain environments. The guiding agent could accelerate/decelerate by changing the pushing/pulling force according to follower's trust level in different situations in guiding. Therefore, trust level is modeled by virtual damped inertial model to find the most sensitive parameter to be used as an indicator.

4. Human-robot interactions were studied when the control policy identified from human guiders was implemented on a robotic arm to perturb the blindfolded subjects' most dominant arm to guide them to a desired position in leftward/rightward directions.

   It is essential to understand how the robot and humans interact when control policy identified from human guiders was implemented on a robotic arm to

perturb the blindfolded subjects' most dominant arm to guide them to a desired position in leftward/rightward directions.

5. To study duo's behavior in human-robot interactions.

   The humans' and robot's behavior are important to understand how they interact. Therefore, the behavioral metrics are chosen such as rise time (RT), best fit model order of the polynomial fitted to the instantaneous error of the human's position relation to a desired angle (N) in transient response, and steady state variability (SSV), steady state error (SSE) steady state response in reaching six desired angles in leftward/rightward directions to understand the humans' behavior. The results of interactions with naive/trained subjects are presented. Moreover, robot's behavior in leftward/rightward movements are presented.

6. To understand spontaneous muscle recruitment in response to leftward/rightward arm perturbations.

   This is important because perception of the guiding command given by the robot depends on how proprioceptive sensors in the muscles are activated.

7. To study how humans trained in primitive haptic patterns given using a wearable sleeve, can generalize their shifts and scale - can recognize linear combinations.

   This study would give an idea as to how humans mentally generalize the cutaneous feedback in different scenarios such as shifting and scaling, how they recognize all trained patterns when played randomly, and how they can recognize linear combination of primitive patterns.

1.4 Contributions

The contribution of this thesis are:

I The structure of control policies are essential when a visually and auditory impaired human is guided by another intelligent agent by using the a hard rein. By modeling how state maps into action by a simple linear Auto-Regressive model (AR), it was found that the guider's control policy can be modeled as a 3rd order predictive model and the follower as a 2nd order reactive model. The model order and reactive/predictive nature will give an insight of humans' behavior in guiding and following when the vision is impaired (section 3.4).

II Studying of how the guider may modulate the pulling force in response to the trust level of the follower in order to study how the above control policy would interact with the follower in an arbitrary path tracking task is necessary to understand the follower's trust on the guider. Modeling the voluntary movements of the follower as a virtual damped inertial system, It was found that virtual damping coefficient is most sensitive to explain the trust level of the follower. This would give an idea as to how the guider should modulate the pushing/pulling force with response to the trust of the follower in haptic based guiding (section 4.3).

III It is important to understand human-robot interactions when the control policy identified from human guiders was implemented on a planar 1-DoF robotic arm to perturb the blindfolded subjects' most dominant arm to guide them to a desired position in leftward/rightward directions. The results show that even though robot's behavior is not significantly different in leftward/rightward movements when it interacts with naive/trained subjects, naive subjects behave differently in leftward/rightward movements. Moreover, it was observed that naive subjects elicit a 2nd order reactive behavior similar to human participants in the human demonstration experiments. However,

trained subjects developed 2^{nd} order predictive following behavior. Moreover, naive and trained subjects' muscle contracted differently when the arm is perturbed in leftward/rightward directions. These spontaneous muscle recruitment and the human behavior would give an insight as to some fact to take into account in designing guidelines how to train humans to follow a guiding robot when the human is guided via a hard rein in low visibility conditions (section 5.3).

IV It is important to understand how humans mentally construct the cutaneous feedback in haptic based guidance. Therefore, cutaneous feedback was studied in different scenarios such as shifting and scaling with respect to trained patterns, how they recognize all trained patterns when they are played randomly, and how they can recognize linear combination of primitive patterns. It was found that humans have a general ability to recognize trained patterns even when they are played in a random order and humans can recognize some linear combinations of trained primitive patterns. The results explain how to use cutaneous feedback to the blindfolded followers to help them mentally construct the shape and stiffness of obstacles that come into contact with a guider robot (section 6.3).

1.5 Contributed papers

Journal papers

- **Ranasinghe, Anuradha**, Jacques Penders, Prokar Dasgupta, Kaspar Althoefer, & Thrishantha Nanayakkara, "*Salient Features of Haptic Based Guidance of People with Limited Vision Using Hard Reins*", IEEE Transactions on Systems, Man, and Cybernetics, Part B, DOI: 10.1109/TCYB.2015.2409772, 2015.

- **Ranasinghe, Anuradha**, Prokar Dasgupta, Kaspar Althoefer, & Thrishantha Nanayakkara, "*Identification of Haptic Based Guiding Using Hard Reins*", PLOS ONE journal,

DOI: 10.1371/journal.pone.0132020, 2015.

Conference papers

- **Ranasinghe, Anuradha**, Jacques Penders, Prokar Dasgupta, Kaspar Althoefer, & Thrishantha Nanayakkara, "*A two party haptic guidance controller via a hard rein*", IEEE/RSJ International Conference on In Intelligent Robots and Systems (IROS), Tokyo, Japan, pp. 116-122, 2013.

- **Ranasinghe, Anuradha**, Althoefer, Kaspar., Penders, Jacques, Dasgupta, Prokar, & Nanayakkara, Thrishantha, " *An Optimal State Dependent Haptic Guidance Controller via a Hard Rein*", IEEE International Conference on Systems, Man, and Cybernetics (SMC), Manchester, UK, pp. 2322-2327, 2013.

  ***(*This paper was short-listed at IEEE SMC2013 conference for the Franklin Taylor Memorial Award for the best paper and the Best Student Paper Award)**

- Penders, J., Jones, P., **Ranasinghe, Anuradha.**, & Nanayakkara, Thrishantha., "*Enhancing trust and confidence in human robot interaction*", UKRE, Sheffield, vol. 25-3, 2013.

Abstract

- **Ranasinghe, Anuradha**, Althoefer, Kaspar., Penders, Jacques., Dasgupta, Prokar., & Nanayakkara, Thrishantha, "*Differential involuntary recruitment of upper arm muscles determine direction dependent haptic perception of uniform external perturbations*", Society of Neuroscience 2014, Washington DC, 2014.

Papers under preparation

- **Ranasinghe, Anuradha**, Prokar Dasgupta, Kaspar Althoefer, & Thrishantha Nanayakkara, "*Characteristics of voluntary movements in response to haptic commands without visual feedback*"

- **Ranasinghe, Anuradha**, Prokar Dasgupta, Kaspar Althoefer, & Thrishantha Nanayakkara, "*Cutaneous feedback for patterns recognition in guiding*"

1.6 Thesis structure

- Chapter 1 introduces the focus of the thesis and explains the motivation for the work.
- Chapter 2 presents previous work and gaps on guiding a impaired human in HHI and HRI experiments in different environments. Moreover, how the previous work focused to study human trust in cooperative studies is considered. The related work on human arm response patterns in proprioceptive and cutaneous perceptions is discussed.
- Chapter 3 presents human-human demonstration experiments to extract control policies in guiding a human in low visibility conditions.
- Chapter 4 describes how to model humans' trust in guiding.
- Chapter 5 presents implementation of extracted control policies on planar 1-DoF robotic arm. Humans' and robot's behaviors in HRI are presented. Moreover, humans' arm muscle activation on arm perturbation in leftward/rightward directions is presented.
- Chapter 6 describes how humans trained in primitive haptic patterns given using a wearable sleeve - can generalize their shifts and scale - can recognize their linear combinations.
- Chapter 7 concludes and summarizes the thesis and discusses possible future directions for this line of research.

CHAPTER 2

BACKGROUND AND RELATED WORK

Abstract

This chapter presents the background and related work of human guidance when the vision is impaired in different environments. First, the chapter presents how a human is guided by an intelligent agent in predictable and unpredictable environments in related works. Then the chapter discusses previous research on haptic based guidance. Next the humans' proprioceptive and cutaneous feedback are discussed in haptic based guidance.

2.1 Human guiding/way finding based on haptic perceptions

There are some situations where humans have to only depend on haptics due to environmental conditions. For example, in indoor fire-fighting. It is important to study how haptics would be used to guide a human by an intelligent agent (man/machine) when the vision is impaired. The touch affordances of the humans in [16] found that humans depend on their nearby surroundings, together with quality of human conversation cooperatively over thousands of years [17]. Being able to explore with hands and communicate at the same time facilitate coordination of action and learning have been more important for human development [18] and human evolution.

Human navigation/way finding consists of two different functions [19]. Those are sensing of the immediate environment and navigating to remote destinations beyond the immediately perceptible environment [20], [21], [22]. According to Loomis *et al* [19], path navigation refers to obtaining information about one's motion and then using that information to compute one's displacement and change in orientation with respect to an origin. In natural unaided navigation one can use visible, auditory, and haptic perception to reach the remote location [19].

Several attempts have been made on guiding people with visual and auditory impairments using intelligent agents [23], [19], [24]. Early research and development based on Electronic Travel Aid (ETA) focused on sensing the immediate environment as shown in Fig. 2.1 [19]. Most of the ETAs are used to detect obstacles and provide auditory or vibrating signals to user such as Sonic pathfinder, Mowat Sensor, and MiniGuide [19]. Two technologically sophisticated devices, the NavBelt and Guide cane were used to provide guiding aids for impaired humans [23].

Infra Red (IR) video sensing and computer processing were used to provide location

speech information to the impaired traveler [24]. The other method for sensing the location was inertial navigation system [25], [26]. Another way of path navigation is downward pointing camera to sense the human's velocity when the vision is impaired [27]. The other approach was using video sensing in conjunction with map correlations [28]. In that study, video images of the environment were matched to images or models of the environment stored in memory.

The idea of using GPS to assist with navigation by the visually impaired goes to three decades [29]. Since then there have been several research projects investigating GPS-based navigation system for visually impaired people [29], [30], [31], [32]. A robotic guide dog with environment perception capability called Rovi has been developed in [4] to guide a human with limited environment perceptions. Rovi could avoid obstacles and reach a target on a smooth indoor floor. However, difficulties arise in rough terrain. An auditory navigation support system for the blind was discussed in [3], where, visually impaired human subjects (blind folded subjects) were given verbal commands by a speech synthesizer. Ulrich *et al.* [33] developed a guide cane without acoustic feedback in 2001 [33]. The guide cane has an ability to analyze the situation and determines appropriate direction to avoid the obstacle, and steers the wheels without requiring any conscious effort [33]. A robotic guide called MELDOG was designed by Tachi *et al* to introduce effective mobility aids for the blind people. Loomis *et al.* [34] developed personal navigation system to guide the blind people in familiar and unfamiliar environments. However, both the MELDOG [35] and Loomis *et al.* [34] navigator could follow only commands given by user to reach the destination.

Personal Guidance System was developed by Loomis *et al.* in 2007 [19] considering their previous work on [36], [37], [38], [39]. The long term goal of this system was to contribute the development of a portable, self-oriented system that would allow visually impaired individuals to travel through familiar and unfamiliar environments without assistance of guidance. The system provided virtual feedback of spatial data.

There are situations where some of the perception modalities such as vision and audition are compromised. In the case of human intervention in disaster response operations like in indoor fire-fighting, where the environment perception is limited due to thick smoke, noise in the oxygen masks and clutter. Not only limit the environmental perception of the human responders, but also this causes stress on them. Nowadays, they depend on touch sensation (haptic) of walls for localizing and ropes for finding the direction [5]. Studies of Penders *et al*. [5] on a swarm robotic approach propose ad-hoc network communication to direct the fire-fighters. The key problem of this approach is lack of bi-directional communication to estimate the behavioral and psychological state of the fire-fighters.

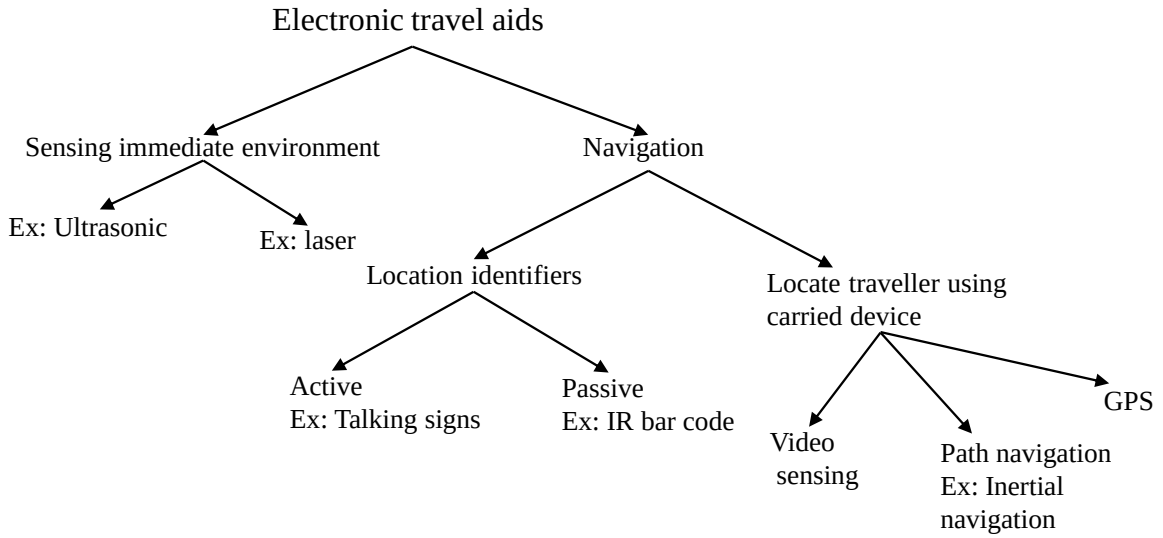

Fig. 2.1 Types of Electronic Travel Aids (ETAs) adapted by [19]

All above navigation aid has drawbacks in cluttered or uncertain environments. Human-Robot Interaction (HRI) is a field to study dedicated to understanding, designing, and evaluating robotic systems for use by or with humans [40]. The need for advanced HRI algorithms that are responsive to real time variations in the physical and psychological states in a human counterpart in an uncalibrated environment has been felt in many applications like in indoor fire-fighting, disaster response, and search and rescue operations [41], [42], [43], [44], [45]. Robots are currently used in urban search and rescue (USAR) operations [43].

An intelligent agent (man/machine) with full environment perceptual capabilities is an alternative to enhance navigation in such unfavorable environments. Since haptic communication is the least affected mode of communication in such cases, the thesis's approach is to understand how to extract guiding/following control policies between the duo where one has environment perception capabilities (An intelligent agent: man/machine) while the other one has limited perceptions of the environment (impaired human) via a hard rein. The guide dog scenario as an inspiration out of many natural examples of guiding via reins, because a hard rein is used to establish a connection between the dog and the visually impaired human. The important point is to notice the division of labor between the handler and the dog [46]. In this situation, the guide dog is not instructed to take the handler to a destination - on the contrary, the handler is taking the dog to a destination. The guide dog and the human depend on the handler's own spatial awareness and ability to read other clues and cues from the environment. However, in this situation, the human makes the navigation decision, dog provides locomotion guidance, and it leaves the the handler (hard rein) the dominant role of being responsible for the navigation [46]. In this research, an intelligent agent would give some navigation guidance while it depends on the state of the human. In this scenario both the intelligent agent and the human actively participated in the communication. Therefore, if an impaired human is guided by an intelligent agent via a hard rein, it is a good paradigm to extract salient features of guiding/following control policies.

The studies on communicative functions of haptic feedback in [18], argued that haptic guidance is a sequence of temporally connected shared events. Therefore, characterization of human-human interaction in a haptic communication scenario, where one partner is blindfolded (limited perception of the environment) while the other human subject has fully perceptual capabilities, can provide a viable basis to design optimal human-robot interaction algorithms to serve humans working in many hazardous/uncertain environments.

2.2 Humans' trust in guiding

The concept of trust is defined by Vries and *et al* [47] as "Trust is believed by someone to compensate for feelings of uncertainty". The authors in [47] argued that trust is considered to be crucial in people's decision to rely on a complex automated system to perform tasks for them. Trust of human's in robot's autonomous decision capabilities is a known major issue that significantly impacts the effectiveness of human-robot collaboration [48].

Trust has been studied in many areas such as automation [49], [50], [51], [52], human-machine interactions [53], and human management models [54]. Model of human machine trust was proposed in [53], and the dynamics of trust between humans and machines examined. Moreover, trust on an automation controller was studied in [49]. The results in [50] indicated that trust is an important factor in understanding automation reliance decisions.

Trust is one of the most critical factors in urban search and rescue missions because it can impact the humans' decisions in uncertain conditions [55]. The study on fire-fighters trust showed that trust in high-reliability task contexts was based on co-workers integrity [56]. Colquitt *et al.* in [56] argued that trust can be rooted in both cognitive and affective sources. All of above studies confirmed that trust is an important factor to build up mutual understanding between two parties in task sharing. Therefore, this thesis attempts to model an impaired human's trust in guiding when the impaired human is guided by another intelligent agent via a hard rein .

Several attempts have been made to study trust of a human with limited perception of the environment [10], [48] in different environmental conditions. Previous studies on a simulated game of firefighting, Stormont *et al.* [10] showed that the fire-fighters become increasingly dependent upon robotic agents when the fire starts to spread along randomly changing wind directions. Freedy [48] has discussed how self confidence correlates with trust of automation in human robot collaboration. Recent studies confirmed that when the

confidence level gets higher the activeness is increased in human robot shared control work in [57], [6].

Any robotic assistant to a person with limited perception of the environment should account for the level of the trust of the person. In HRI, it is increasingly becoming important to consider trust of the human on the robotic counterpart in uncertain environments like real fire. In [58], [55] studied how human trust can be explained quantitatively. However, this work is not only to quantify the human trust but also to model it in real time. This thesis discusses novel optimal state-dependent controller that accounts for the level of trust of the follower as part of the state. Those results are mainly intended to be used in a robot to guide people with good vision working in low visibility environments like in indoor fire-fighting or in other disaster response scenarios in future.

2.3 Proprioceptive and cutaneous feedback in guiding

The human brain has the remarkable ability to use a reduced number of sensory modalities to accomplish tasks. Humans used to do it without any sensor deprivation as well as the ability to derive complex perceptions by combining different sensory modalities [1]. Knowledge about the modified behavioral characteristics due to reduced sensory modalities will help to design external assistive agents like robots to optimally assist human movements. There have been many studies on proprioceptive and cutaneous feedback in guiding and reaching in different scenarios.

2.3.1 Proprioceptive feedback in guiding

Proprioception is known to be playing an important role in the control of reaching movements [59], [60]. It is well known that humans use haptic perception of errors they make in reaching movements to learn internal models to compensate for external force fields with

[61], [62] and without visual feedback [63], [64], [65], [66]. For a smooth trajectory, proprioceptive and visual feedback may guide adaptive updating of motor commands [61]. Robert *et al*. in [61] claimed that visual feedback prevents compensation direction error in reaching movements. However, in this thesis proprioceptive feedback is considered to monitor the current human's position to reduce the relative error in guiding in real time when the guiding controller derived from human demonstration experiments in [67], [68] was implemented a planar 1-DoF robotic arm.

Most of the reaching movement studies, average out error correction patterns in different directions that makes it difficult to decipher anisotropic nature of haptic perception of reaching errors. Most of the studies of Franklin, Burdet, and Milner use forward movement with detailed online information [62]. This thesis presents humans' behavior, perceptions, and arm muscle activation when naive/trained humans' most dominant arm is perturbed in leftward/rightward directions.

2.3.2 Cutaneous feedback in guiding

The humans' sense of touch is a complex and robust system [69]. As a perceptual system it covers the entire surface of the human body and much of its internal structure. Human hand consists with around 17,000 cutaneous mechanoreceptors [70]. Some studies have demonstrated how to convey signals by stimulating cutaneous mechanoreceptors in guiding [71], [72], [73], [74], [75].

In some studies vibrotactile displays have used in a way as sensory substitution system [76]. Those were used to improve the quality of life in different ways such as reading devices for those with visual impairments [77] to provide feedback of body tilt [78], balance control and postural stability [79], and navigation aid in unfamiliar environments [80]. Those were evaluated as aids to navigate in unfamiliar and hazardous environments [76].

Vibration stimulation was used to convey different types of messages to the users in

guiding with/without vision [74], [75]. Mobile devices were used to provide pedestrian navigation systems [81], [82], [83] in low visibility conditions. Authors in [74] introduced an active belt that would enable users to obtain multiple directional information in guiding. The direction is sensed by GPS direction sensor and 7 vibroactuators. Another interesting work on cooperative human robot haptic navigation was demonstrated in [84] using a vibrotactile bracelet very recently. In this study, the subjects were free to decide their own pace and a warning vibrational signal was generated by the bracelet when a large deviation occurred with respect to desired trajectory. The novel vibro-tactile bracelet would be used for path navigation for in an unknown environment with a mobile robot.

Previous studies have demonstrated mechanical and psychophysical studies of surface wave propagation during vibrotactile simulations [85]. Most of the studies focused on vibrotactile localization on the arm [73], [69] and number of tactors [86], [73], [69], [86].

In this regard this thesis focuses on how trained in primitive haptic patterns given using a wearable sleeve, can recognize their shifts and linear combinations. The results would give an idea as to how humans mentally construct the cutaneous feedback in different scenarios. The results would add cutaneous feedback to the blindfolded followers to help them mentally construct the shape and stiffness of obstacles that come into contact with the robot in future. These experiments will help to formulate several new hypotheses about the abilities of the human brain to use a reduced number of sensory modalities to accomplish tasks that they used to do without any sensory deprivation as well as the ability to derive complex perceptions by combining different sensory modalities.

2.4 Discussion

This chapter presents the previous work on navigation of a human with/without auditory and visual perceptions from the environment by an intelligent agent. Moreover, the chapter states how the thesis focus is different from previous literature. Next the chapter discusses

an approach to estimate the follower's trust in the guider with and elaboration on related work. Then the studies on proprioceptive and cutaneous feedback are presented when the vision is impaired. The discussion of the above major topics is a good basis to design a robot to navigate a human in low visibility conditions like indoor in indoor fire-fighting.

CHAPTER 3

IDENTIFICATIONS OF HUMAN GUIDING USING A HARD REIN

Abstract

This chapter presents identifications of human-human interaction where one person with limited auditory and visual perception of the environment (a follower), is guided by an agent with full perceptual capabilities (a guider), via a hard rein along a given path. Several identifications of the interaction between the guider and the follower were investigated such as, a) how to identify human control policies in guiding and following, b) how to test the order of the control policy, and c) how learning may successively apportion the responsibility of control across different muscles of the guider in Human-Human Interaction (HHI) experiments when 10 pairs participated in 20 experimental trials. It was found that the guiding agent's control policy can be modeled as a 3^{rd} order predictive AR system and the human follower can be modeled as a 2^{nd} order reactive AR system. Moreover, it was found that the guider exhibits to optimize the total cost over trials.

3.1 Introduction

The main goal of this chapter is to identify the control policies in HHI where one person with limited auditory and visual perception of the environment (a follower), is guided by another human with full perceptual capabilities (a guider), via a hard rein along a given path. As described in the introduction Chapter 1, the motivation of this thesis is to understand precise and efficient haptic based guiding when a human has lost visual and auditory perceptions due to the surrounding environment.

Several attempts have been made on guiding people with visual and auditory impairments using intelligent agents in cases such as fire-fighting [5] and guiding blind people using guide dogs [2]. Search and rescue scenarios are often complicated by low or no visibility conditions, because of smoke or dust. How does a robot guides impaired human through an obstacle-laden environment that is very noisy and there is no-visibility? Because of these conditions the guidance should consist entirely of haptic feedback. In such situations impaired human will be highly vulnerable and subject to unpredictable environmental stress. The best way to test this scenario is to study how a human with full perceptual capabilities guide an impaired human. Therefore, this chapter presents identifications of human guiding using a hard rein in human demonstrations.

This chapter explores the context of identifications of control policies from human demonstration experiments when a blindfolded human is guided by another human to be applied in robot assisted guidance in no-visibility conditions like in indoor fire-fighting or other disaster responders.

3.1.1 The questions addressed in human demonstration experiments

1. How to identify guider's and follower's control policies

2. How learning may successively apportion the responsibility of control across different

muscles of the guiding agent

3.2 Methodology

Human-human demonstration experiments were conducted to understand the control policies of guiding and following.

3.2.1 Identification of guiding control policy and following state transition policy

The experiment was conducted to understand guiding control policy and following state transition policy when one human with limited visual and auditory environmental perceptions is guided by another human with perceptual capabilities in an arbitrary complex path.

3.2.1.1 Experimental protocol

The experiment was conducted with 10 pairs of subjects after giving informed consent (see ethical approval in Appendix A). They were healthy and in the age group of 23 - 43 years. Fig. 3.1A shows how the guider and the follower held both ends of hard rein to track the wiggly path. Fig. 3.1B shows the follower was blindfolded and cutoff from using auditory feedback. Fig. 3.1C shows the relative orientation difference between the guider and the follower (referred to as state (ϕ) hereafter), and angle of the rein relative to the agent (referred to as action (θ) hereafter).

For clarity, the detailed wiggly path is shown in Fig. 3.2. The path of total length 9m was divided into nine milestones as shown in Fig. 3.2. In any given trial, the guider was asked to take the follower from one milestone to another at six milestones up or down (ex. 1-7, 2-8, 3-9, 9-3, 8-2, and 7-1). The starting milestone was pseudo-randomly changed from trial to trial in order to eliminate the effect of any memory of the path. Moreover, the follower

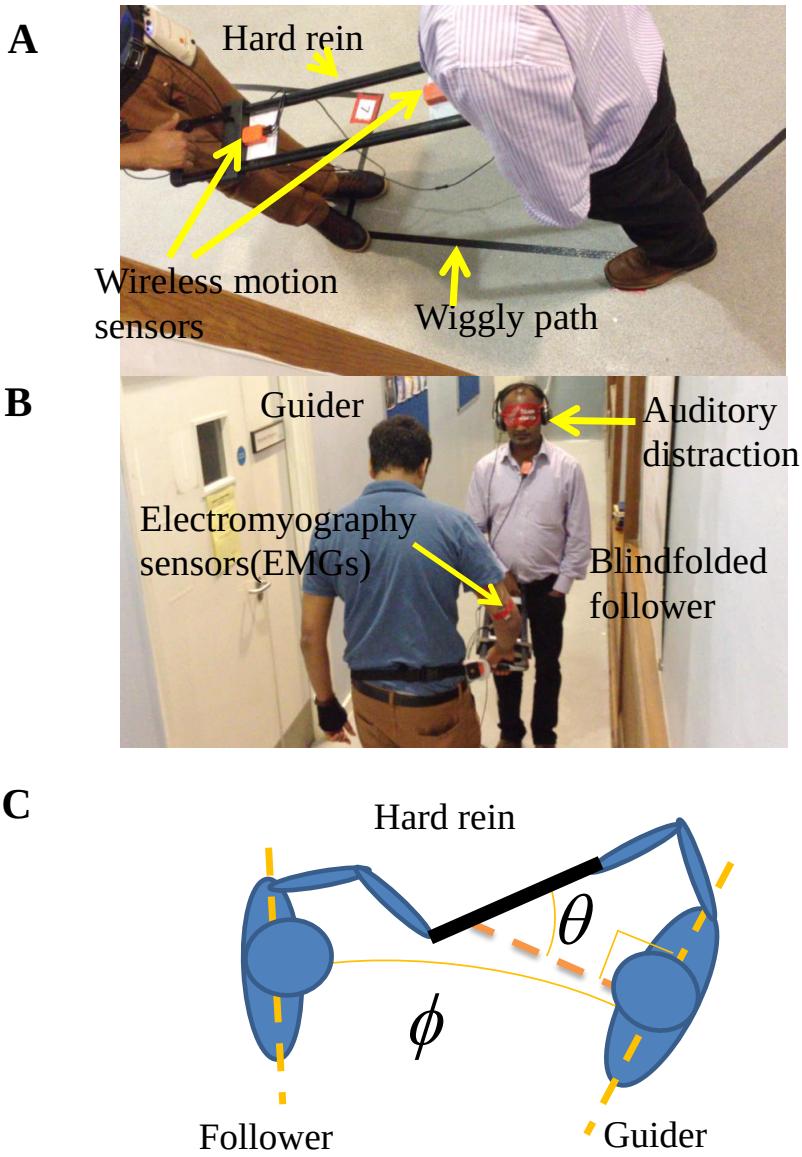

Fig. 3.1 Human-human demonstration experimental layout: A) The hard rein with wireless MTx motion trackers. The guider and follower hold the hard rein, B) Tracking the path by the duo, and C) The hard rein with wireless MTx motion sensors attached to measure the state ϕ and the action θ. Here ϕ is the relative orientation difference between the guider and the follower and θ is angle of the rein relative to the agent.

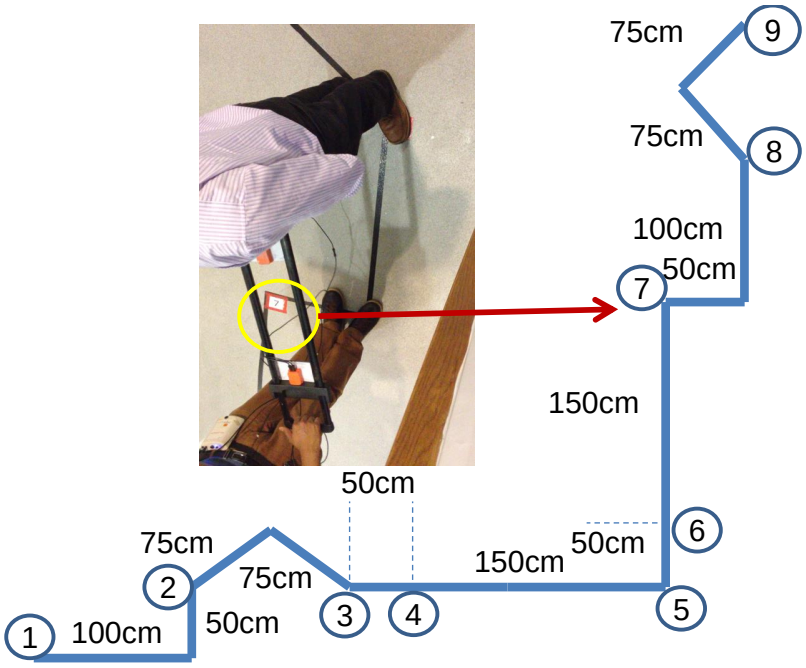

Fig. 3.2 The detailed diagram of labeled wiggly path on a floor.

was disoriented before starting every trial. The guider was instructed to move the handle of the hard rein only on the horizontal plane to generate left and right turn commands. Furthermore, the guider was instructed to use push and pull commands for forwards and backward movements. The follower was instructed to pay attention to the commands via the hard rein to follow the guider. The follower started to follow the guider once a gentle tug was given via the hard rein.

3.2.1.2 Sensing

MTx motion capture sensors (3-axis acceleration, 3-axis magnetic field strengths, 4-quaternions, 3-axis Gyroscope readings (Xsens,USA)) were used to measure the states and actions of the duo. Two MTx sensors were attached on the chest of the guider and the follower to measure the rate of change of the orientation difference between them (state). Another motion tracker was attached on the hard rein to measure the angle of the rein relative to the sensor on the chest of the guider (action from the guider). Four Electromyography (EMG) (Noraxon, USA) electrodes at 1500Hz were fixed on the guider's Anterior Deltoid, Biceps, Posterior

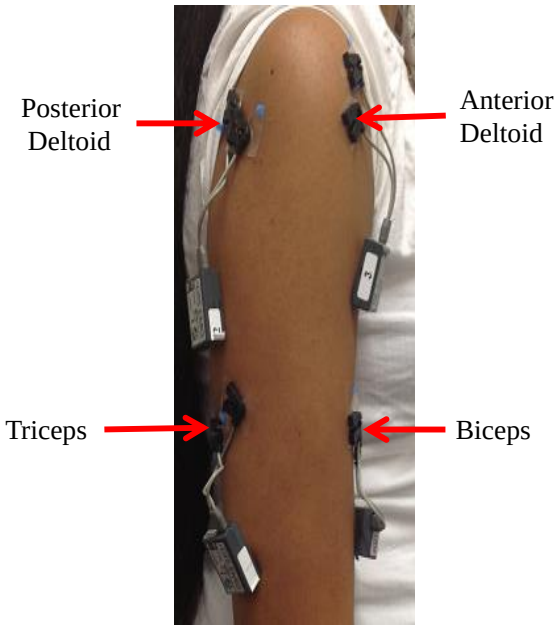

Fig. 3.3 EMG sensors are attached on the upper arm of the guider: EMG sensors are attached on Anterior Deltoid, Posterior Deltoid, Biceps, and Triceps of the guider's arm.

Deltoid, and Lateral Triceps along the upper arm as shown in Fig. 3.3. Before attaching EMG electrodes, the skin was cleaned with alcohol.

3.2.1.3 Synchronization of MTx motion sensors and EMG sensors

Since the sampling frequency of MTx motion sensors and EMG are different, synchronization method was introduced. Synchronization was achieved by adding external channel of the EMG recorder. An extra motion tracker with a switch was worn by the guider on his waist. A copper wire which winds around the motion tracker connects via a switch and the battery serially connected to the EMG external channel. Before starting the trial, the guider was asked to turn on the switch of the circuit, the induced magnetic field around the wire could be seen in magnetic data of the MTx motion sensor while it could be seen by a trigger in newly added channel in the EMG recorder. In the analysis, the triggers were used to align the motion tracker and EMG data.

3.3 Modeling

This section presents how to model the guiding and following policies of the guider and the follower. The map from state to action (the guider's policy) or the map from action to state (the state transition policy of following) were formulated by Auto-Regressive (AR[1]) model. The intention is to find the model order and the nature (predictive/reactive) of the model.

3.3.1 The guider's closed loop control policy

The guider's control policy is modeled as a N-th order state dependent discrete linear controller. The order N depends on the number of past states used to calculate the current action.

Let the state be the relative orientation between the guider and the follower given by ϕ, and the action be the angle of the rein relative to the sensor on the chest of the guider given by θ as shown in Fig. 3.1C. Then the linear discrete control policy of the guider is given by

$$\theta_g(k) = \sum_{r=0}^{N-1} a_r^{gRe} \phi_g(k-r) + a_N^{gRe} \tag{3.1}$$

if it is a reactive controller, and

$$\theta_g(k) = \sum_{r=0}^{N-1} a_r^{gPre} \phi_g(k+r) + a_N^{gPre} \tag{3.2}$$

if it is a predictive controller, where, k denotes the sampling step, N is the order of the polynomial, $a_r^{gRe}, a_r^{gPre}, r = 1, 2, \cdots, N-1$ is the polynomial coefficient corresponding to the r-th state in the reactive and predictive model respectively, and a_N^{gRe}, a_N^{gPre} are corresponding scalars.

[1] An auto-regressive (AR) model is a representation of a type of random process. The (AR) model specifies that the output variable depends linearly on its own previous values [87].

3.3.2 The follower's state transition policy

While the guider's control policy is represented by Eqs. 3.1 and 3.2, the follower's state transition policy was modeled as an N-th order action dependent discrete linear controller to understand behavior of the follower. The order N depends on the number of past actions used to calculate the current state. Then the linear discrete control policy of the follower is given by

$$\phi_f(k) = \sum_{r=0}^{N-1} a_r^{fRe} \theta_f(k-r) + a_N^{fRe} \tag{3.3}$$

if it is a reactive controller, and

$$\phi_f(k) = \sum_{r=0}^{N-1} a_r^{fPre} \theta_f(k+r) + a_N^{fPre} \tag{3.4}$$

if it is a predictive controller, where, k denotes the sampling step, N is the order of the polynomial, $a_r^{fRe}, a_r^{fPre}, r = 1, 2, \cdots, N-1$ is the polynomial coefficient corresponding to the r-th state in the reactive and predictive model respectively, and a_N^{fRe}, a_N^{fPre} are corresponding scalars. These linear controllers in Eqs. 3.1, 3.2, 3.3, and 3.4 can be regressed with the experimental data obtained in the guider-follower experiments above to obtain the behavior of the polynomial coefficients across trials. The behavior of these coefficients for all human participants across the learning trials will give us useful insights as to the predictive/reactive nature, variability, and stability of the control policy learned by duo. Furthermore, a linear control policy given in Eqs. 3.1, 3.2, 3.3, and 3.4 would make it easy to transfer the fully learned control policy to a robotic guider in a low visibility condition.

3.4 Results

The experiments were conducted with human participants to understand how the coefficients of the control policy relating states ϕ and actions θ given in Eqs. 3.1 to 3.4 settle

down across learning trials. In order to have a deeper insight into how the coefficients in the discrete linear controller in Eqs. 3.1 to 3.4 change across learning trials, the following scientific questions were tested, 1) whether the guider and the follower tend to learn a predictive/reactive controllers across trials and 2) what would be the order of the control policy of the guider in Eqs. 3.1 and 3.2 and the order of the control policy of the follower in Eqs. 3.3 and 3.4.

3.4.1 Data Analysis

All data were analyzed using MATLAB R2012a (The MathWorks Inc). Daubechies wave family (db10) of the MATLAB Wavelet Toolbox was used to extract the action of the guider and the state of the follower. Symlet wave family (sym8) of MATLAB was used for EMG analysis. Statistical significances were computed using the Mann-Whitney U test ($\alpha = 0.05$).

3.4.2 Adoption of Wave families for action and state vector profiles

To find regression coefficients, since the raw motion data have noise, Wavelet Toolbox (The MathWorks Inc) was used to reduce the noise in the action and the state vectors. The guiders action are continuous swing and pulls on the horizontal plane. However, for clarity, the guider's arm movement was plotted in horizontal and vertical planes for a random trial as shown in Fig. 3.4. The vertical movements are very low to compare with the horizontal movements. Therefore, only horizontal movements was considered to represent the arm action. Therefore, the Daubechies wave family was chosen (for sinusoidal waves) [88] in the wavelet analysis. Moreover, according to the previous studies [89], [60], human arm movements are continuous and smooth. Therefore, a continuous mother wavelet (db10) was taken to represent the swing actions in wavelet analysis. For further clarity, the percentage of energy representation of db10 and harr wave families were compared as shown in Fig. 3.5A. Considering higher percentage value, db10 was selected for swing type action analysis.

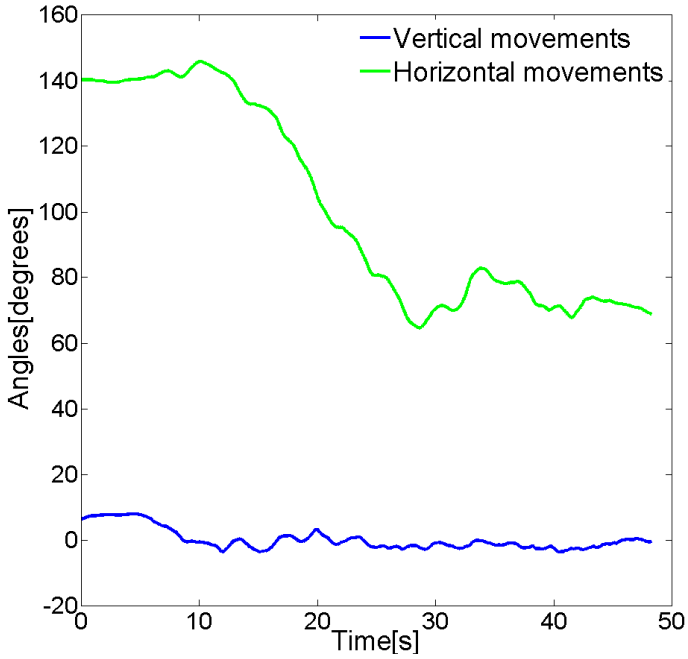

Fig. 3.4 The vertical movements and horizontal action vector for the guider in a representative trial.

Then different decompression levels were tested for db10. The percentage of energy corresponding to approximation for different decompression levels were found to be 99.66%, 93.47%, and 86.73% for decompression levels 4, 8, and 15 respectively. The highest percentage of energy was gained when the decompression level is 4.

Fig. 3.5B shows the percentage energy corresponding to the 1 to 4 decomposition levels of the action vector. Since the 4^{th} decomposition level has the highest percentage (88%) value, 4^{th} decomposition level was adopted of db10 wave family to analyze raw data of the action. Moreover, the same procedure was tested for state vector profile and the results agreed with action vector profile. Therefore, based on the results, 4^{th} decomposition level was adopted of db10 wave family to analyze raw data of both the action and the state.

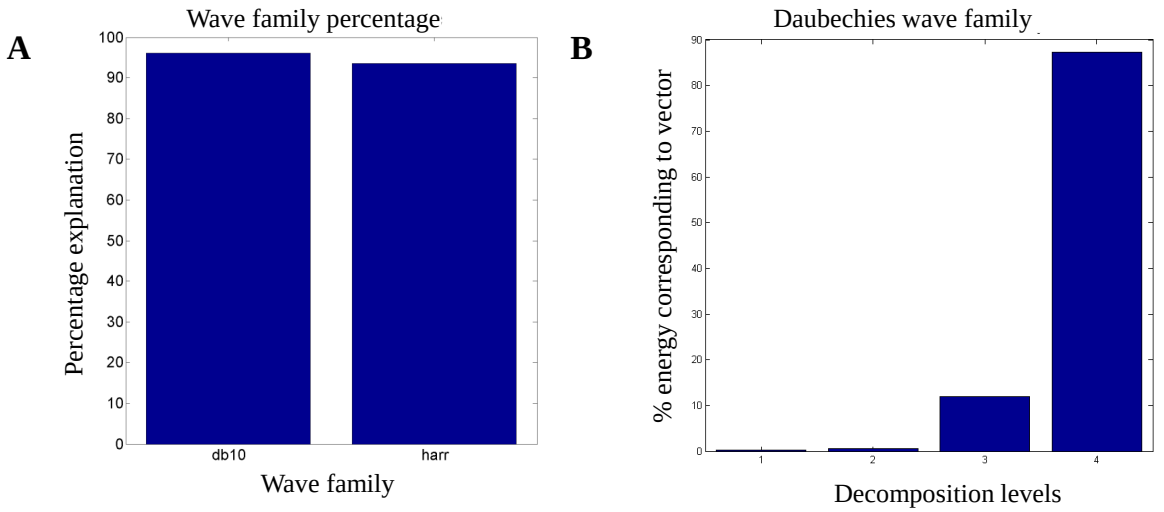

Fig. 3.5 Selection of wave family for action vector profiles: A) Selection of wavelet family for guiding agent action vectors. The percentage of energy representation of action vector of all subjects in all trials for db10 and harr wavelet families, and B) The percentage of energy corresponding to 1 to 4 decomposition levels in db10 wave family. The averaged action vector across the all subjects over trials are taken.

3.4.3 Determination of the guider's control policy

The 4^{th} decomposition level of db10 of action θ and state ϕ vectors are used for regression in Eqs. 3.1 and 3.2. Once the coefficients of the polynomial in Eqs. 3.1 and 3.2 are estimated, the best control policy (Eqs. 3.1 or 3.2), and the corresponding best order of the polynomial should give the best R^2 value for a given trial across all subjects. Here, twenty experimental trials are binned to five for clarity.

First, the R^2 of the reactive and predictive from 1^{st} to 4^{th} order polynomials over trials for the individual guider are shown in Fig. 3.6. The average R^2 value across the 10 subjects is shown by a dashed line in Fig. 3.6. Since the individual subject has a higher variability, hereafter the average R^2 value across all subjects is taken to find the guider's control policy as shown in Fig. 3.7. Therefore, the average R^2 from 1^{st} to 4^{th} order polynomials over trials for guider predictive and reactive are shown in Fig. 3.7A.

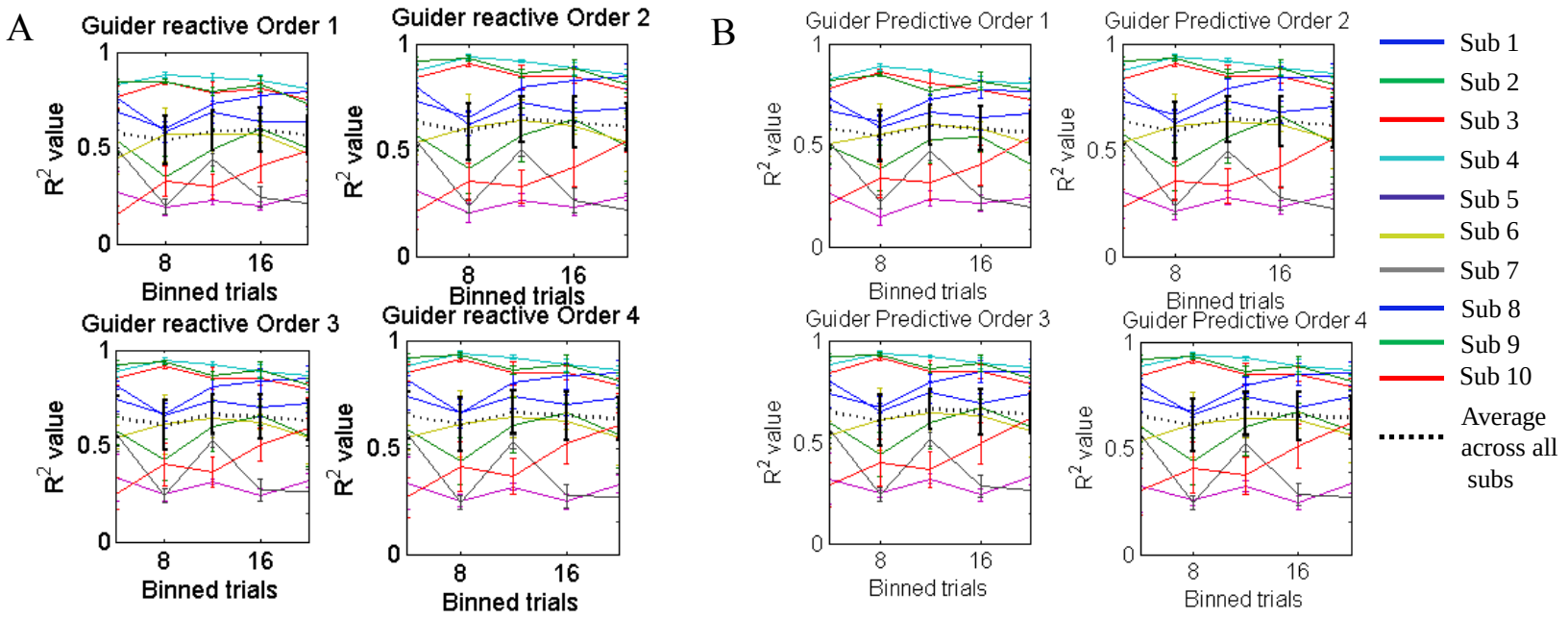

Fig. 3.6 The individual guider's R^2 value representation across the trials for predictive and reactive models: A) The R^2 value variation of the reactive from 1st to 4th order polynomials over trials for the individual guiders, and B) The R^2 value variation of the predictive from 1st to 4th order polynomials over trials for the individual guiders. The average R^2 across all subjects are shown by a dashed line.

3.4.4 Determination of predictive/reactive nature of the guider's control policy

To select best fit policies, coefficients of Eqs. 3.1 and 3.2 are estimated from 1st order to 4th order polynomials as shown in Fig. 3.7A. Dashed line and solid line were used to denote reactive and predictive models respectively. From Fig. 3.7A, the R^2 values corresponding to the 1st order model in both Eqs. 3.1 and 3.2 are the lowest. The relatively high R^2 values of the higher order models suggest that the control policy is of order > 1. Therefore, the percentage (%) differences of R^2 values of higher order polynomials relative to the 1st order polynomial for both Eqs. 3.1 and 3.2 were taken to assess the fitness of the predictive control policy given in Eq. 3.2 relative to the reactive policy given in Eq. 3.1. Fig. 3.7B shows that the marginal percentage (%) gain in R^2 value (%$\triangle R^2$) of 2nd, 3rd, and 4th order polynomials in Eq. 3.2 predictive control policy, (solid line) grows compared to those of the reactive control (dashed line) policy in Eq. 3.1. Therefore, the conclusion is that the guider gradually gives more emphasis on a predictive control policy than a reactive one. Moreover, individual guider's predictive/reactive nature and the model order were tested as shown in the tree diagram in Fig. 3.7C.

3.4.5 Determination of the model order of the guider's control policy

The percentage (%) gain of of 3rd order polynomial is highest compared to 2nd and 4th order polynomials as shown in Table 3.1 by numerical values and the Fig. 3.7B. There is a statistically significant improvement from 2nd to 3rd order models ($p = 0.008$), while there is not significant information gain from 3rd to 4th order models ($p = 0.54$). It means that the guider predictive control policy is better explained with a 3rd order model. No any information is added for higher orders after $N = 3$. Therefore, hereafter, 3rd order predictive control policy is considered to explain the guider's control policy.

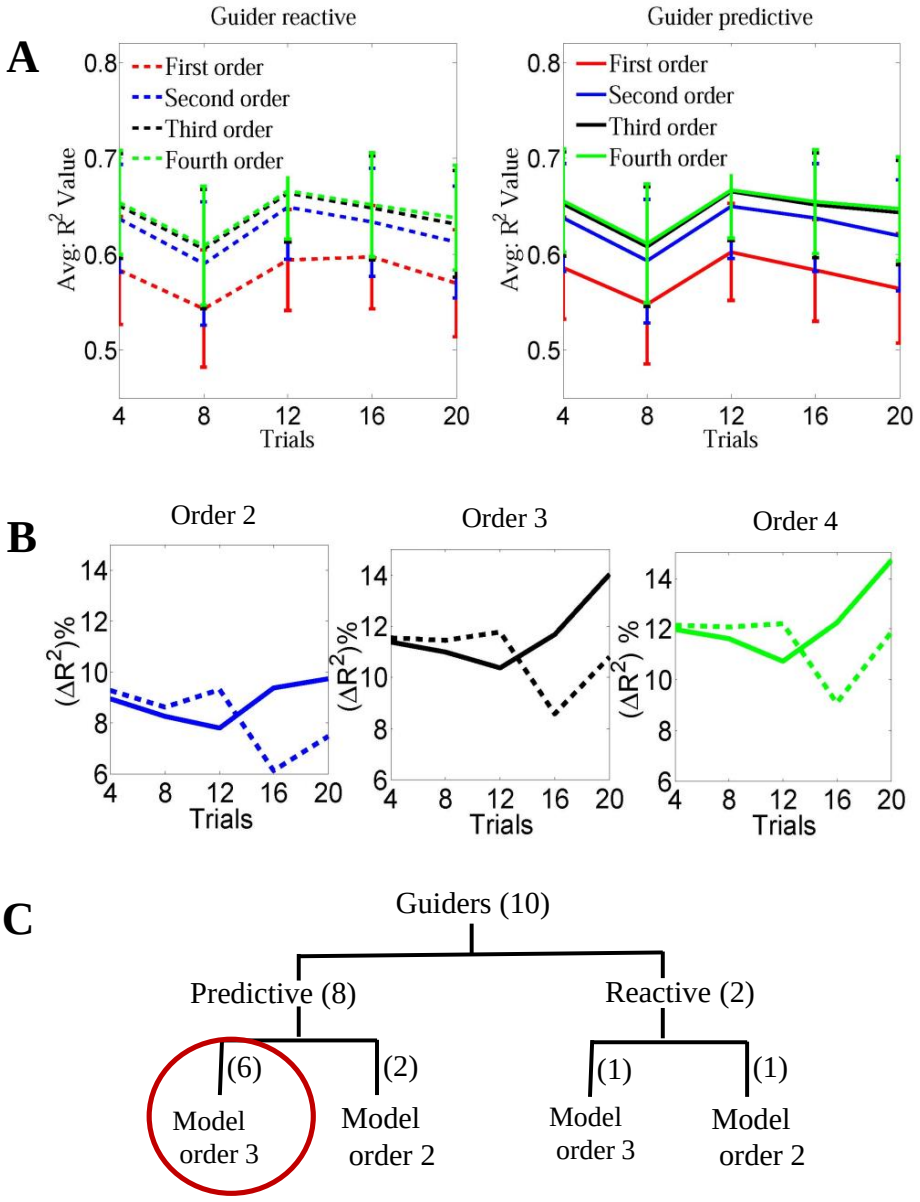

Fig. 3.7 The guider's model order and predictive/reactive nature selection: R^2 values from 1st order to 4th order polynomials for the guider. Reactive models (dashed line) and predictive models (solid line): A) The R^2 value variation of the reactive and predictive from 1st to 4th order polynomials over trials for the guider, B) The percentage (%) differences of R^2 values of 2nd to 4th order polynomials with respect to 1st order polynomial for the guider's: 2nd order (blue), 3rd order (black), 4th order (green), and C) Individual guider's model orders and the predictive/reactive nature distribution by a tree diagram. On average the guider is most likely on 3rd order predictive.

Therefore, the guider's control policy can be written by

$$\theta_g(k) = a_0^{gPre}\phi_g(k) + a_1^{gPre}\phi_g(k+1) + a_2^{gPre}\phi_g(k+2) + a_3^{gPre} \tag{3.5}$$

a_i^{gPre}, $i = 0, \cdots, 3$ are the polynomial coefficient of the 3rd order predictive controller [90], [91].

Table 3.1 Guider predictive $\triangle R^2\%$ of 2nd to 4th order polynomials w.r.t 1st order. Statistical significance was computed using the Mann-Whitney U test ($\alpha = 0.05$)

Trial No:	2nd **order**	3rd **order**	4th **order**	p values
4	8.94	11.37	11.97	
8	8.26	10.98	11.62	
12	7.81	10.36	10.74	$p(2^{nd} \leftrightarrow 3^{rd}) < 0.009^*$,
16	9.38	11.68	12.25	$p(3^{rd} \leftrightarrow 4^{th}) > 0.5$
20	9.74	14.00	14.70	

3.4.6 Determination of the follower's state transition policy

Next attempt is to understand the identifications of the follower's state transition policy in response to guider's actions.

3.4.7 Determination of predictive/reactive nature of the follower's control policy

First, the R^2 of the reactive and predictive from 1st to 4th order polynomials over trials for the follower for the individual subjects are shown in Fig. 3.8. The average R^2 value across the 10 followers is shown by a dashed line as shown in Fig. 3.8. Since the individual subjects has a higher variability, the average R^2 value across all subjects is taken as shown in Fig. 3.9. Therefore, the average R^2 from 1st to 4th order polynomials over trials for follower predictive and reactive are shown in Fig. 3.9C.

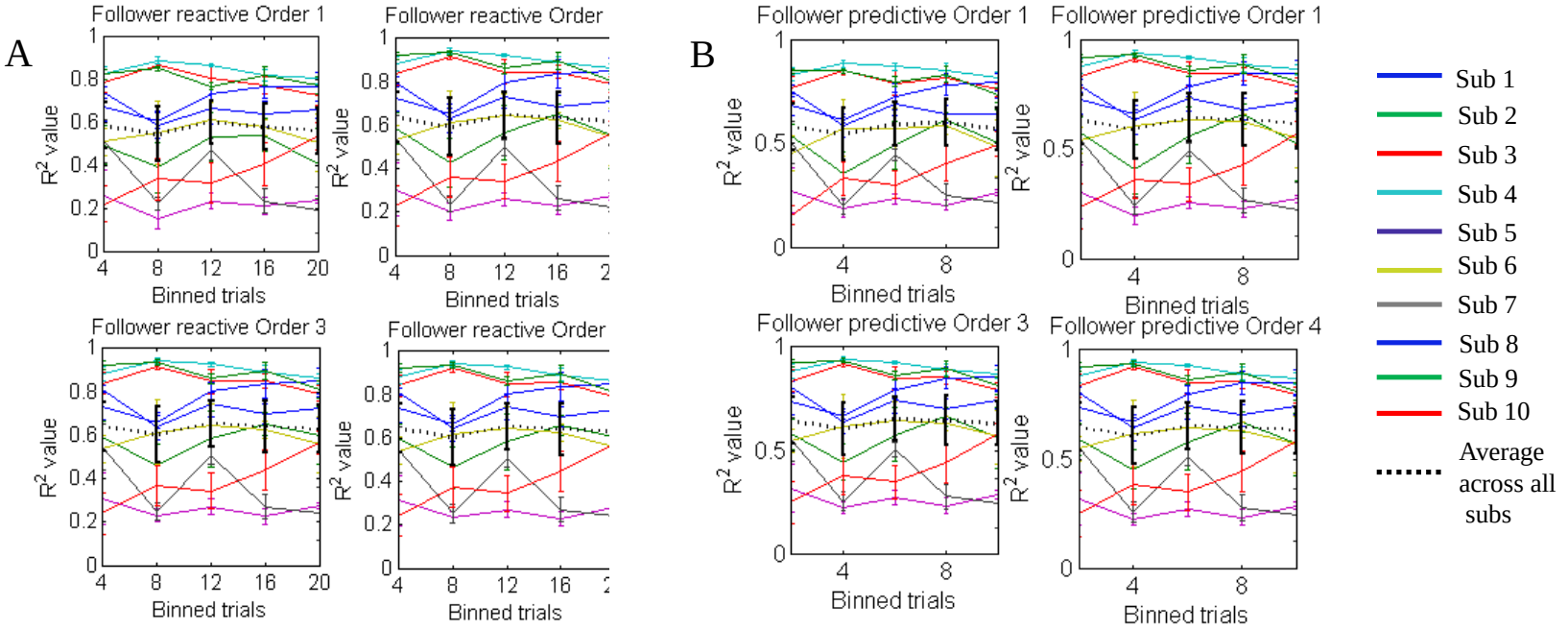

Fig. 3.8 The individual follower's R^2 value representation across the trials for predictive and reactive models: R^2 values from 1st order to 4th order polynomials for the individual follower: A) The R^2 value variation of the reactive from 1st to 4th order polynomials over trials for the individual subject, and B) The R^2 value variation of the predictive model from 1st to 4th order polynomials over trials for the individual subjects. The average R^2 across all subjects are shown by a dashed line.

The experimental data for state θ and action ϕ in Eqs. 3.3 and 3.4 were used to extract features of the follower's policy from 1st to 4th order polynomials over trials as shown in Fig. 3.9C. Here, same mathematical and statistical method were used as guider's model. Interestingly, Fig. 3.9C shows that the marginal percentage (%) gain in R^2 value (%$\triangle$R^2) of 2nd, 3rd, and 4th order polynomials in Eq. 3.3 reactive control policy, (dashed line) grows compared to those of the predictive control policy (solid line) in Eq. 3.4. Moreover, individual follower's predictive/reactive nature and the model order selection are shown in the tree diagram in Fig. 3.9(C). Therefore, conclusion is that the follower gradually gives more emphasis on a reactive policy than a predictive one.

3.4.8 Determination of the model order of the follower's state transition policy

The percentage (%) gain of of 2nd order polynomial is highest compared to 3rd and 4th order polynomials as shown in Table 3.2 by numerical values and the Fig. 3.9D. Interestingly, there is no statistically significant improvement from 2nd to 3rd order models ($p = 0.42$) or from 3rd to 4th order models ($p = 0.54$). Therefore, the follower reactive policy is more explained when the order is $N = 2$. Therefore, hereafter, 2nd order reactive policy is considered to explain the follower's state transition policy.

Therefore, the follower's state transition policy can be written as,

$$\phi_f(k) = a_0^{fRe}\theta_f(k) + a_1^{fRe}\theta_f(k-1) + a_2^{fRe} \tag{3.6}$$

a_i^{fRe}, $i = 0, \cdots, 3$ are the polynomial coefficient of the 3^{rd} order reactive controller [91]

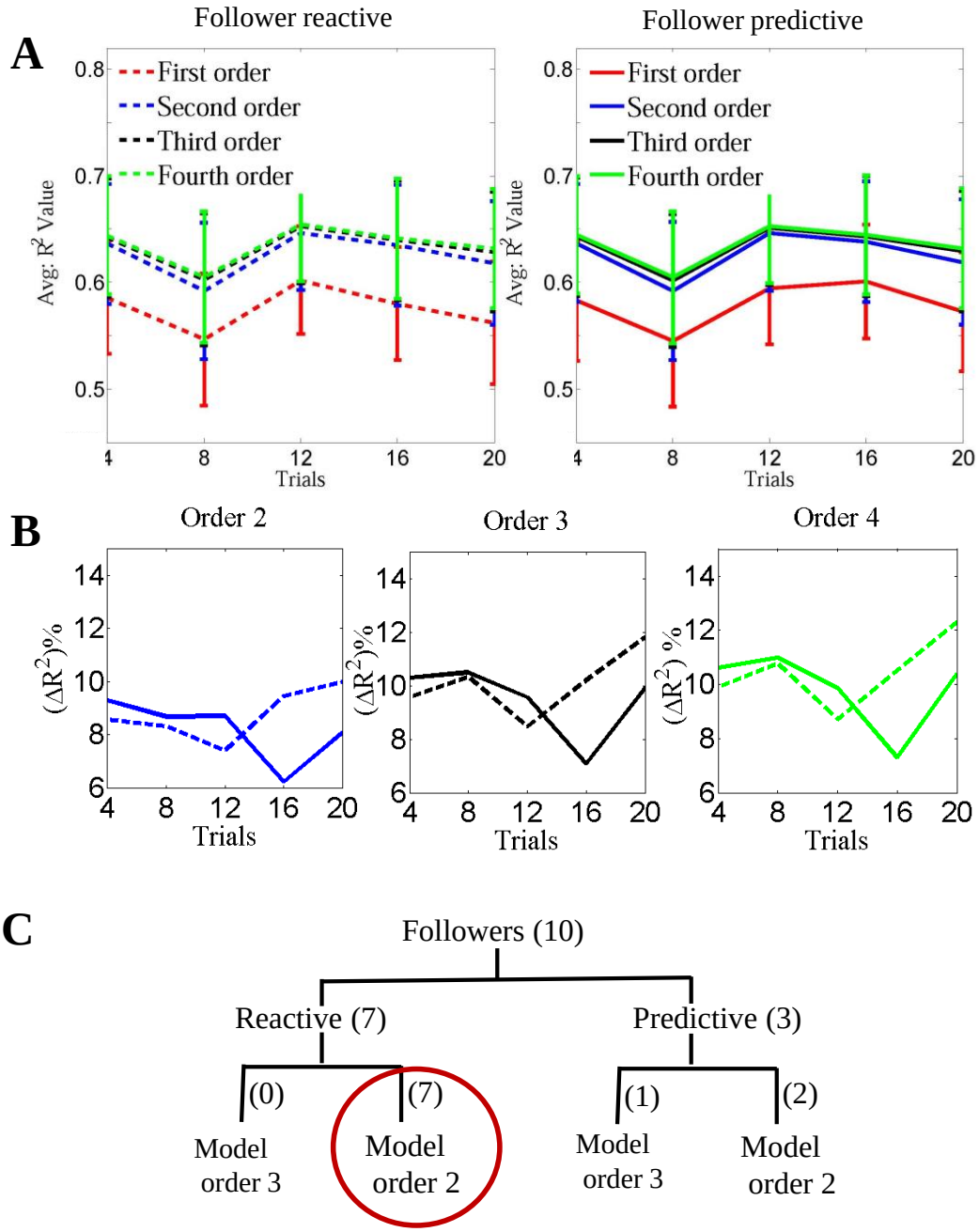

Fig. 3.9 The follower's model order and predictive/reactive nature selection: R^2 values from 1st order to 4th order polynomials for the follower. Reactive models (dashed line) and predictive models (solid line): A) The R^2 value variation of the reactive and predictive from 1st to 4th order polynomials over trials for the guider and the follower respectively, B) The percentage (%) differences of R^2 values of 2nd to 4th order polynomials with respect to 1st order polynomial for the guider's and the follower's control policies respectively: 2nd order (blue), 3rd order (black), 4th order (green), and C) Individual follower's model orders and the predictive/reactive nature distribution by a tree diagram. The follower is most likely on 2rd order reactive models.

Table 3.2 Follower reactive $\triangle R^2\%$ of 2nd to 4th order polynomials w.r.t 1st order. Statistical significance was computed using the Mann-Whitney U test ($\alpha = 0.05$)

Trial No:	2^{nd} **order**	3^{rd} **order**	4^{th} **order**	p values
4	8.58	9.57	9.91	
8	8.31	10.33	10.77	
12	7.41	8.46	8.70	$p(2^{nd} \leftrightarrow 3^{rd}) > 0.4$,
16	9.45	10.21	10.51	$p(3^{rd} \leftrightarrow 4^{th}) > 0.5$
20	9.96	11.82	12.29	

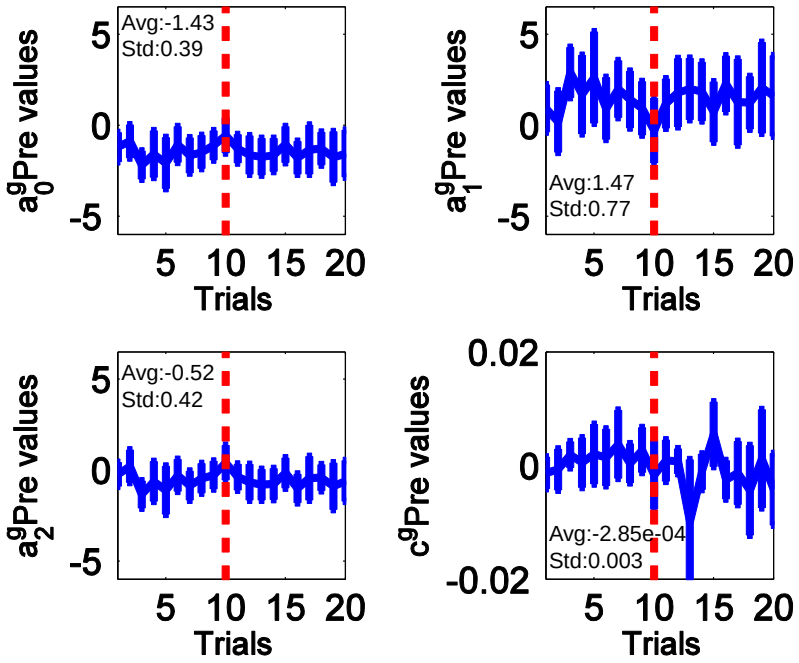

Fig. 3.10 The evolution of coefficients of the 3rd order auto regressive predictive controller of the guider.

3.4.9 Polynomial parameters of auto-regressive state dependent behavioral policies of the duo

The polynomial parameters of the guider's 3rd order predictive and the follower's 2nd order reactive policies would evolve across learning trials in Eqs. 3.2 and 3.3 for the guider and the follower respectively. In Figs. 3.10 and 3.11 show the history of the polynomial coefficients fluctuates within bounds for both the guider predictive and the follower reactive.

The average and standard deviation (denoted by avg: and std: respectively) values of the coefficients are labeled in Figs. 3.10 and 3.11. This could come from the variability across participants and variability of the parameters across trials itself. Therefore, the above control policies are estimated as bounded stochastic decision making process.

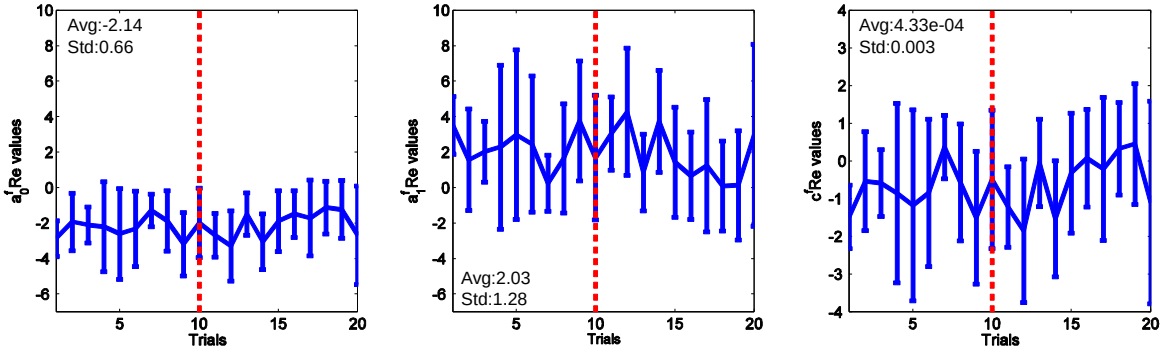

Fig. 3.11 The evolution of coefficients of the 2nd order auto regressive reactive controller of the follower.

3.4.10 Optimality of muscle recruitment

To understand the optimality of muscle activation, first the responsibility assignment of muscles from EMG recordings is discussed. Since the raw EMG data has noise, again Wavelet Toolbox (The MathWorks Inc.) was used to reduce noise. The raw EMG signal is a sinusoidal continuous wave as shown in Fig. 3.12A. Therefore, the *sym8* in Symlets wave family (The MathWorks Inc) was used [88] for EMG analysis. For further clarity, the percentage of energy corresponding to the approximation of *sym8* (Symlets) and *harr* (Harr) are demonstrated by a bar chart as shown in Fig. 3.12B by 72.91% and 68.46% respectively. Considering the highest energy percentage, *sym8* was chosen for our EMG wave analysis. Then different decompression levels were tested for *sym8*. The percentage of energy corresponding to approximation for different decompression levels were found to be 99.52%, 95.97%, 92.05%, 85.41%, and 20.36% for decompression levels 3, 4, 5, 6 and 7 respectively. The highest percentage of energy was gained when the decompression level

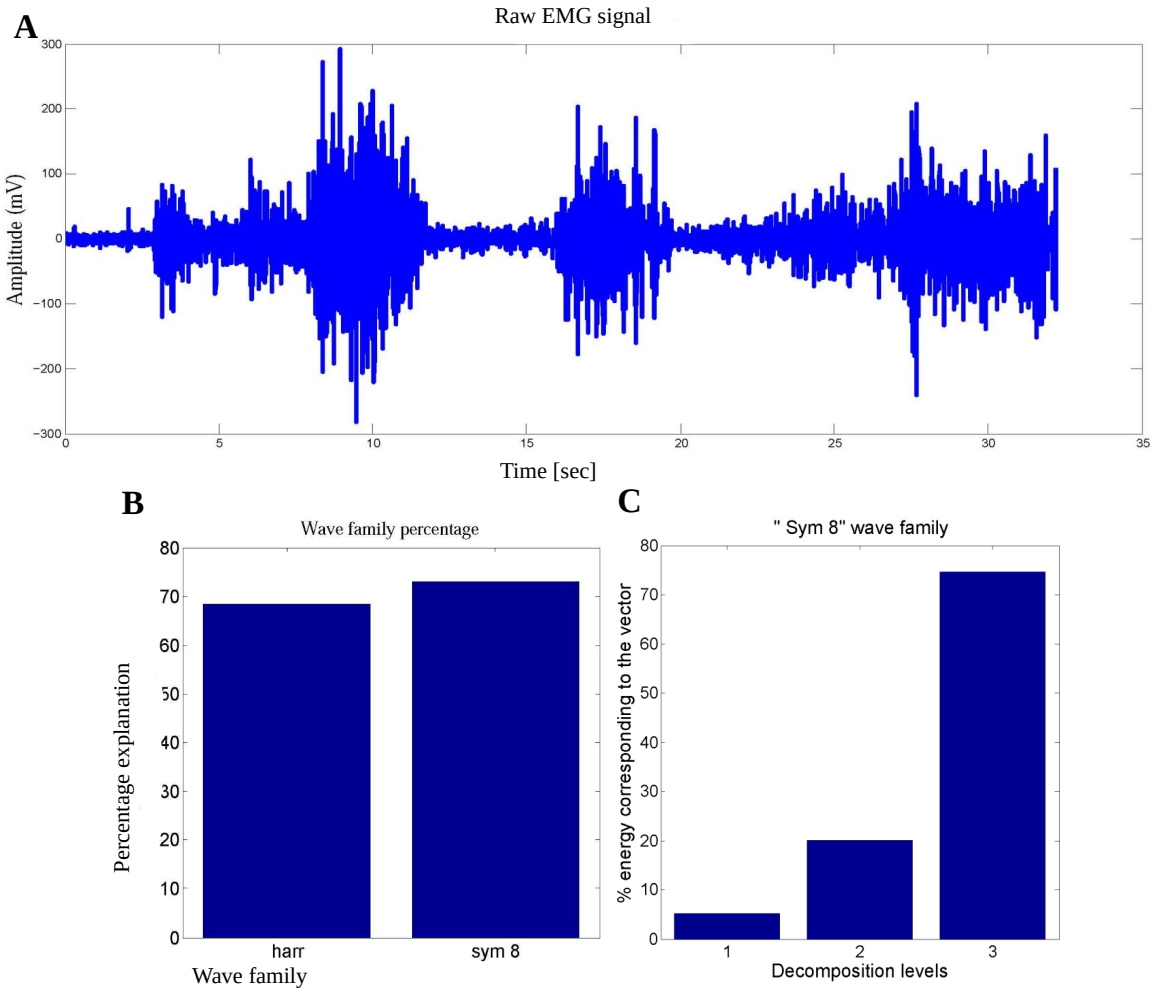

Fig. 3.12 Selection of wavelet family for EMG vector: A) A representative raw EMG signal from the guider, B) The percentage of energy representation for harr and sym8 wavelet families for raw EMG signal, and C) The percentage of energy corresponding to 1 to 3 decomposition levels for sym8 wave family for the EMG signal.

is 3. To understand the percentages of energy corresponding to the 1 to 3 decomposition levels, Fig. 3.12C shows the percentage energy corresponding to the 1 to 3 decomposition levels of the EMG signal. Since the 3rd decomposition level has highest percentage energy level (76%), hereafter the 3rd decomposition level is used to analyze raw EMG data.

3.4.11 Behavior of antagonist muscles

When the guider takes the arm action in horizontal plane, it can be pushing/ pulling or swinging in horizontal plane. The Anterior Deltoid and Posterior Deltoid are recruited for

arm pushing and pulling. The guider can use the elbow joint in two different ways: one is to swing the rein in the vertical plane by flexing the elbow without moving the shoulder joint, and the other is to pull the rein if the elbow is flexed in synchrony with a shoulder joint flexion. To understand the muscle recruitment, average normalized activation of each individual muscle was plotted over trials and the averaged normalized EMG ratio between frontal and dorsal muscles over trials as shown in Fig. 3.13A and Fig. 3.13B respectively. There is a downward trend in ratio of Anterior Deltoid and Posterior Deltoid muscles over trials in Fig. 3.13B: M1 while ratio of Biceps and Triceps muscles has a upward trend over trials as shown in Fig. 3.13B: M2. This indicates that a forward model of task dynamics is learnt across trials. For further clarity, the significance test was conducted between the first 5 trials and last 5 trials of M1 and M2 using single tailed t-test (because data were normally distributed, $p = 0.85$). The results show that the ratio of first five trials and last five trials of Anterior Deltoid and Posterior Deltoid (M1) are significantly different ($p = 0.001$) while there is no significance between the ratio of first five trials and last five trials of Biceps and Triceps (M2) ($p = 0.85$). This suggests that the forward model [92], [93] that predicts the consequence of guiding actions accounts for the activity of Deltoids than the elbow joint. This may be due to the fact that the elbow joints is mainly responsible to keep the guider's actions on the horizontal plane.

3.4.12 Behavior of total EMG over trials

To obtain an estimation of the total energy consumed during guiding, the average EMG for all four muscles of all ten subjects are computed. The results reflect the average energy consumed in a trial given by $J = \sqrt{\sum_{i=1}^{4}\sum_{j=1}^{S_N} EMG_{ij}^2}$, where S_N is the number of subjects, EMG_{ij} is the average rectified EMG of the ith muscle of the jth subject. The behavior of this energy consumption indicator J is shown in Fig. 3.14. It is observed from the 2nd order best fit curve that J increases to a maximum in the first half of the trials - decreases

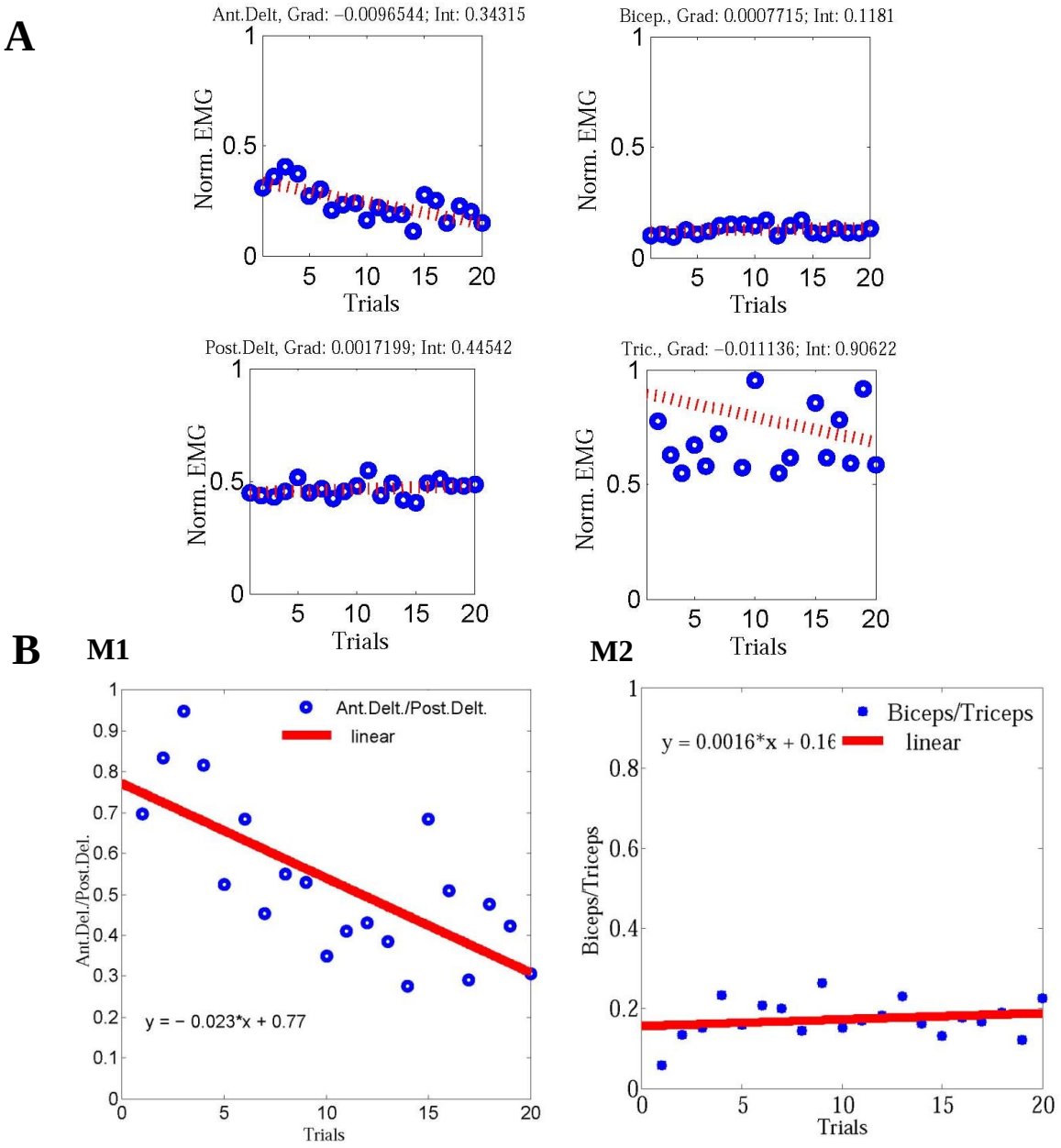

Fig. 3.13 The behavior of the average normalized muscle EMGs: A) Average normalized muscle EMG anterior Deltoid, posterior Deltoids, Biceps, and Triceps. The gradient and intercept of individual muscles are (-0.005, 0.315), (0.004,0.426), (0.001, 0.133), and (-0.013, 0.995) for Anterior Deltoid, Posterior Deltoid, Biceps, and Triceps respectively, and B) Frontal and dorsal muscle ratio: M1- Biceps triceps muscle ratio, M2- anterior Deltoid posterior Deltoid muscle ratio

in last 10 trials. This suggests that optimization is a non-monotonic process. During the first half of trials, it may have given priority to predictive control policy order selection (Eq. 3.2) and the formation of the forward model to predict follower's state into the future than optimization in the muscle activation space, which is also reflected in the behavior of R^2 values in Fig. 3.7. Once the optimal order is selected, subjects exhibit monotonic optimization in the muscle activation space as seen in the last 10 trials of Fig. 3.14, with a corresponding increase of R^2 values in Fig. 3.7.

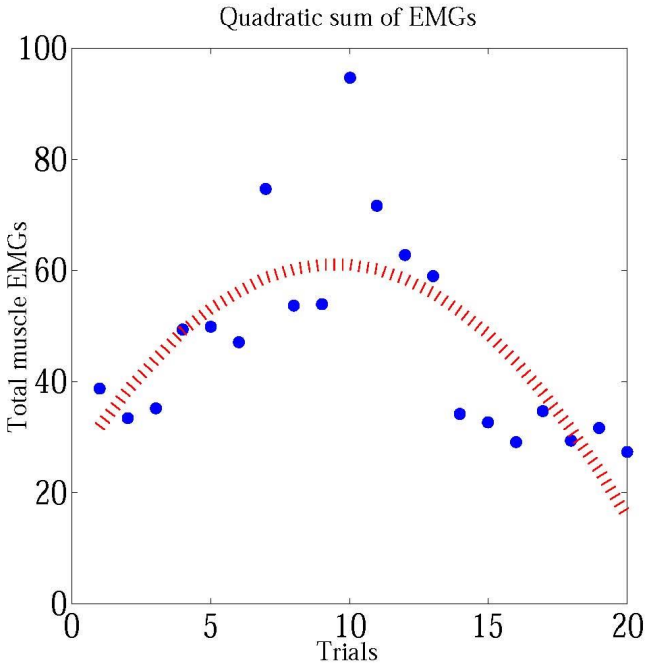

Fig. 3.14 The behavior of this cost indicator: The behavior of this cost indicator J of the 2nd order best fit curve for average EMGs of all four muscles of the ten subjects across trials.

3.4.13 Discussion

This chapter presents identification of state dependent control policy to guide a person with limited visual and auditory perceptions in an uncalibrated environment. If an intelligent agent (man/machine) guides the above person, the guiding agent could learn variability of movements and uncertainty of behavior [94]. Therefore, this study was conducted to

understand how two human participants interact with each other using haptic signals through a hard rein to achieve a path tracking goal when one partner was cut off from auditory and visual feedback from the environment (the follower), while the other (the person with environmental perceptions) gets full state feedback of the follower to find variability of movement and uncertainty of the behavior. It was found that on average guider gives more emphasis on 3rd order predictive controller and the follower gives more emphasis on 2nd order reactive model.

The proposed control policy based on human-human demonstrations is mainly intended to be used in a robot to guide people with good vision working in low visibility environments like in indoor fire-fighting or in other disaster response scenarios. The results suggest that in general, the guider depends on more historical information to generate an action, while the follower depends on less. Therefore, the interpretations as to why the follower's auto-regressive reactive policy is a 2nd one, whereas the guider's auto-regressive predictive policy in a 3rd or higher order is that a reactive behavior does not need as many past states as in a predictive behavior to take action. The novel findings provide a novel theoretical basis to design advanced human-robot interaction algorithms in a variety of cases that require the assistance of a robot to perceive the environment by a human counterpart.

CHAPTER 4

ESTIMATE THE TRUST OF A HUMAN IN FOLLOWING ANOTHER AGENT BY THE COEFFICIENTS OF A VIRTUAL DAMPED INERTIAL MODEL OF THE HUMAN IN REAL TIME

Abstract

This chapter presents how the trust of a human in following another agent can be estimated by the coefficients of a virtual damped inertial model of the human in real time. In Human Robot Interactions (HRI), the human will try to 'read' the situation by nature, and anticipate the movements of the robot companion. A major pre-condition for successful HRI in these circumstances is the human trust in the robot. If the robot can adjust itself in order to trust level of the human, it is easy to develop a mutual understanding between the robot and the human in guiding. By modeling the follower's dynamics by a time varying virtual damped inertial system, it shows that the coefficient of virtual damping is most sensitive to the trust level of the follower at any given time. These experimental insights would be used to derive a novel controller that integrates an optimal order control policy with a push/pull force modulator in response to the trust level of the follower monitored using a time varying virtual damped inertial model.

4.1 Introduction

Human mutual trust to follow an other party is more important to have a successful HRI. According to Oxford dictionary trust is defined as [95] "firm belief in the reliability, truth, or ability of someone or something".

So far, there has been little discussion about human trust on robots in unstructured environments. Trust is one of the most critical factors in urban search and rescue missions because it can impact the decisions human make in uncertain conditions [55]. If any robotic assistant to a person with limited perception of the environment could monitor the level of trust of the person to be relevant to the psychological context of the person being assisted, would be the best way to construct a mutual understanding between two parties. Few attempts have been made to study trust of a human with limited perception [10], [48] in different environments. In a simulated game of fire-fighting, Stormont *et al* [10] showed that the fire-fighters become increasingly dependent upon robotic agents when the fire starts to spread along randomly changing in wind directions. Freedy [48] has discussed how self confidence correlates with trust of automation in human robot collaboration. Previous studies on human trust on a guiding agent have shown that humans tend to depend entirely on the guiding agent when they are in hazardous environments [10] until sudden a change occurs [96]. This implies that the degree of compliance in a follower should drop if the follower loses trust in the guiding agent. Moreover, [58], [55] studied how human trust can be explained quantitatively. However, this chapter explains not only quantifies the human trust but also models it in real time.

The results from human-human demonstrations provide useful design guidelines to HRI that should account for the real-time trust of the human counterpart. In a HRI scenario such as a fire-fighter being guided by a robot through thick smoke, the estimate of the followers' trust using the above method could be used to adopt the behavioral changes of the intelligent

agent.

4.1.1 The objectives addressed by Chapter 4

1. How the guiding agent may modulate the pulling force in response to the trust level of the follower in different paths

4.1.2 Modeling the follower as a virtual time varying damped inertial system

In order to study how the above control policy would interact with the follower in an arbitrary path tracking task, the voluntary following behavior of the blindfolded human subject (follower) was modeled as a damped inertial system, where a tug force $F(k)$ applied along the follower's heading direction at sampling step k would result in a transition of position given by

$$F(k) = M\ddot{P}_f(k) + \zeta \dot{P}_f(k) \tag{4.1}$$

where M is the virtual mass, P_f is the position vector in the horizontal plane, and ζ is the virtual damping coefficient. It should be noted that the virtual mass and damping coefficients are not those real coefficients of the follower's stationary body, but the mass and damping coefficients felt by the guider while the duo is in voluntary movement. This dynamic equation can be approximated by a discrete state-space equation given by

$$x(k+1) = Ax(k) + Bu(k+1) \tag{4.2}$$

where, k is the sampling step, $x(k+1) = \begin{bmatrix} P_f(k+1) \\ P_f(k) \end{bmatrix}$,

$A = \begin{bmatrix} (2M+T\zeta)/(M+T\zeta) & -M/(M+T\zeta) \\ 1 & 0 \end{bmatrix}$, $B = \begin{bmatrix} T^2/(M+T\zeta) \\ 0 \end{bmatrix}$, $u(k) = F(k)$

and T is the sampling time.

Given the updated position of the follower $P_f(k)$, the new position of the guider $P_g(k)$ can be easily calculated by imposing the constraint $\left\|P_f(k) - P_g(k)\right\| = L$, where L is the length of the hard rein. The guider's location was obtained by assuming the guider is always on the known desired path. Therefore, given a follower's position $P_f(k)$ the intersection of the desired path and the circle with center at $P_f(k)$ and radius L will give the guider's location.

4.2 Methodology

The experiment was conducted to study how to model the trust of the follower in different path tracking. Fourteen naive pairs of healthy subjects with age 23 - 29 years participated to the study after giving informed consent (see ethical approval in Appendix A). They were healthy and in the age group of 23 - 29 years. Fig. 4.1A shows how the guider and the follower held both ends of hard rein to track the different paths. The follower was blind-folded and cutoff from using auditory feedback. MTx motion sensors were attached to the follower's chest to measure the acceleration as shown in Fig. 4.1A. In addition to MTx motion sensors, ATI Mini40 6-axis force torque transducer was attached to the hard rein to measure tug force sampled at 1000Hz along the horizontal plane to guide the follower as shown in Fig. 4.1B. There were 10 trials each for three different paths shown in Fig. 4.1C.

Moreover, to study the trust from the human follower, a trust scale 1 to 10 ranging from lowest to highest was introduced before starting the experiments and subjects were asked to rate their trust to follow the guider after each trial. After each trial, subjects (follower) reported trust value orally.

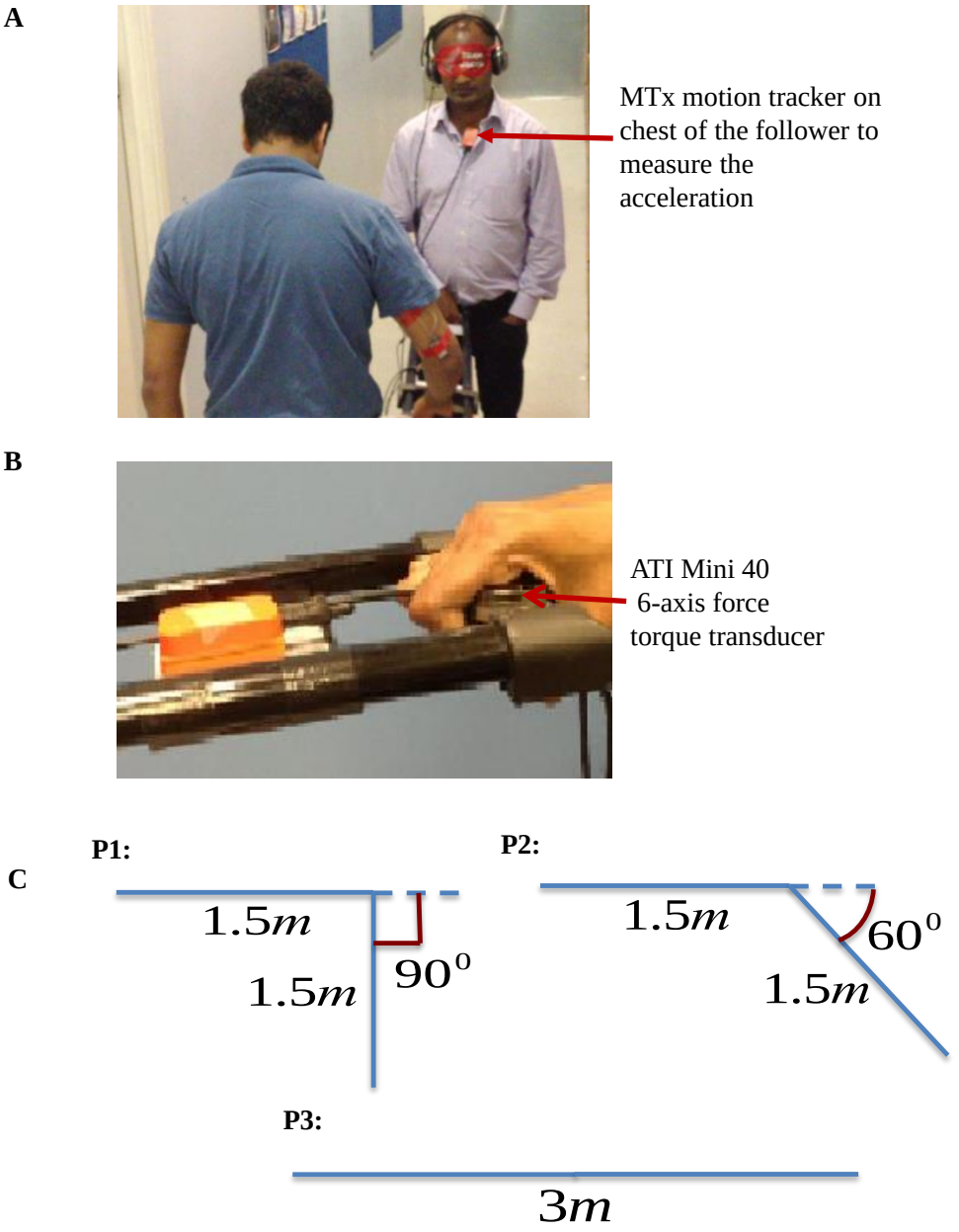

Fig. 4.1 The study of trust level of the follower in different paths: A) The guider and the follower in path tracking: The MTx motion tracker was attached on the follower's chest to track the motion data, B) ATI Mini40 6-axis force torque transducer at 1000Hz attached to the hard rein to measure pushing/pulling force, and C) The detail diagram of experimental layout of trust studies of following subject in three different paths: P1: Ninety degree turn, P2: Sixty degree turn, and P3: Straight path.

4.3 Results

4.3.1 The instantaneous trust level of the follower

The instantaneous trust level of the follower in the state-space was incorporated with the closed loop controller. The results of variability of voluntary movements of a blindfolded follower in a haptic based guidance scenario are shown in a virtual damped inertial dynamic system. The attempt is to address the question of how the follower's trust towards the guider should be accounted for in designing a closed loop controller. Here, the trust of the follower in any given context should be reflected in the compliance of his/her voluntary movements to follow the instructions of the guider. By modeling the impedance of the voluntary movement of the follower using a time varying virtual damped inertial system, the variability of the impedance parameters are observed - in virtual mass and damping coefficients - in paths with different complexities (paths).

The experimental results of 14 pairs of subjects in three types of paths - 90° turn, 60° turn, and a straight - are shown in Fig. 4.2. Here motion data are extracted within a window of 10 seconds around the 90° and 60° turns, and for fairness of comparison, the same window is taken for the straight path for our regression analysis to observe the virtual damping coefficient and the virtual mass in three different paths. Fig. 4.2A and Fig. 4.2B show the variability of the virtual damping coefficient and the virtual mass for the above three contexts respectively. The Fig. 4.2A shows that the variability of the virtual damping coefficient is highest in the path with a 90° turn, with relatively less variability in that with a 60° turn, and least variability in the straight path.

In Fig. 4.2A and in Fig. 4.2B, the average values of the virtual damping coefficient and the virtual mass distribution in straight path are lowest. This suggests that the trust level of the follower is greater in the straight path. Furthermore, Table 4.1 and Table 4.2 show the results of Mann Whitney U test ($\alpha = 0.05$) for different paths (90° turn, 60° turn,

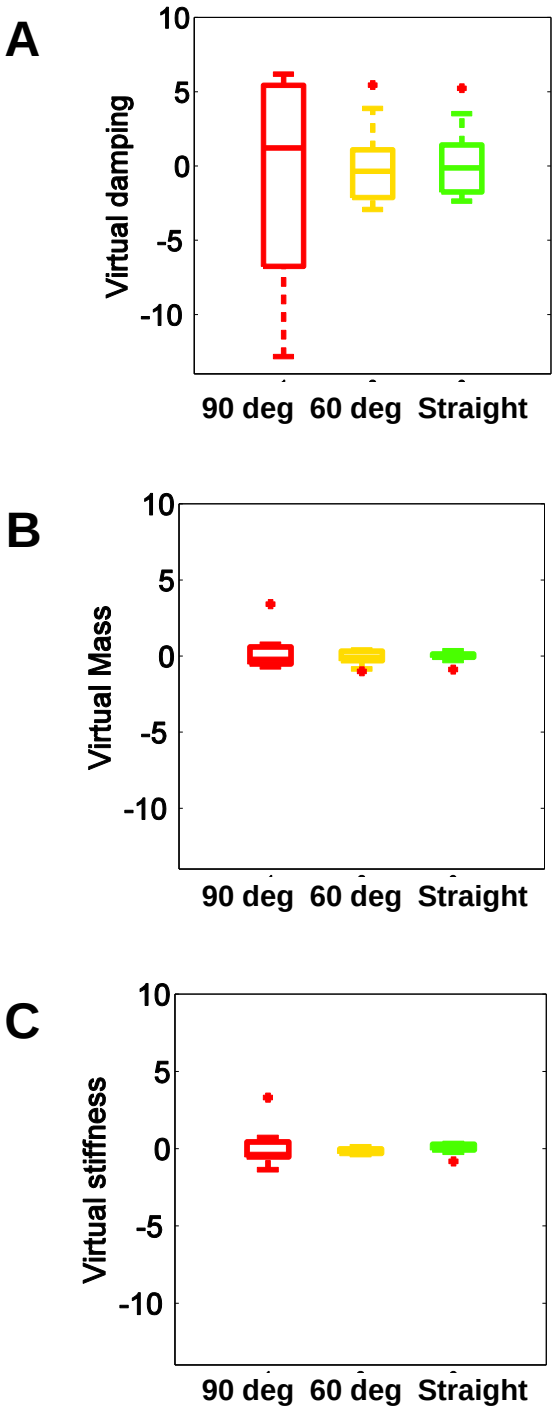

Fig. 4.2 The follower's trust in different context: Regression coefficients in Eq. 4.1 of different paths: A) Virtual damping coefficient for paths: 90° turn (red), 60° (yellow) turn, and straight path (green). The average values are 3.055, 1.605, and -0.586 for 90° turn, 60° turn, and straight path respectively, B) Virtual mass coefficient for paths: 90° turn (red), 60° turn (yellow), and straight path (green). The average values are 2.066, -0.083, and 0.002 for 90° turn, 60° turn, and straight path respectively, and C) Virtual stiffness coefficient for paths: 90° turn (red), 60° (yellow) turn, and straight path (green). The average values are 0.0325, -0.1385, and 0.0117 for 90° turn, 60° turn, and straight path respectively.

and straight path) of coefficients in Eq. 4.1 (Since the data are not normally distributed, non parametric Mann-Whitney U test was conducted). Results in Table 4.1 show that the virtual damping coefficient in 90° turn is significantly different from that in straight path ($p = 0.009$). Moreover, virtual damping coefficient in 60° turn is also significantly different from that in straight path ($p = 0.01$). There is no statistically significant difference between the virtual damping coefficient in path 90° turn and 60° turn ($p = 0.90$). Furthermore, the virtual mass distribution in Eq. 4.4 is shown in Fig. 4.2B. Interestingly, only straight path is statistically significantly different from 90° turn ($p = 0.006$). However, the Mann Whitney U test in between 60° turn and straight path is not significantly different ($p = 0.80$). This may come from the fact that the follower has more trust to follow the guider in a straight path than other two paths. Therefore, these results confirm that the follower's trust level is reflected in the time varying parameter of the virtual damped inertial system. The virtual damping coefficient presents itself to be more sensitive parameter to the level of trust than the virtual mass.

Table 4.1 Virtual damping coefficients. Statistical significance was computed using the Mann-Whitney U test

Paths	**Mean**	
90° turn	3.055	$p(90^0 turn \leftrightarrow 60^0 turn) > 0.6$,
60° turn	1.605	$p(60^0 turn \leftrightarrow Straight path) < 0.02^*$,
Straight path	-0.586	$p(90^0 turn \leftrightarrow Straight path) < 0.01^*$

When the follower voluntarily moves forward according to the small tug-signal of the guider, any increase of force felt by the guider must come from a reduction in the "voluntary" nature of follower's movement. Therefore, the follower was modeled as a virtual damped inertial model. To represent the variable "voluntary" nature of the follower, virtual stiffness is not considered. For that reason, the original location is irrelevant in a voluntary movements. However, the variability of virtual stiffness was tested by adding the stiffness to Eq. (4.1) as shown in Eq. (4.3) for clarity.

Then the Eq. (4.1) becomes

$$F(k) = M\ddot{P}_f(k) + \zeta\dot{P}_f(k) + \mathbf{k}P_f(k) \tag{4.3}$$

Table 4.2 Virtual mass coefficients. Statistical significance was computed using the Mann-Whitney U test

Paths	**Mean**	
90° turn	2.066	$p(90^0 turn \leftrightarrow 60^0 turn) > 0.8$,
60° turn	-0.083	$p(60^0 turn \leftrightarrow Straight path) > 0.7$,
Straight path	0.002	$p(90^0 turn \leftrightarrow Straight path) < 0.01^*$

Fig. 4.2C shows the variability of the virtual stiffness for 90° turn, 60° turn, and straight path. The variability of the mass and the stiffness are low as shown in Fig. 4.2B and Fig. 4.2C while variability of damping coefficient is high as shown in Fig. 4.2A. In Fig. 4.2A, in Fig. 4.2B, and in Fig. 4.2C the average values of the virtual damping coefficient, the virtual mass, and the virtual stiffness distribution in straight path are lowest. This shows that the trust level of the follower is greater in the straight path. Furthermore, Table 4.1, Table 4.2, and Table 4.3 show the results of Mann-Whitney U test for different paths (90° turn, 60° turn, straight path) of coefficients in Eq. (4.3).

However, the virtual stiffness is significantly different - 90° to straight ($p = 0.002$), 90° turn and 60° turn ($p = 0.004$), and 60° turn and straight ($p = 0.001$) - three paths. Even though the virtual stiffness is significantly different for three defined paths the variability is very low. However, the variability of virtual damping coefficient is higher than virtual mass and stiffness. Therefore, these results confirm that the follower's trust level is reflected in the time varying parameter of the virtual damped inertial system. It is noted that the virtual damping coefficient presents itself to be more sensitive parameter to the level of trust than the virtual mass or stiffness.

The results confirm that, the virtual damping coefficient can be a good indicator to control the push/pull behavior of an intelligent guider using a feedback controller of the form

Table 4.3 Virtual stiffness coefficients. Statistical significance was computed using the Mann-Whitney U test

Paths	**Mean**	
90° turn	0.0325	$p(90^0 turn \leftrightarrow 60^0 turn) < 0.05^*$,
60° turn	-0.1385	$p(60^0 turn \leftrightarrow Straight path) < 0.05^*$,
Straight path	0.0117	$p(90^0 turn \leftrightarrow Straight path) < 0.05^*$

given in Eq. 4.4, where F(k) is the pushing/pulling tug force along the rein from the human guider at k^{th} sampling step, M is the time varying virtual mass, M_0 is its desired value, ζ is the time varying virtual damping coefficient, k is the sampling step, and ζ_0 is its desired value.

$$F(k+1) = F(k) - (M - M_0)\ddot{P}_f(k) - (\zeta - \zeta_0)\dot{P}_f(k) \tag{4.4}$$

Human participants consistently confirmed that their trust level to follow the guider

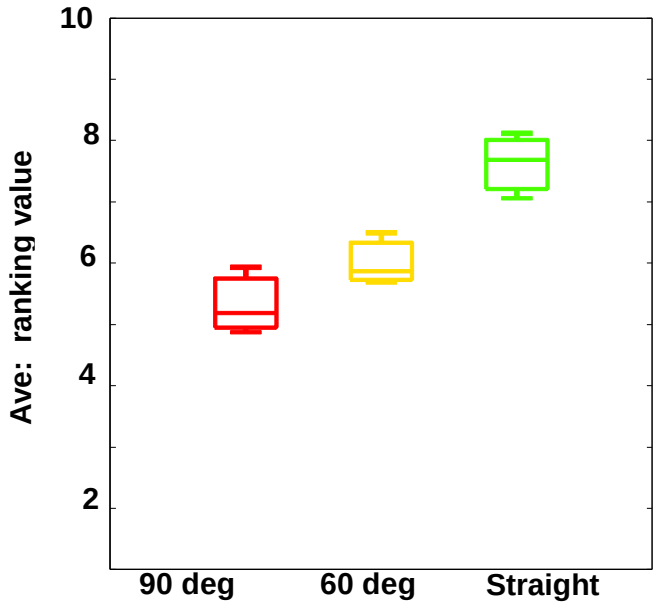

Fig. 4.3 The follower's trust in different context: The trust scale varies from 1 to 10 from the lowest to the highest. The average response value across straight, 60°, turn and 90° turn are shown with variability.

dropped from the straight path to that with a 60° turn, to that with a 90° turn. Moreover, the follower's response towards the defined trust scale is presented in Fig. 4.3, where the average trust scale values across all the subjects for straight, 60° turn, and 90° turn are shown. The variability of 90° turn is higher than the 60° turn and straight paths as shown in Fig. 4.3. For further clarity, the significance was computed by Mann-Whitney U test as shown in Fig. 4.3. The significance between straight and 90° turn ($p = 0.01$) and straight and 60° turn ($p = 0.03$) are significantly different . The follower's response after each trial confirms that the follower is more confident to follow the guider in straight path than 90° turn and 60° turn.

Moreover, followers' trust ranking over the trials are shown in Fig.4.4. Fig.4.4 shows that followers' rank is increases over trials. However, on average subjects gave higher ranking value for straight path, and lowest in 90° turn.

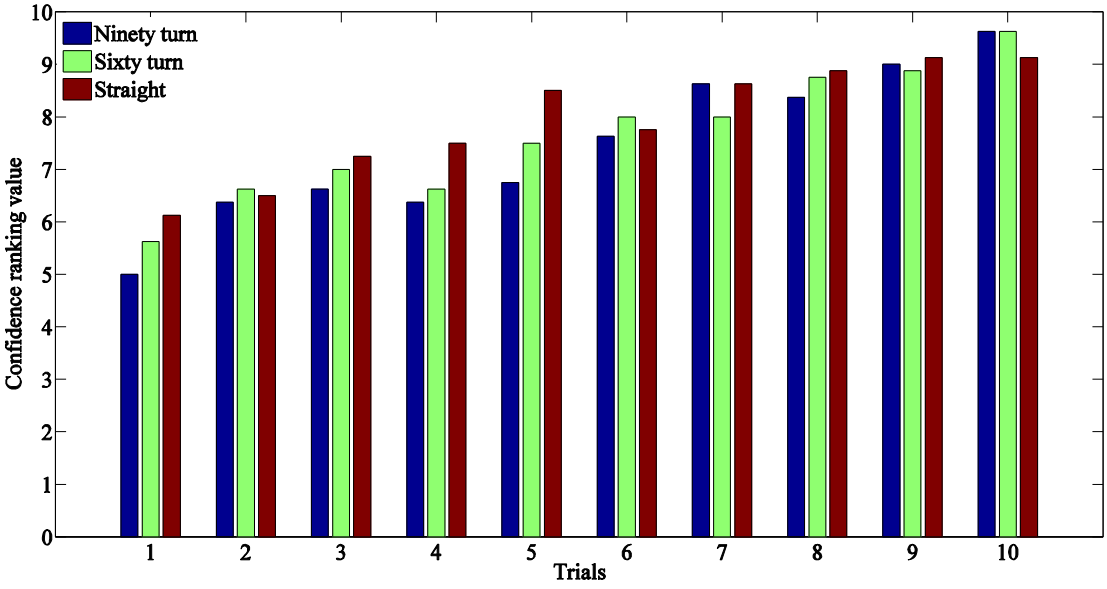

Fig. 4.4 Average ranking over the trials: Subject's ranking values distribution over the trials for straight path, 60° turn, and 90° turn.

4.3.2 Developing a closed loop path tracking controller incorporating the follower's trust level

The guider's 3rd order predictive policy in Eq. 3.5 in Chapter 3 is combined to control the swing movement of the hard rein, with the tug force modulation rule in Eq. 4.4 to form a controller that accounts for the state of the follower that indicates his/her trust level.

The last 10 trials coefficients values are used as marked on Fig. 3.10 and Fig. 3.11 by red dashed line to calculate the statistical features of the regression coefficients in order to make sure the model reflects the behavior of the human participants at a mature learning stage in model order selection experiments on human demonstrations in Chapter 3. The model parameters were then found to be: $a_0 = N(-1.9216, 0.2590^2)$, $a_1 = N(2.0125, 0.4735^2)$, $a_2 = N(2.0125, 0.4735^2)$, and $c = N(-0.7429, 0.2416^2)$.

In order to ascertain whether the control policy obtained by this systems identification process is stable for an arbitrarily different scenario, numerical simulation is conducted to study forming a closed loop dynamic control system of the guider and the follower using the control policy given in Eq. 3.5 together with the discrete state space equation of the follower dynamics given in Eq. 4.2.

To understand the variability of the virtual model parameters based on the model, the virtual mass $M = 15$[kg] from $t = 2$s to $t = 3$s and the virtual damping coefficient $\zeta = 6$[Nsec/m] from $t = 6$s to $t = 7$s are set to observe tug force variation in Eq. 4.2 as shown in Fig. 4.5. The length of the hard rein is $L = 0.7$m. The tug force variation in Fig. 4.5 shows that the virtual damping coefficient more influenced to vary the tug force than the virtual mass. The results again suggest that virtual model parameter would be used to indicate the trust of the follower.

By modeling the impedance of the follower as a virtual damped inertial system, variability was considered of the follower's impedance parameters (the virtual mass and damping

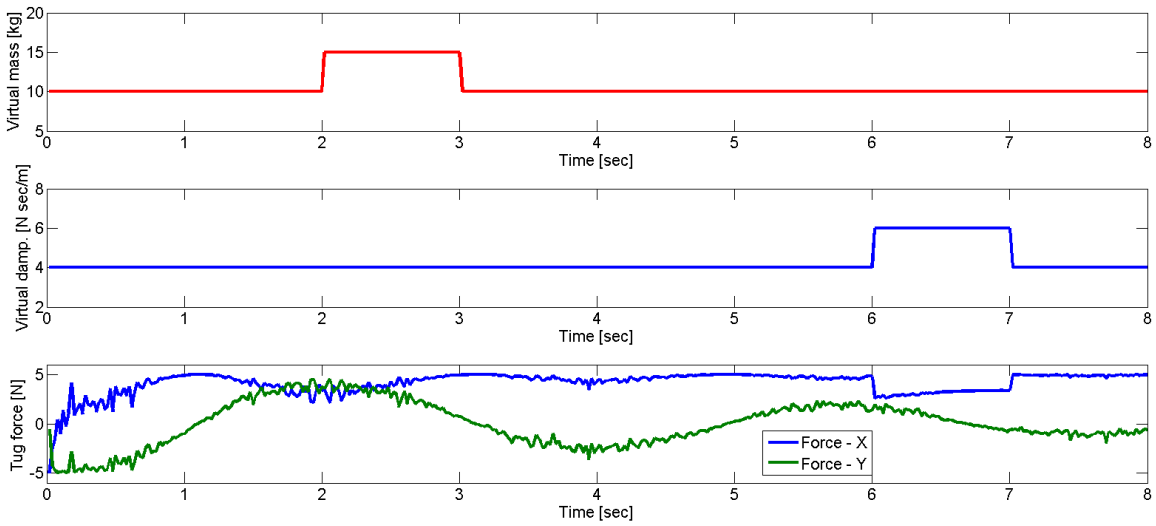

Fig. 4.5 Simulation results: The tug force variation of the follower in order to sudden change of the virtual mass $M = 15$[kg] from $t = 2$s to $t = 3$s and the virtual damping coefficient $\zeta = 6$[Nsec/m] from $t = 6$s to $t = 7$s.

coefficients) at different turn angles. From the three types of paths are shown Fig. 4.2, the blindfolded subjects who played the role of the follower confirmed that their trust in following the guider was highest in the straight path and it dropped in the other paths so that the trust was medium in the path with a 60° turn, and least in that with a 90° turn. The results of virtual impedance parameters in Eq. 4.4 are shown in Fig. 4.2A and Fig. 4.2B. The experimental results of human subjects also show that the variability of the virtual damping coefficients correlates more with the complexity of the path in Fig. 4.2 - reflecting the trust level of the follower - than that of the virtual mass coefficient. Fig. 4.2A and Fig. 4.2B show that the higher trust of the follower in the straight path results in a lower average value of the virtual damping coefficient. When the follower drops his trust in 90° turn and 60° turn, the guider has to exert a higher tug force to take following agent into desired trajectory that leads to higher average values for the virtual mass and virtual damping coefficient.

Moreover, the experimental average trust scale test results in Fig. 4.3 suggest that the follower's trust drop in 90° turn and 60° turn.

4.4 Discussion

Previous studies on human trust on a helping agent have shown that humans tend to depend entirely on the helping agent when they are in hazardous environments [10] until sudden a change occurs [96]. This implies that the degree of compliance in a follower should drop if the follower loses trust in the helping agent. By modeling the impedance of a follower as a virtual damped inertial system, variability of the follower's impedance parameters (the virtual mass and damping coefficients) was considered at different turn angles. From the three types of paths, the blindfolded participants who played the role of the follower confirmed that their trust in following the guider was highest in the straight path and it dropped in the other paths so that the trust was medium in the path with a 60° turn, and least in that with a 90° turn. The experimental results of human participants also show that the variability of the virtual damping coefficients correlates more with the complexity of the path in Fig. 4.2 - reflecting the trust level of the follower - than that of the virtual mass coefficient or the virtual stiffness. Fig. 4.2 shows that the higher trust of the follower in the straight path results in a lower average value of the virtual damping coefficient. When the follower drops his trust in 90° turn and 60° turn, the guider has to exert a higher tug force to take following agent into desired trajectory that leads to higher average values for the virtual mass and virtual damping coefficient.

Experimental results from human-human demonstrations provides useful design guidelines to human-robot interaction that should account for the real-time trust level of the human counterpart. In a human-robot interaction like in indoor fire-fighter being guided by a robot through thick smoke, the estimate of the followers' trust using the above method could be used to change acceleration/deceleration of the intelligent agent.

CHAPTER 5

HUMAN INTERACTION WITH THE GUIDER'S CONTROL POLICY IMPLEMENTED IN A ROBOT

Abstract

This chapter describes studies on human-robot interactions when the control policy identified from human guiders was implemented on a planar 1-DoF robotic arm to perturb the blindfolded subjects' most dominant arm to guide them to a desired position in leftward/rightward directions. The chapter discusses how the robot and humans behave in leftward/rightward movements when robot interacts with naive and trained subjects. Furthermore, the human's arm muscle contribution immediately after the arm perturbation from leftward/rightward directions and stability of the controller are presented. The results show that even though robot's behavior is not significantly different in leftward/rightward movements when it interacts with naive/trained subjects, naive subjects behave differently in leftward/rightward movements. Moreover, it was observed that naive subjects elicit a 2^{nd} order reactive behavior similar to human participants in the experiments in Chapter 3. However, trained subjects developed a 2^{nd} order predictive following behavior.

5.1 Introduction

The human brain has the remarkable ability to use a reduced number of sensory modalities to accomplish tasks that they used to do without any sensor deprivation as well as the ability to derive complex perceptions by combining different sensory modalities [1]. For instance, in the case of indoor fire-fighting, fire-fighters move inside the buildings under low visibility conditions using only haptic sensation. In such cases, a knowledge about the modified behavioral characteristics due to reduced sensory modalities will help to design external assistive agents like robots to optimally assist human movements.

It is important to study how robot's behavior depends on human's behavior and vice versa in human-robot interactions. Therefore, robot's behavior in leftward/rightward arm commands and human's behavior in leftward/rightward movements are presented when human's arm is perturbed by planar 1-DoF robotic arm to bring human into a desired angular position. In this scenario, humans' behavioral metrics such as rise time (RT), best fit model order of the polynomial fitted to the instantaneous error of the human's position for a given desired angle (N), steady state variability (SSV), and steady state error (SSE) are presented to discuss the human's interaction behavior with robot. Moreover, robot's action command distribution in leftward/rightward directions is presented to understand robot's behavior in leftward/rightward arm actions in human-robot interactions. Human-robot interaction experiments were conducted with naive/trained subjects to test any difference in the behavior in robot and human in moving leftward/rightward directions. Furthermore, humans' spontaneous arm muscle response immediately after the arm perturbation is analyzed to understand arm muscles' activation when the arm is perturbed from leftward/rightward directions. Moreover, the stability of the implemented controller is discussed.

For more clarity, the summary of the carried experiments in human-robot interaction experiments is shown in Fig. 5.1.

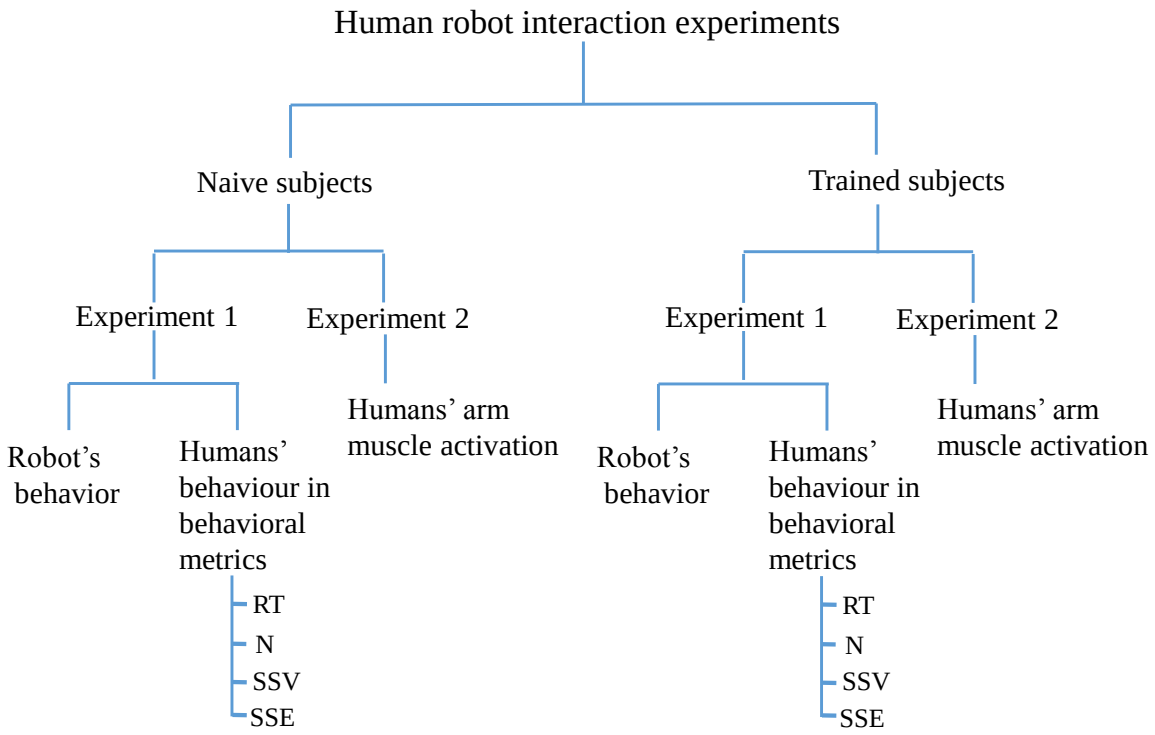

Fig. 5.1 The summary of the human-robot interaction experiments. The same experiments were carried out with naive and trained subjects to study robot's behavior, human's behavior, and human's muscle activation. Experiment 1 is to test the human's and the robot's behavior. Experiment 2 is to test human's arm muscle activation. RT, N, SSV, and SSE were taken as behavioral metrics of the humans.

5.1.1 The objectives addressed by human-robot interaction experiments

1. To understand the influence of guiding direction (leftward/rightward) and training of the followers in the four behavioral metrics shown in Fig. 5.1.

2. What would be the model order of following and its reactive/predictive nature of naive/trained subjects.

3. To understand the differences in spontaneous muscle recruitment in responses to leftward/rightward perturbations given by the robot. This is important because perception of the guiding command given by the robot depends on how proprioceptive sensors in the muscles are perturbed.

4. Whether the implemented closed loop guider's control policy is stable or not.

5.2 Materials and Methods

Human-human demonstration experiments in Fig. 5.2A were replicated by human-robot interaction experiments as shown in Fig. 5.2B. This chapter presents two experiments. Experiment 1 was designed to study how humans' behavior depends on robot behavior and vice versa when the humans' most dominant arm is perturbed from leftward/rightward directions. The model order and the reactive/predictive nature of the naive/trained subjects are also presented. Moreover, the stability of the implemented controller is discussed. Experiment 2 was designed to study the arm muscle recruitment immediately after given a single tug from leftward/rightward directions. Both Experiment 1 and Experiment 2 were conducted with naive and trained subjects.

5.2.1 Experimental setup

The schematic diagram of replication of human-human experiments in Fig. 5.2A was replicated by human-robot experiments as shown in Fig. 5.2B. In Fig. 5.2B, the angle (ϕ) is the error of following (The angle of the line connecting from motor axis to the human's position and the desired position), the angle (θ) is the robotic arm's swing angle on the horizontal plane. Moreover, the replicated experimental setup is shown in Fig. 5.3. In Fig. 5.3, the guider's arm was replaced by planar 1-DoF robotic arm to generate the swing arm action in horizontal plane. The cord was attached to the waist belt of the blindfolded subjects and the encoder on the shaft platform to measure the relative error between the human and the motor shaft (ϕ). The planar 1-DoF robotic arm was actuated by a motor. The motor shaft was driven by a Maxon EC 60 (ϕ) mm brush less 400 Watt with Hall sensors motor. An EPOS2 50/5 digital position controller was used to control the motor. Here, NI LabVIEW

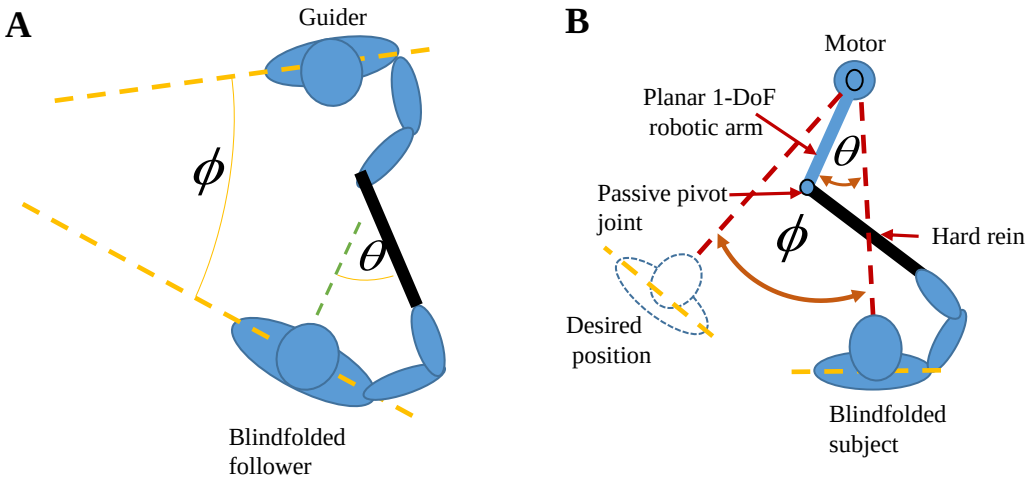

Fig. 5.2 Replicating human-human demonstration experiments by human-robot interaction: A) Human-human demonstration experiment set up, B) The schematic diagram of human-robot interaction experiments: The guider's arm is replicated by a planar 1-DoF robotic arm. The hard rein is connected via a passive joint to the robotic arm. Blindfolded subject hold the other end of the rein. The angle (ϕ) is the error of following (The angle of the line connecting from motor axis to the human's position and the desired position.), the angle (θ) is the robotic arm's swing angle on the horizontal plane.

2009 was used for programming and communicating with other hardware devices to control the robotic arm. The joint between the robotic arm and the hard rein was made as a passive joint. The other end of the hard rein was held by the human follower as shown in Fig. 5.3.

For more clarity, more detailed diagram of closed loop human-robot interaction experiments is shown in Fig. 5.4. Here, the human's movement error (ϕ) was fed the guider's control policy derived from human demonstration experiments in equation 3.2 to calculate the robot's next arm action (θ).

5.2.2 Subject's training phase

Experiments 1 and 2 were repeated after training to compare any difference in naive and trained subjects' behavior. In the training phase, the subjects were trained to give an idea how to move proportional to the perturbed tug force. The subjects move from the initial position (home) to the desired positions A, B, C, D, E, and F for the desired angles $+10^{\circ}$,

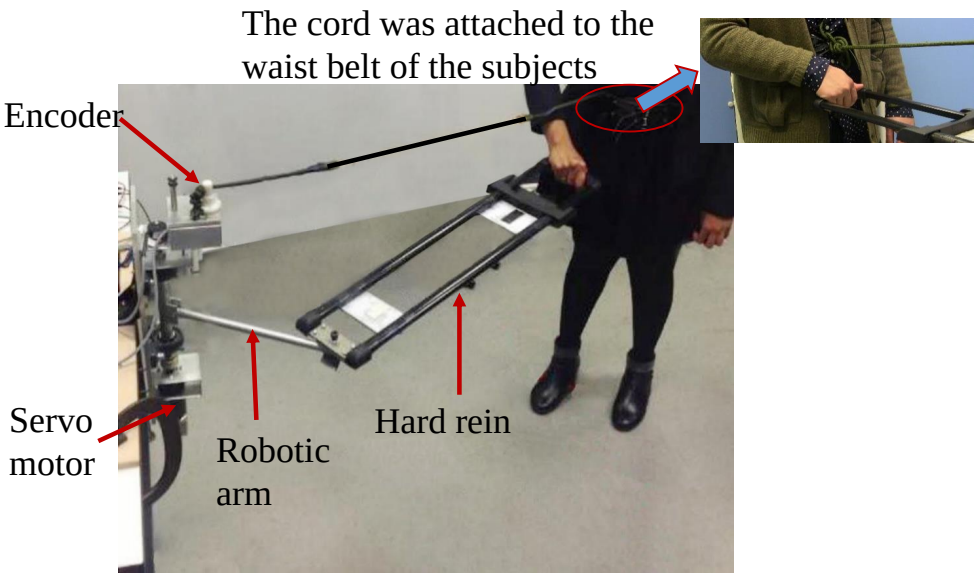

Fig. 5.3 Experimental set up: The cord was attached to the waist belt of the blindfolded subjects and the encoder on the shaft platform to measure the relative error between the human and the motor shaft (ϕ).

$+20°$, $+30°$, $-10°$, $-20°$, and $-30°$ as shown in Fig. 5.5. Here, the subject's most dominant arm was perturbed by a single tug force. For each desired angle in training phase, the subjects performed 5 trials.

5.2.3 Experiment 1: Study the human's and robot's behavior in human-robot interaction

The Experiment 1 was conducted to study the human's and robot's behavior in human-robot interaction. Humans' behavior were studied in behavioral metrics in transient and steady state such as RT, N, SSV, and SSE. These results would give an idea as to how humans' behavior depends on the robot arm actions and how the robot's arm action depends on human movements when the same controller is used to generate the tug perturbation from leftward/rightward directions. Moreover, humans' model order and reactive/predictive nature of following in human-robot interaction are presented. Furthermore, stability of the controller is presented. Experiment 1 was conducted with naive/trained subjects.

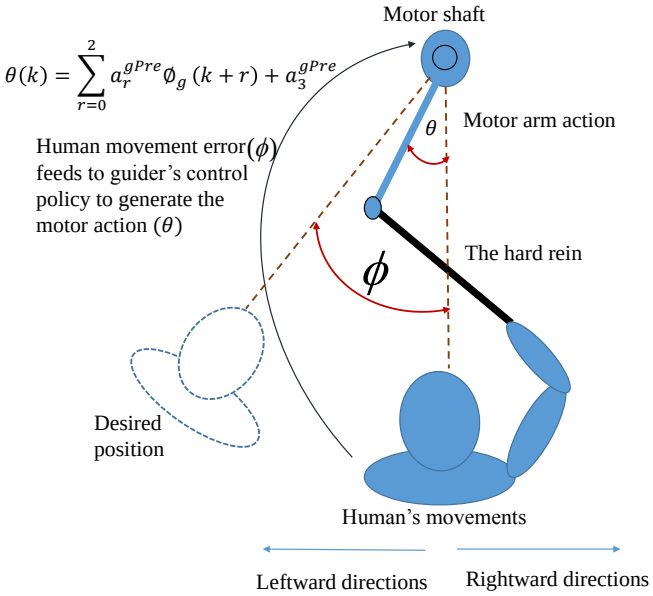

Fig. 5.4 Human-robot interactions: Human's movements angle (ϕ) was fed to calculate the robot's next arm action (θ) in horizontal plane by using guider's third order predictive control policy derived from human demonstration experiments.

5.2.3.1 Experimental protocol

In the first experiment, the subjects were given the Oldfield 1971 handedness questionnaire [97] to avoid adding ambidextrous in to the analysis. Eight (4-male, 4-female) naive and 12 (7-male, 5-female) trained right-handed subjects participated in the experiment after giving informed consent (please refer annex 1). They were healthy and in the age group of 21 - 30 years. Visual feedback to the subject was cut off by blindfolding, while the auditory feedback was cut off by playing a sound track of less than 70 dB (For example noise in a cocktail party).

5.2.3.2 Experimental procedure

In any given trial, the blindfolded subjects started to move from their home position. The subjects were instructed to move proportionally to the signal direction of the perturbation. In addition to that, they were asked not to manipulate any force. When the subjects perceived

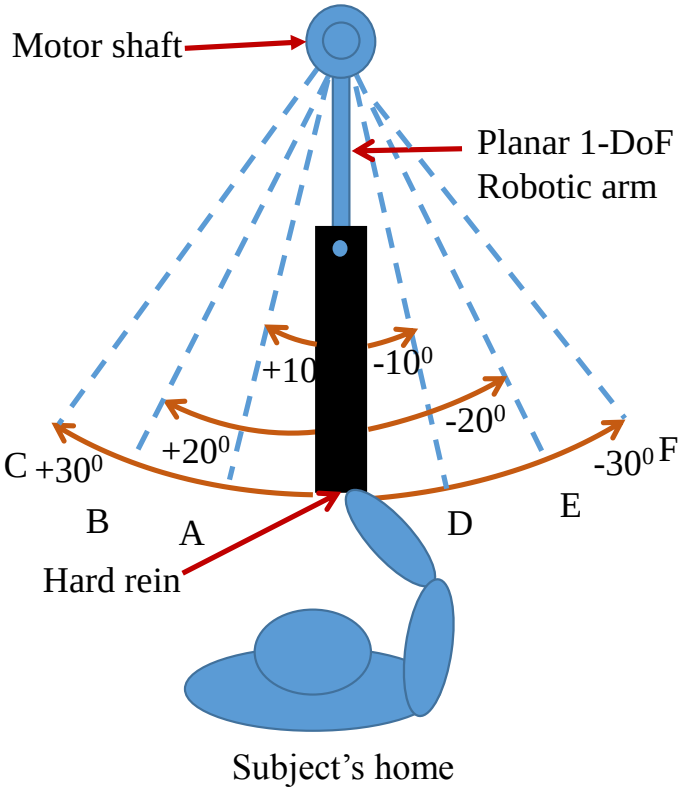

Fig. 5.5 Subject's training phase: Blindfolded subjects move from the initial position (home) to the desired positions A, B, C, D, E, and F for the desired angles $+10°, +20°, +30°, -10°, -20°$,and$-30°$.

the tug perturbation, they were asked to make a voluntary movement in the direction of the perturbation. The generated tug was used to perturb the subject's most dominant arm in three magnitudes in right ($-25°$, $-45°$, and $-65°$) and left ($+25°$, $+45°$, and $+65°$) directions from the subject's home.

Once the trial was started, the encoder mounted on top of the motor shaft axis as shown in Fig. 5.3 read instantaneous error of the blindfolded subject's position relation to the desired angle (ϕ). The closed loop the guider's control policy in equation 3.2 computed a desired tug force (θ) in real time as shown in Fig. 5.4. The mechanism of the planar 1-DoF robotic arm is to generate discrete tugs. Withing a single trial (90s time interval), 23 tugs were generated. Subjects continuously moved as long as they felt the tug perturbation towards the target angular position. The current tug force is not considered to generate the

next tug perturbation. The subjects' current position is only considered to generate next tug perturbation. The encoder is attached to the wrist belt of the subject as shown in Fig. 5.3 to measure the subjects' current angular displacement. Then the encoder reading feeds to the equation 3.2 to compute the next tug perturbation. For a given desired angle, same trial was repeated three times. As a result, each subject performed eighteen trials during the experiment. Subjects were given a five minutes break after every six trials to minimize fatigue.

5.2.4 Experiment 2: Study humans' arm muscle spontaneous responses immediately after the arm's perturbation

The Experiment 2 was conducted to study humans' arm muscle responses when the human's arm is perturbed from leftward/rightward directions. For simplicity, -45° and $+45^{\circ}$ were taken as the desired angular positions and the subject's most dominant arm was perturbed by a single tug perturbation to study arm muscles recruitment immediately after the arm perturbation. Five trials were recorded for each desired angles. Five naive subjects (2-male, 3-female) and ten (6-male, 4-female) trained subjects participated the experiments.

Surface EMGs were recorded by using the EMG (Noraxon, USA) sensors from the following muscles of the blindfolded subject's most dominant arm: Anterior Deltoid(AD), Posterior Deltoid (PD), Biceps (Bc), Median Triceps (MT), Brachioradialis (Br), Flexor Carpi Radialis (FCR), Extensor Carpi Ulnaris (ECU), and Extensor Carpi Radialis (ECR). Before attaching EMG electrodes, the skin was cleaned with alcohol. The electrodes were 2 mm in diameter and 12 mm apart. EMG records were carefully monitored for stimulus artifacts, noise, and cross-talk by firmly attaching to the skin using double-sided adhesive tape.

5.3 Results

It is important to understand robot's and human's behaviors when human's arm is perturbed in leftward/rightward directions to bring them to desired angular positions in human-robot interactions. Therefore, results on robot's interaction with naive and trained subjects are presented. Moreover, naive/trained subjects' muscle activation immediately after the perturbed arm and the stability of the implemented controller are discussed.

5.3.1 Naive subjects-robot interactions

First, interactions between robot-naive subjects are described. Since the human-robot interaction is a closed loop as shown in Fig. 5.4, a two-way ANOVA ($\alpha = 0.05$) analysis was conducted to test how actions of human and robot depend on variables such as direction of robot and human. The first 20% of raw data (transient state) were considered. The results show that human's action depends on robot's direction ($F(1,30) = 11.89$, $p = 0.001$) and human's direction ($F(1,30) = 132.26$, $p = 0$). The ANOVA test results confirm that human's and robot's actions depend on each other when robot interacts with naive subjects.

Behaviors, perceptions, and symmetry/asymmetry would give an idea as to how robot and human interact in guiding. Therefore, human's and robot's behaviors are presented to understand the interaction, perception, and symmetry/asymmetry in moving leftward/rightward directions when robot interacts with naive subjects.

5.3.1.1 Naive subjects' behavior

The naive subjects' behavioral metrics such RT, N, SSV, and SSE are presented to understand how they behave when the arm is perturbed from leftward/rightward directions.

Transient response behavioral metrics, RT and N are shown in Fig. 5.6. The RT was calculated for six desired angles (-65°, -45°, -25°, $+25^\circ$, $+45^\circ$, and $+65^\circ$). In this

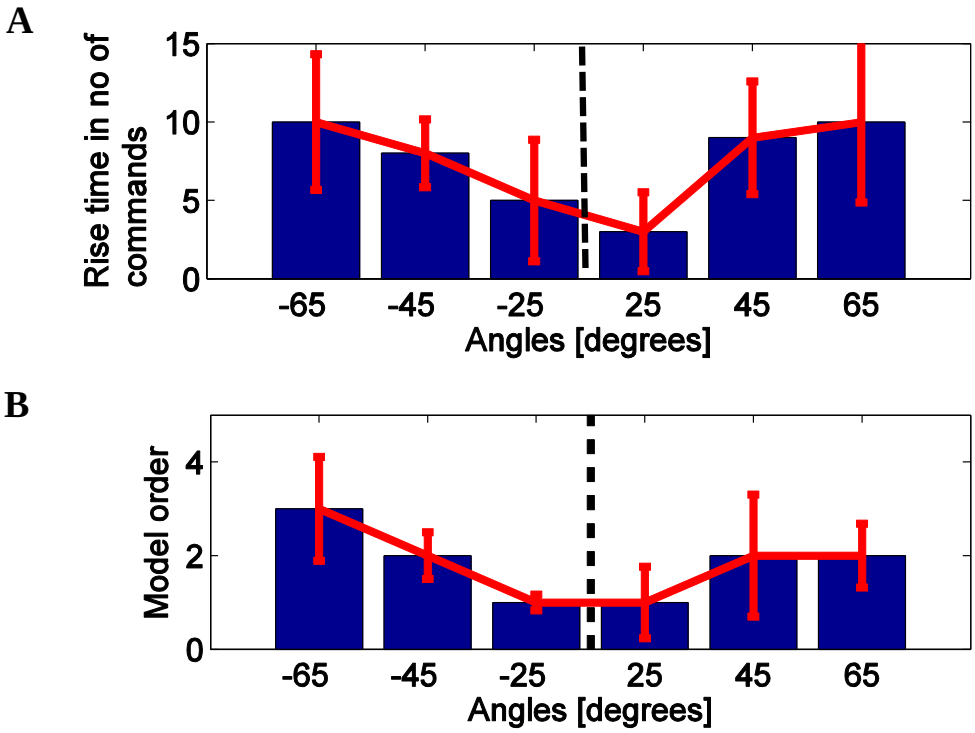

Fig. 5.6 The behavioral metrics for naive subjects in transient response: A) Rise time (RT): Average rise time distribution across the naive subjects in number of commands for reaching desired angles $-65°$, $-45°$, $-25°$, $+25°$, $+45°$, and $+65°$, and B) Model order (N): Average model order distribution for naive subjects for reaching six desired angles.

regard, the RT is considered as measured number of commands to reach from 10% to 90% of the desired angles. The results of rise time for reaching different desired angles are shown in Fig. 5.6A. The standard error across all subjects are shown by an error bar. Here, the average value is taken of last 5 recordings as a final value to calculate the rise time. Moreover, the order of the best fit polynomial gives an idea of the transient response of the controller. Here, Akaike Information Criterion (AIC) is used to find the best fit order of the polynomials [98]. To understand the optimal order of the polynomial, the average model order across the all subjects is shown in Fig. 5.6B for reaching six desired angles.

Moreover, behavioral metrics in Fig. 5.6 was used to test whether any significance difference in moving leftward/rightward directions in RT, and N as shown in Table 5.1. The Mann-Whitney U test ($\alpha = 0.05$) was conducted to test the significance. Asymmetry is

noticed in N in moving leftward/rightward when the desired angle is 45°.

Table 5.1 The significance test results in behavioral metrics for naive subjects in transient responses

Desired angular position in leftward/rightward directions	25°	45°	65°
RT	$p = 0.99$	$p = 0.11$	$p = 0.29$
N	$p = 0.80$	$p = 0.04^*$	$p = 0.40$

Next, steady state variability (SSV), and steady state error (SSE) are presented to understand naive subjects' behaviors in steady state in reaching six desired angles in leftward/rightward directions.

It would be interesting to test how the subjects can understand the arm perturbation given by the robotic arm to settle down at the desired target point. Therefore, the last 10% of experimental recordings of the instantaneous error of the subject's position relative to the desired angle/target point (ϕ) is taken for steady state analysis. Fig. 5.7A shows the distribution of the average steady state response across all subjects in reaching six desired angles. Moreover, for a stable controller, steady responses as close as possible to the desired angular position is essential. Therefore, steady state error is presented in reaching six desired angular positions in leftward/rightward directions as shown in Fig. 5.7B.

Again, behavioral metrics in Fig. 5.7 were used to test whether there is any significance in moving leftward/rightward directions in SSV, and SSE in naive subjects as shown in Table 5.2. Asymmetry is again noticed in SSV in moving leftward/rightward when the desired angles are 45°, and 65° as shown in Table 5.2. Here again significance was tested by Mann-Whitney U test ($\alpha = 0.05$).

It would be interesting to test the human followers' predictive/reactive nature and the model order during the following as observed in human demonstration experiments in Chapter 3. Following the same method described in Chapter 3, it was found that on average naive subjects give more emphasis on a 2^{nd} order reactive model as noticed in follower's behav-

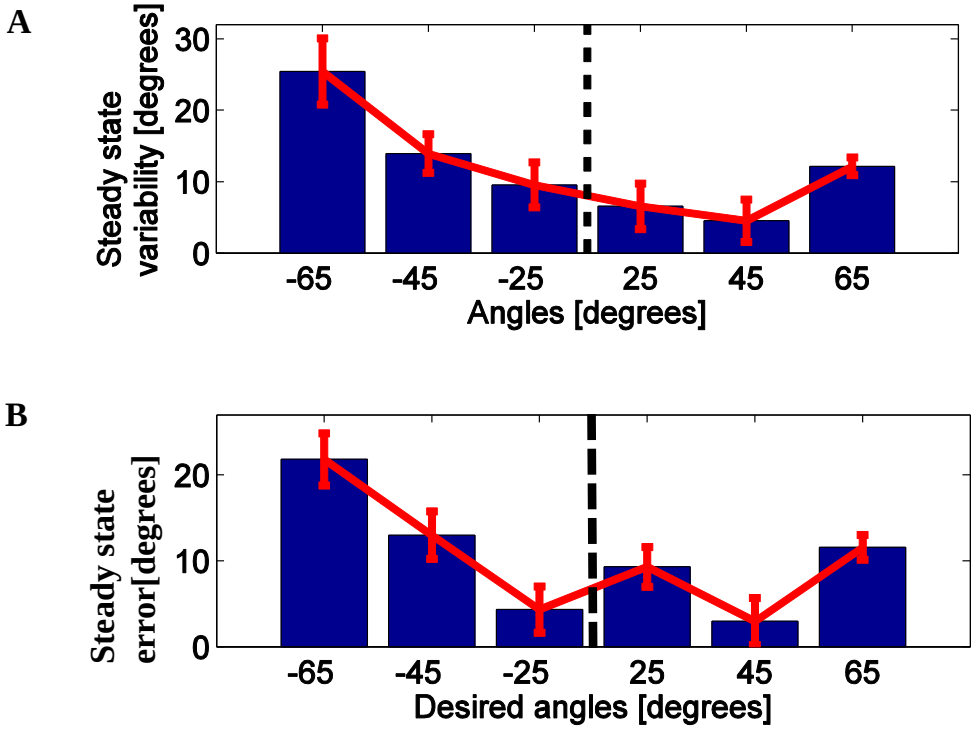

Fig. 5.7 The behavioral metrics in steady state for naive subjects: A) Steady state variability (SSV): Average steady state variability for reaching six desired angles $-65°$, $-45°$, $-25°$, $+25°$, $+45°$, and $+65°$, and B) Steady state error (SSE): Average steady state error distribution across the naive subjects for reaching the six desired angles.

Table 5.2 The significance test results in behavioral metrics for naive subjects in steady state responses

Desired angular position in leftward/rightward directions	$25°$	$45°$	$65°$
SSV	$p = 0.79$	$p = 0.01^*$	$p = 0.03^*$
SSE	$p = 0.58$	$p = 0.24$	$p = 0.48$

iors in human demonstration experiments in Chapter 3 (Note that only transient data were taken for the analysis).

5.3.2 Possible causes of asymmetry in naive subjects' behavioral metrics

5.3.2.1 Robot's behavior

An asymmetry was noticed in the behavioral metrics of naive subjects'- N in transient and SSV in steady state responses. Naive subject's action depends on motor direction as noticed in ANOVA test results. However, the asymmetry in behavioral metrics in Table 5.1 and Table 5.2 might come from the behavior of the robot in generating perturbation force in leftward/rightward directions differently. To test that, robot behavior in generation action perturbation in leftward and rightward directions is presented in Fig. 5.8A and Fig. 5.8B respectively. To test whether there is any significance difference generating tug perturbation from leftward/rightward directions, Here also Mann-Whitney U test ($\alpha = 0.05$) was conducted between Fig. 5.8A and Fig. 5.8B. It was found that leftward/rightward robotic arm actions are not significantly different ($p = 0.112$). This confirms that robot's arm actions are not significantly different in leftward/rightward directions.

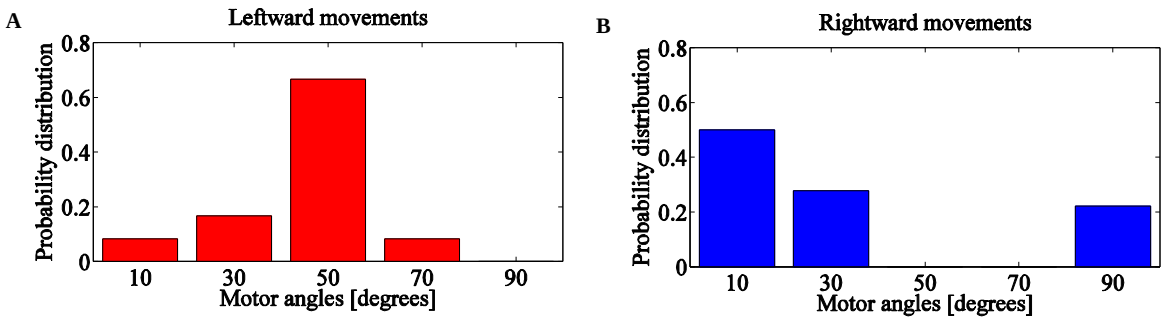

Fig. 5.8 Robot's behavior in leftward/rightward directions: A) The probability distribution in robot's leftward movements, and B) The probability distribution in robot's rightward movements.

The naive subjects' behavior metrics show asymmetry in leftward/rightward movements in some behavioral metrics in transient and steady state as shown in Table 5.1 and Table 5.2 respectively. However, when the robot interacts with naive subjects, the robot's arm action in

leftward/rightward directions are not significantly different. The significance in behavioral metrics might come from the way naive subjects perceive the arm perturbation. Therefore, spontaneous muscle response of naive subjects immediately after the arm perturbation is presented.

5.3.2.2 Naive subjects' spontaneous muscle response

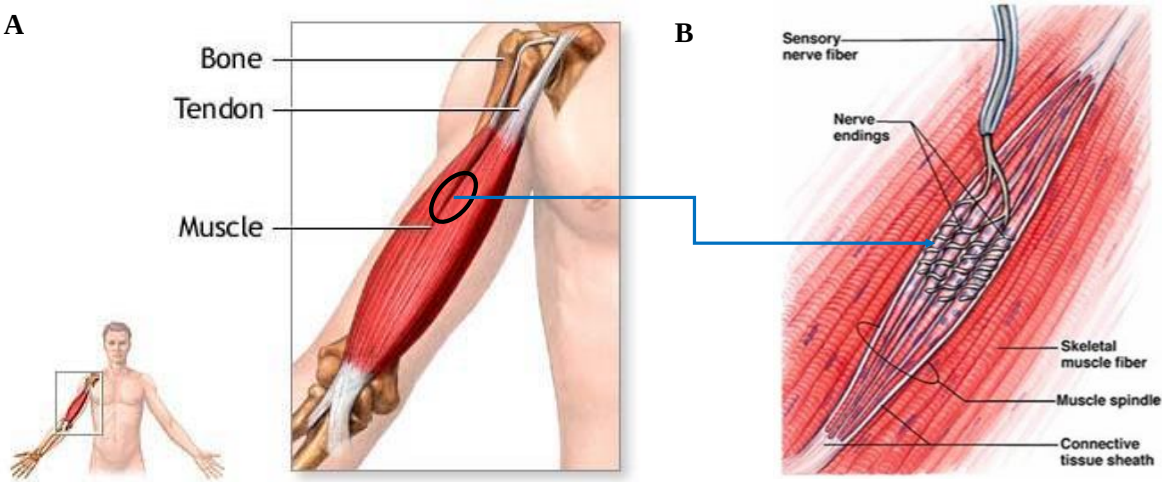

Fig. 5.9 Arm muscle anatomy: A) The muscle is connected to the bond via tendon, and B) Muscle spindle is embedded with muscle fibers. Adapted by [99], [100].

Proprioceptors are the sensors that provide information about joint angle, muscle length and muscle tension. Proprioceptive sensor stimulation in the muscles depends on how muscles are spontaneously recruited in response to leftward/rightward perturbations. In Fig.5.9 shows how proprioceptive sensor is embedded in the muscle. Moreover, in Fig.5.9A shows how a muscle is connected to the bone via tendon. A tendon is a tough band of fibrous connective tissues that connects muscle to bone [101]. Muscle spindles are embedded with muscle fibers as shown in Fig.5.9B. They are sensory receptors that preliminary detects changes in the length of the muscles.

When the arm is perturbed the muscle lengthens and muscle spindle is stretched. This contraction in muscle tension provides different degrees of pull on the tendon. Therefore,

arm muscles' spontaneous responses was tested in EMG in Experiment 2 immediately after the arm perturbation. Note that, in Experiment 2, the naive subject's most dominant arm was perturbed by a single tug to test the muscle recruitment immediately after the given tug for reaching $+45^{\circ}$ and -45° as shown in Fig. 5.10A.

EMG is a non-invasive method to quantify the relationship between a specific movement and the activation of the underlying muscle groups [102]. Therefore, the EMG signals in arm flexion/extension were studied in moving leftward/rightward directions as shown in Fig. 5.10A. Fig. 5.10B shows the average normalized rectified raw EMG recording across the arm muscles of Anterior Deltoid (AD), Posterior Deltoid (PD), Biceps (Bc), Median Triceps (MT), Brachioradialis (Br), Flexor Carpi Radialis (FCR), Extensor Carpi Ulnaris (ECU), and Extensor Carpi Radialis (ECR) in anti clock wise direction across all subjects. Butterworth filter (MATLAB 2012b) was used for subtracting noise from low magnitude surface EMG [103]. The spontaneous muscle response in extension and flexion of the arm is shown by blue and brown colors. Moreover, standard errors are shown by red and black colors for the arm's flexion and extension respectively.

First, the raw EMG data were normalized to test individual muscle activation patterns as shown in Fig. 5.10B. Fig. 5.10B shows that different muscles are contracted differently. Moreover, it is noticed that antagonist muscle co-contraction as shown in Fig. 5.10B in anterior and posterior arm pairs. For example Anterior and Posterior Deltoids pair. The Mann-Whitney U test ($\alpha = 0.05$) was conducted between arm flexion and extension to test any significance difference in muscle activation in Fig. 5.10B in leftward/rightward arm perturbations. There is no significance difference in arm flexion and extension ($p = 0.95$) in normalized muscle activation in Fig. 5.10B. However, for more clarity, the total number of peaks occurred during the arm action was studied that seems to be consisted with other research [104] that focused on EMG peaks to study limb patterns during the multi-joint movements.

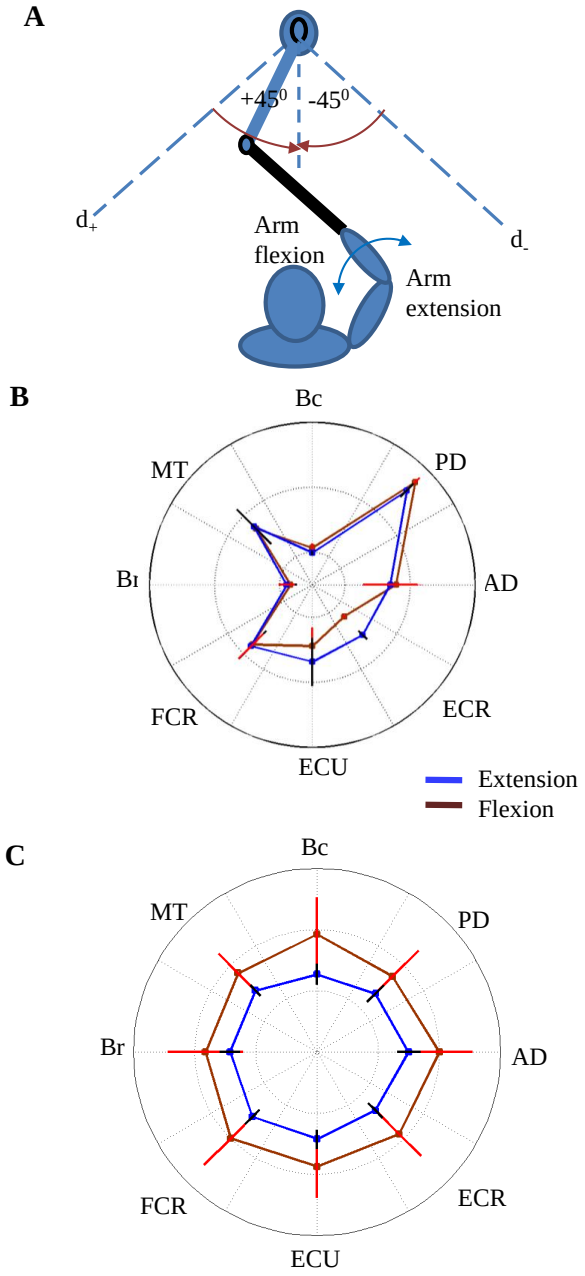

Fig. 5.10 Right-handed naive subjects' muscle recruitment patterns of perturbed arm: A) The right-handed naive subject's arm flexion/extention in leftward/rightward movements, B) The normalized rectified raw muscle activation of EMG recordings for naive subjects' arm flexion/extension in rightward/leftward movements respectively, and C) The total number of peaks occurred in EMG recordings across all naive subjects of muscles: The extension and flexion of the arm are shown by blue and brown colors respectively. The standard error for extension and flexion are shown by black and red. The arm muscles were chosen as Anterior Deltoid(AD), Posterior Deltoid (PD), Biceps (Bc), Median Triceps (MT), Brachioradialis (Br), Flexor Carpi Radialis (FCR), Extensor Carpi Ulnaris (ECU), and Extensor Carpi Radialis (ECR).

The average number of peaks occurred in EMG recording across the all subjects is shown in Fig. 5.10C in leftward/rightward movements. In general, the total number of peaks occurred in EMG is less for flexion as shown in Fig. 5.10C. However, significance was noticed between flexion and extension ($p = 0.00015$). The results show that when the arm is perturbed from leftward/rightward directions, muscle activation is significantly different. This suggests that the muscles contracted differently depending on leftward/rightward perturbations. This could occur as a result of spontaneous reaction reflection. Because as the result of embodiment perception of the muscles [105], [106], naive subjects could perceive leftward/rightward perturbations differently.

The multiple sensors from different muscles in the arm give perceptions of angle, speed and force and this could be affected to naive subjects the way they perceive the arm perturbation differently. That might be the fact that naive subjects behave differently as noticed some behavioral metrics in Table 5.1 and Table 5.2 in leftward/rightward movements. The other possible facts for asymmetry in behavioral metrics could be any asymmetry of the robotic command in leftward/rightward directions. However, robot's arm commands distribution in leftward rightward directions in transient responses in Fig. 5.8 shows that symmetry in leftward/rightward directions. It would be interesting to train subjects to test whether there is any significant different in perception and behavior after the calibration. Therefore, the same Experiment 1 and Experiment 2 were repeated with trained subjects (please refer subjects' training phase in materials and methods section) to test any difference after the training process.

5.3.3 Trained subjects-robot interactions

The robot-trained subjects interaction is presented to test any asymmetry in behavioral metrics and muscle recruitment as noticed in naive subjects. Moreover, it would be interesting to test whether any asymmetry in robot's behavior in leftward/rightward in arm actions after

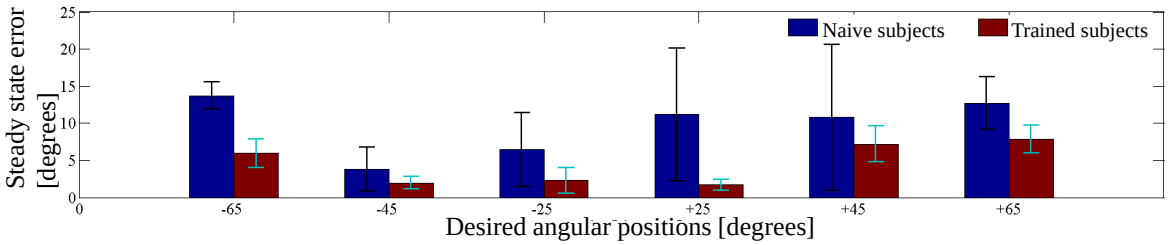

Fig. 5.11 The steady state error for the naive and the trained subjects: The standard error is shown by error bars.

the calibration. First, two-way ANOVA test ($\alpha = 0.05$) was conducted again to test how trained subjects' and robot's actions depend on other variables such as robot's direction, and human's direction. The first 20% of transient state human's and robot's actions and directions were considered. The results again show that trained subjects' action depends on robot's direction ($F(1,30) = 6.28$, $p = 0.01$) and human's direction ($F(1,30) = 155.99$, $p = 0$) as noticed in robot-naive subjects interaction experiments.

First, the naive and the trained subjects are compared as shown in Fig. 5.11 to test any improvement after the training. Fig. 5.11 shows the variability and the error of reaching desired angles for naive and trained subjects in steady state for 8 naive subjects and 8 trained subjects. Moreover, the percentage of reduction of variability in naive and trained subjects in reaching desired angular positions are shown in Table 6.6. The trained subjects were able to minimize the reaching error by a reasonable percentage for all desired angular position as shown in Table 6.6 comparatively with naive subjects. Therefore, it is interested to test again robot's behavior, trained subjects behavior, and muscle activation.

Table 5.3 The percentage of reduction of variability in naive and trained subjects in reaching desired angular positions

Desired angular position	$-65°$	$-45°$	$-25°$	$25°$	$45°$	$65°$
% reduction after training	43.24	51.70	35.39	15.28	66.89	61.57

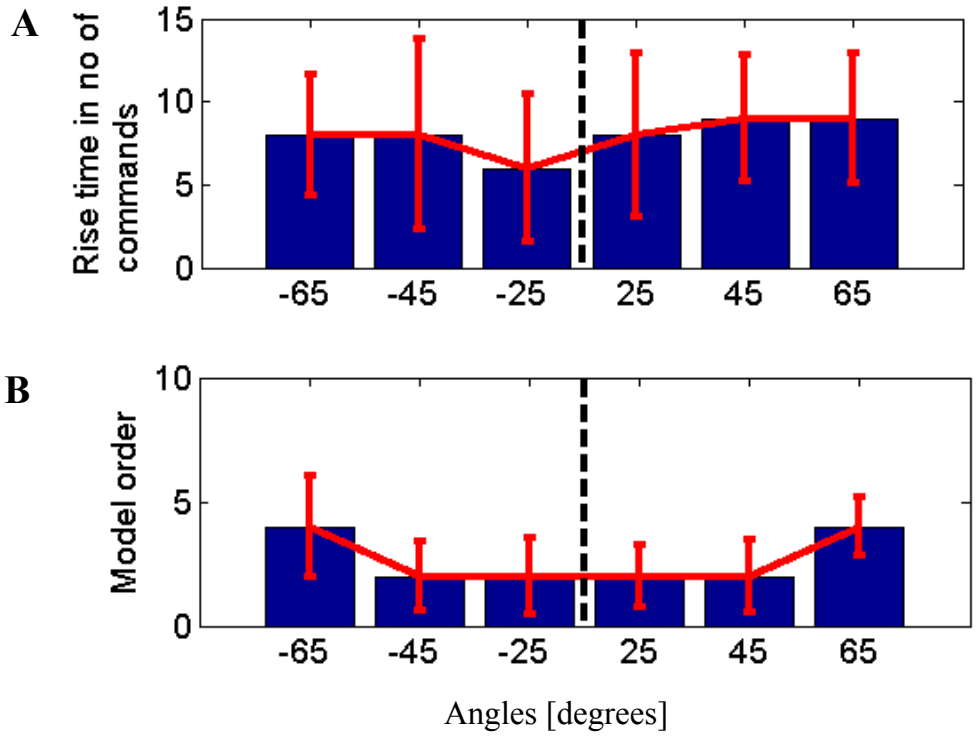

Fig. 5.12 The behavioral metrics in transient responses for trained subjects: A) Rise time (RT): Average rise time distribution across the trained subjects in number of commands for reaching $-65°$, $-45°$, $-25°$, $+25°$, $+45°$, and $+65°$ six desired angles, and B) Model order (N): Average model order distribution for trained subjects for reaching six desired angles.

5.3.3.1 Trained subjects' behavior

Trained 12 subjects' behavioral metrics are presented to understand behavior in moving leftward/rightward directions. First transient response behavioral metrics, RT and N are presented as shown in Fig. 5.4. Moreover, Mann-Whitney U test ($\alpha = 0.05$) was conducted to test whether any asymmetry in behavioral metrics as noticed in N, and SSV in naive subjects. Interestingly, the significance test results in Table 5.4 shows that none of the behavioral metrics in transient response is not significantly different for trained subjects.

Next the behavioral metrics for steady state was considered for trained subjects. Behavioral metrics SSV and SSE are shown in Fig. 5.13. Again Mann-Whitney U test ($\alpha = 0.05$) was conducted to test any asymmetry in leftward/rightward movements in steady state. The

Table 5.4 The significance test results in behavioral metrics for trained subjects in transient responses

Desired angular position in leftward/rightward directions	25°	45°	65°
RT	$p = 0.22$	$p = 0.60$	$p = 0.85$
N	$p = 0.70$	$p = 0.59$	$p = 0.13$

significance test results in Table 5.5 show that again none of the behavioral metrics in steady state is significantly different. The significance test results in human behavioral metrics in Table 5.4 and Table 5.5 show that trained subjects' movements in leftward/rightward directions are not significantly different in transient or steady state as noticed in some behavioral metrics for naive subjects. The symmetry in behavioral metrics in trained subjects might come from the way robot interacts with trained subjects. To test the possible causes of symmetry in behavioral metrics in trained subjects again robot's behavior and trained subjects' arm muscle activation are presented.

Table 5.5 The significance test results in behavioral metrics for trained subjects in steady state responses

Desired angular position in leftward/rightward directions	25°	45°	65°
SSV	$p = 0.12$	$p = 0.21$	$p = 0.90$
SSE	$p = 0.21$	$p = 0.28$	$p = 0.12$

Moreover, following the same method in Chapter 3, trained subject's model order and reactive/predictive nature were tested. Interestingly, it was found that on average trained subjects give more emphasis on 2^{nd} order predictive model after the training. However, human demonstration experiments in Chapter 3 was conducted with naive subjects. The results suggest that if those subjects were trained, the followers might be developed a predictive model.

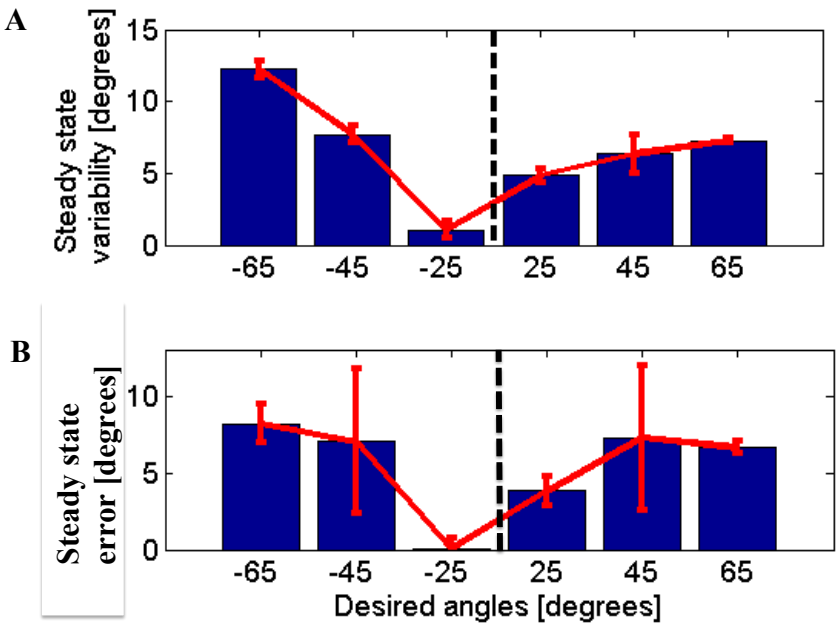

Fig. 5.13 The behavioral metrics in steady state for trained subjects: Steady state variability (SSV): Average steady state variability distribution across the trained subjects for reaching $-65°$, $-45°$, $-25°$, $+25°$, $+45°$, and $+65°$ six desired angles, and B) Steady state error (SSE): Average steady state error distribution across the trained subjects for reaching $-65°$, $-45°$, $-25°$, $+25°$, $+45°$, and $+65°$ six desired angles

5.3.4 Possible causes of symmetry in trained subjects' behavioral metrics

5.3.4.1 Robot's behavior

The robot's behavior is shown in Fig. 5.14 when robot interacts with trained subjects. To test any difference in robotic arm movement in leftward/rightward directions for trained subjects, again Mann-Whitney U test ($\alpha = 0.05$) was conducted between leftward movements in Fig. 5.14A and rightward movements in Fig. 5.14B. Interestingly there is no significance in leftward/rightward movements in robot's behavior ($p = 0.22$). After the training, the robot or the human leftward/rightward movements are not significantly different. That

might come from predictive model nature of trained subjects or trained subjects perceive differently after the calibration. Therefore, it would be interesting to test again arm muscle contribution immediately after the arm perturbation for trained subjects.

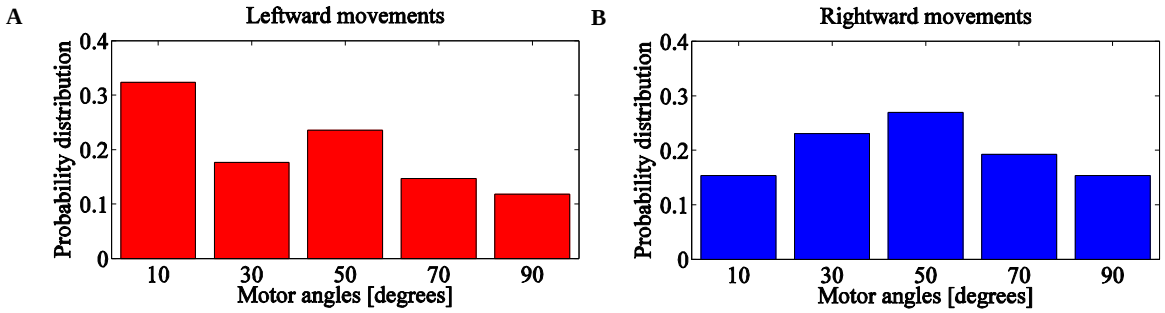

Fig. 5.14 Robot's behavior when it interacts with trained subjects: A) The probability distribution in robot's leftward movements, and B) The probability distribution in robot's rightward movements.

5.3.4.2 Trained subjects' spontaneous muscle responses

Trained subjects' spontaneous muscle responses immediately after the tug perturbation are shown in Fig. 5.15. It is important to test any significance difference in muscle recruitment in moving leftward/rightward as noticed in naive subjects in Fig. 5.10C. The Mann-Whitney U test ($\alpha = 0.05$) was conducted to test any significance difference in arm extension and flexion. Interestingly, significance test results show that the arm's flexion and extension is significantly different ($p = 0.002$) for trained subjects as noticed in naive subjects. The results show that even though trained subjects perceive differently in leftward/rightward perturbations, their behavioral metrics are symmetric in leftward/rightward movements as shown in Table 5.4 and Table 5.5. This might come from there is an internal model in the brain to compensate the perception differently after training the subjects.

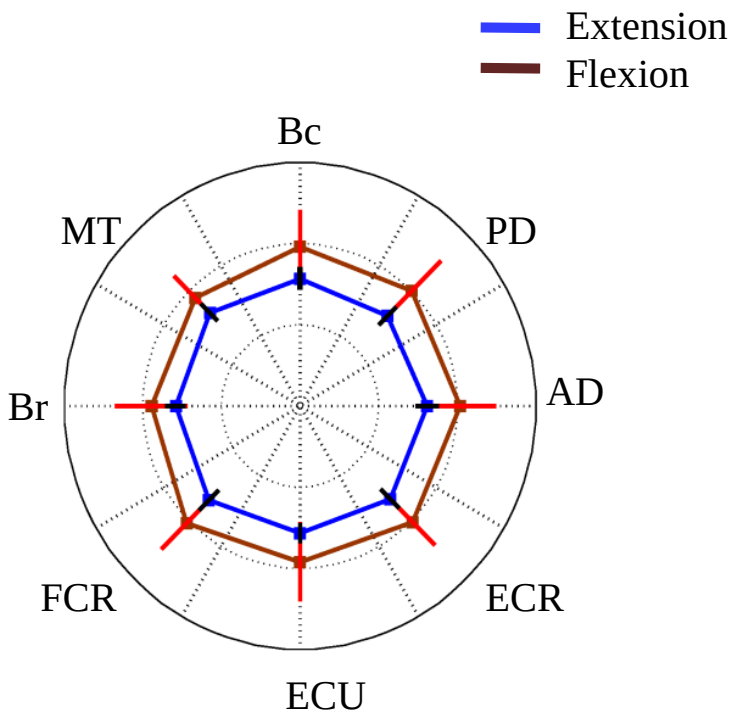

Fig. 5.15 Trained subjects' muscle recruitment patterns: The total number of peaks occurred immediately after the perturbation in EMG recordings across all the trained subjects: The extension and flexion of the arm are shown by blue and brown colors respectively. The standard error for extension and flexion are shown by black and red. The arm muscles were chosen as Anterior Deltoid(AD), Posterior Deltoid (PD), Biceps (Bc), Median Triceps (MT), Brachioradialis (Br), Flexor Carpi Radialis (FCR), Extensor Carpi Ulnaris (ECU), and Extensor Carpi Radialis (ECR).

5.4 Discussion

This chapter presents robot's and humans' behavior when guider's control policy identified from human demonstration experiments was implemented on a planar 1-DoF robotic arm. Experiments were carried out with naive and trained subjects to test any behavioral changes in the duo after training.

First considering the stability of the implemented controller, the behavioral metrics in RT show that naive/trained subjects can settle down in the desired angular positions in a reasonable time. For example, subjects reach to their rise time on average number of com-

mands 8 for naive subjects as shown in Fig. 5.6A and 7 for trained subjects as shown in Fig. 5.4A out of 23 commands during the trial. Moreover, the low model order in behavioral metrics N confirms less oscillation in settling down. For example the average model order across the subjects is 2 for both naive and trained subjects. Furthermore, the low variability in steady state again in trained subjects confirms the stability of the controller. Those results confirm that implemented guider's control policy is stable.

It is noticed that naive subjects move differently when their arm is perturbed from leftward/rightward directions as shown in Table 5.1 and Table 5.2 in some behavioral metrics such as N and SSV. However, robot's behavior is symmetric in leftward/rightward arm commands. Again it was found that on average naive subjects give more emphasis on a 2^{nd} order reactive model as noticed in human demonstration experiment in Chapter 3. Moreover, naive subjects arm spontaneous muscle response immediately after the perturbation is significantly different when the arm is perturbed in leftward/rightward directions. However, when subjects were trained, none of the behavioral metrics or robot's behavior is significantly different in moving leftward/rightward directions as noticed in some naive behavioral metrics. Interestingly, the reactive behavior in naive subjects was changed to predictive behavior after the training while the order remained the same.

Humans' current movement is a combination of the way of perceiving the perturbation and the human action. Naive and trained subjects spontaneous muscle response in response to leftward/rightward perturbation given by the robot show that proprioceptive sensors in the muscles are contracted differently when the arm is perturbed from leftward/rightward directions. Even though humans perceive the muscle contraction differently from leftward/rightward directions as noticed in spontaneous muscle response in naive and trained subjects, the humans' behavior can change after training as noticed in trained subjects' behavioral metrics. Therefore, one of the possible reasons of symmetry in the behavioral metrics in trained subjects might come from any internal model in the brain to compensate

their perception differently after the training. That could change their behavior to predictive nature. Therefore, trained subjects might predict the next action to make a current movement in order to move desired direction accurately. Moreover, when humans are trained they might be able to move more passively as noticed in predictive nature.

Sensor morphology, perception and the interaction with the environment provide an alternative avenue for tackling the challenges faced by robotics in embodiment perceptions [105]. The experiments with naive and trained subjects show that how humans perceive the same perturbation differently depending on the direction and how the training could effect them to move symmetrically. Therefore, these spontaneous reactions of the humans give an insight as to some fact to take into account in designing guidelines how to train humans to follow a guiding robot when the human is guided via a hard rein in low visibility conditions.

CHAPTER 6

WEARABLE HAPTIC BASED PATTERN FEEDBACK SLEEVE

Abstract

This chapter presents how humans trained in primitive haptic patterns given using a wearable sleeve, can recognize their shifts and linear combinations. The wearable sleeve consisted of 7 vibroactuators to stimulate subject's forearm to convey the primitive patterns. The used primitive haptic patterns are the Gaussian template (T), shifted right (R), shifted left (L), half Gaussian (H), and shrink (S) hereafter denoted by templates. The results of this chapter would give an idea as to how humans mentally construct the cutaneous feedback in different scenarios such as shifting and scaling with respect to trained patterns, how they recognize all trained patterns when played randomly, and how they can recognize linear combination of primitive patterns. Moreover, the results would be used to convey a message to the human to give an idea of the shape and stiffness of obstacles that come into contact with the robot during guiding in low visibility conditions in future.

6.1 Introduction

Haptics would be the best way to convey messages in critical tasks to provide spatial information [107]. Some of the studies demonstrated that haptic perceptions can be used to assist humans in navigation in unfamiliar environments [108], [109]. Therefore, it is important to understand how humans perceive haptic feedback patterns to convey messages during guiding like in indoor fire-fighting. Therefore, this chapter presents how humans recognize primitive vibroactuator array patterns given in a sleeve worn in the forearm when the patterns are shifted, scaled and linearly combined.

Mechanoreceptors on the skin respond to mechanical pressure or distortion. There are four main types of mechanoreceptors in glabrous skin: Pacinian corpuscles, Meissner's corpuscles, Merkel's discs, and Ruffini endings as shown in Fig. 6.1. However, Pacinian corpuscles are sensitive for mechanical vibration [69]. Pacinian corpuscles have a threshold frequency that a vibration stimulus must overcome in order to trigger a signal to the brain [110]. A perceptible frequency range of humans was found in [69] from 20-400 Hz. Therefore, the maximum frequency was chosen 400 Hz in the vibroactuator haptic sleeve array. If a vibration is not strong enough to cause the Pacinian corpuscle to reach this threshold, the brain would not be able to sense the vibration.

There have been many studies on using vibroactuators for different purposes in navigation. For example, the study in [74] presented an active belt which is a wearable tactile display that can transmit directional information in combination with GPS directional sensor and vibration motor. Another research on cooperative human robot haptic navigation in [84], used a wrist belt with vibro-tactile sensors to guide a human to a target location. Moreover, haptic feedback was used to navigate people by using a mobile phone in [75]. Furthermore, vibro-tactile way-point navigation was presented in [81] in pedestrian navigation.

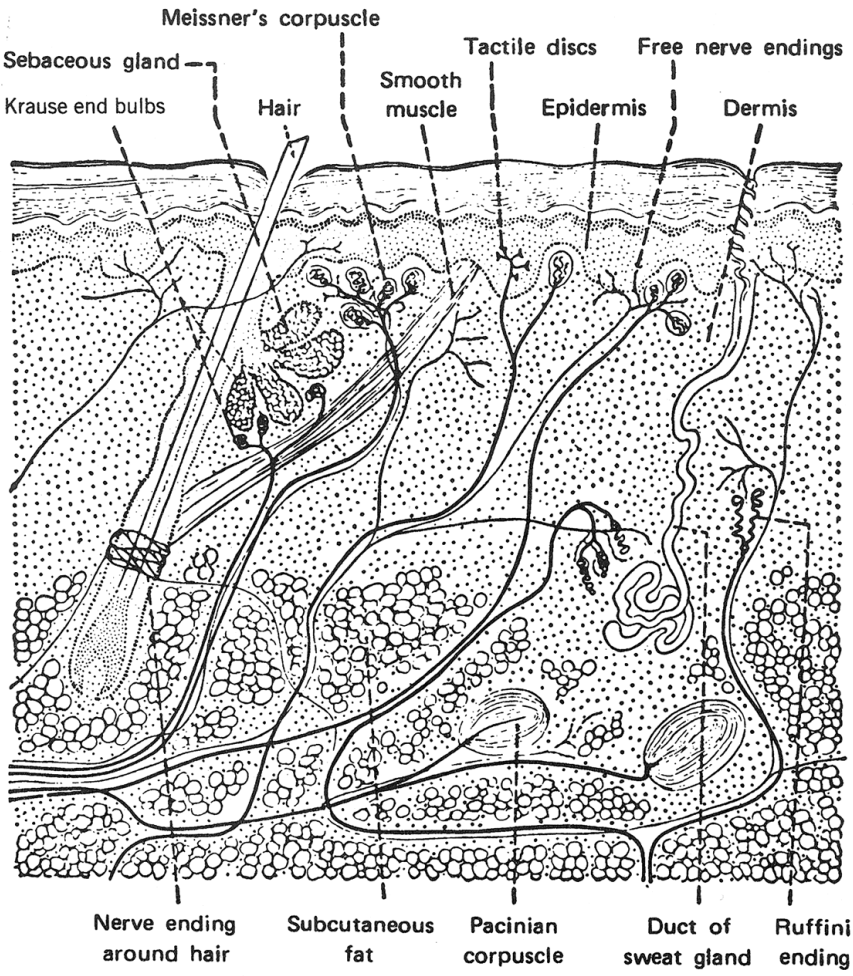

Fig. 6.1 Cross section of the skin adapted from [69].

Studies conducted on variability of haptic perception found out that the perception depends on vibrotatile location on the body [76], the area of contractor [73], [111], frequency [69], and duration of vibration [76]. Therefore, in addition to the frequency, identification of the sensitive location, and the duration of stimuli are important to design a vibroactuator haptic sleeve.

6.1.1 Localization of the vibroactuators

It is noted that in [76] when subjects were asked to identify the location of vibro-tatctile stimulation, the accuracy was only 53%. Since the localization accuracy is low, it is impor-

tant to study how humans would generalize haptic feedback patterns to a given set of discrete locations of the skin, because an attempt of generalization may change the level of error at individual locations. Moreover, it has been found that the level of accuracy can be improved when the vibro-tactile sensors are mounted on the forearm or back [86], [111]. Therefore, vibro-tactile sensors were mounted on the forearm during the experiments. Moreover, the two point resolution varies across the body as shown in Fig. 6.2 [69]. For example two point resolution for the forearm is more than 35mm. Therefore, wearable haptic based pattern feedback sleeve with vibroactuators was designed to make a gap of 70mm between two vibroactuators to avoid unnecessary ambidextrous cross talks.

6.1.2 Importance of the duration of stimuli

The study in [112] argued that if the tactile stimulus increases from 80 to 320 ms, the ability of patterns identification is also improved. However, people prefer that the stimulus is between 50 and 200 ms and they feel longer durations are perceived to be annoying [113]. The study in [69] experienced that shorter length of time vibrating reduces the adaptation. Therefore, duration of the experimental trials are limited to 100 - 150 ms.

6.1.3 The questions answered in wearable haptic based pattern feedback sleeve experiments

1. How humans generalize a Gaussian pattern in scaling and shifting
2. How humans can recognize trained haptic feedback patterns when they are presented in a random order
3. How humans can recognize random linear combinations of trained primitive patterns given by a set of discrete vibroactuators on the forearm

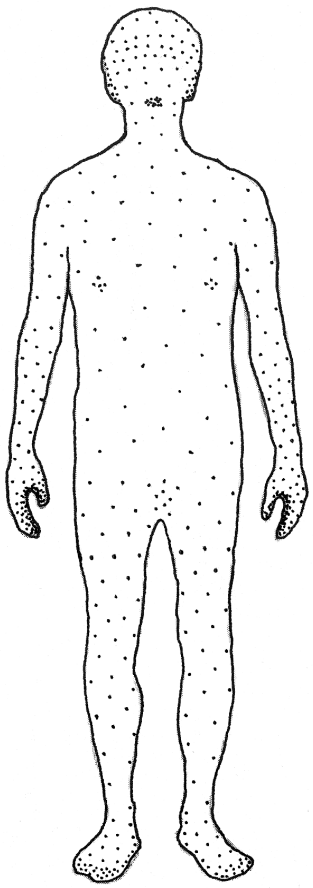

Fig. 6.2 Map of two point discrimination of the human body adapted from [69].

6.2 Materials and Methods

6.2.1 Experimental setup

Pico Vibe 10 mm vibration motor - 3mm type (Precision Micro-drives) in Fig. 6.3A was used to make wearable haptic based pattern feedback system as shown in Fig. 6.3B. There are 7 Pico Vibe 10 mm vibroactuators array arranged in equal distance as shown in Fig. 6.3B. The 7 Pico Vibe 10 mm vibroactuators are attached to the seven belts which can be adjusted with the size of the human arm as shown in Fig. 6.4A. The different intensities for the vibrators are generated by Arduino Mega motherboard and the amplitude is modulated by a simple power amplifier circuit as shown in Fig. 6.4B.

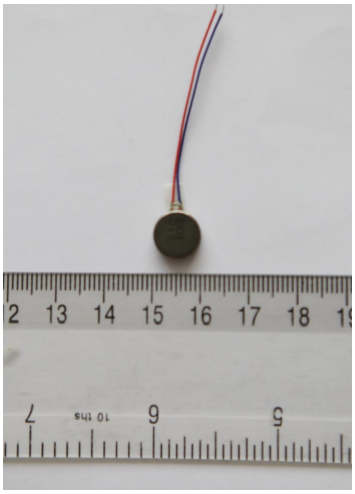

Fig. 6.3 Pico Vibe 10 mm vibroactuator

6.2.2 Experiment 1: How humans generalize a Gaussian pattern in scaling and shifting

Ten healthy subjects (6 - male, 4 - female) age between 24 to 39 participated in the Experiment 1. The Experiment 1 was conducted to test how humans generalize a primitive template pattern (T) with respect to scaling and shifting. The shifting was done by left shift (L) and right shift (R), not up or down and scaling was done by shrinking (S), and half in magnitude (H).

The intensities for the template (T) were generated from Gaussian curve membership function (gaussmf) in MATLAB R2012b. The T, R, L, S, and H are implemented as shown in Table 6.1. Moreover, for clarity the all templates patterns are shown in Fig. 6.6.

Table 6.1 Intensity table for different templates

Intensities (Hz):	Vib. 1	Vib. 2	Vib. 3	Vib. 4	Vib. 5	Vib. 6	Vib. 7
T	103.33	140.60	281.96	400.00	281.96	140.60	103.33
R	100.00	100.10	103.33	140.60	281.96	400.00	281.96
L	281.96	400.00	281.96	140.60	103.33	100.10	100.00
S	100.00	100.10	140.60	400.00	140.60	100.10	100.00
H	51.66	70.30	140.98	200	140.98	70.30	51.66

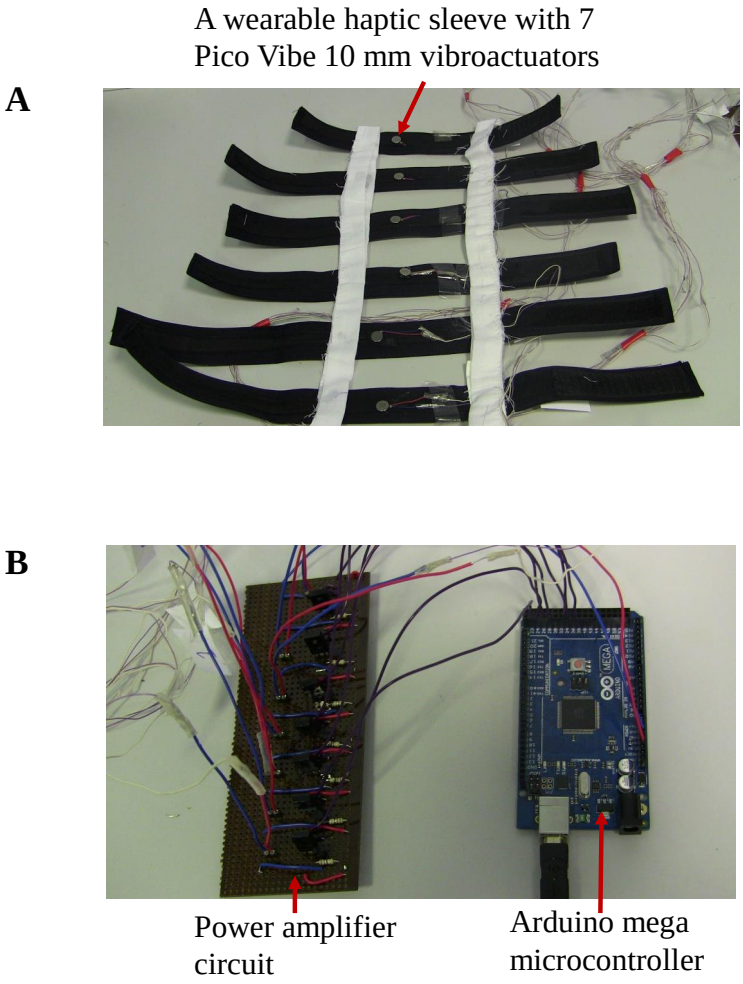

Fig. 6.4 Hardware design for wearable haptic sleeve: A) A wearable haptic sleeve with 7 Pico Vibe 10 mm vibration motor, and B) Arduino Mega motherboard and power amplifier circuit to generate different intensity patterns.

6.2.2.1 Experimental procedure

Subjects wore the haptic based pattern feedback sleeve as shown in Fig. 6.5A. Subjects were asked to keep the arm stretched during the experiments. The intensity patterns were selected as shown in Fig. 6.6 to generate different stimulation patterns. Single trial ran average 10 to 15 seconds. During the first five trials, the template (T) in Fig. 6.6A was played. Before playing each template, subjects were shown the printed template. The subjects were explained the defined area for drawing on the ipad screen as shown in Fig. 6.5A. Subjects

were asked to draw a smooth curve representing what they perceive on an ipad sketching app (Draw free app (Apple Inc)) after each trial as shown in Fig. 6.5B. A drawing area on the ipad was clearly demarcated to match the size of the printed template as shown in Fig. 6.5A. After first five training trials, L, R, S, and H patterns were played randomly. Whenever the template T was played, it was shown prior to the trial and subjects drew what they felt during the trial. Pattern T repeated four times like in a block. Likewise four blocks of templates were played during the experiments after first five trials. The rest of four intensity patterns (R, L, H, and S) played six times each during the experiment randomly. Therefore, subjects participated in 45 trials during the experiments. For more clarity, The trial number and respective played patterns are shown in Table 6.2.

Table 6.2 Experiment 1: The pattern order in different trials

Pattern	Trial nos:
T	1-5, 11-14, 20-23, 29-32, 38-41
R	6, 10, 18, 27, 33, 45
L	7, 17, 24, 35, 37, 44
S	9, 16, 26, 28, 34, 42
H	8, 15, 19, 25, 36, 43

6.2.3 Experiment 2: How humans can recognize trained haptic feedback patterns when they are presented in a random order

The second experiment was conducted to test how subjects recognize all trained haptic feedback patterns when they are presented in a random order. Eight healthy subjects (6 - male, 2 - female) aged 24 to 28 participated in the Experiment 2. Since the subjects were not able to distinguish the pattern S from other patterns in Experiment 1, only patterns L, R, H, and T were considered for the second experiment. During the second experiment, first 20 trials were designed to train the subjects to learn the patterns T, R, L, and H. Each pattern was played 5 times. During that 20 trials, subjects were shown the printed out pattern before

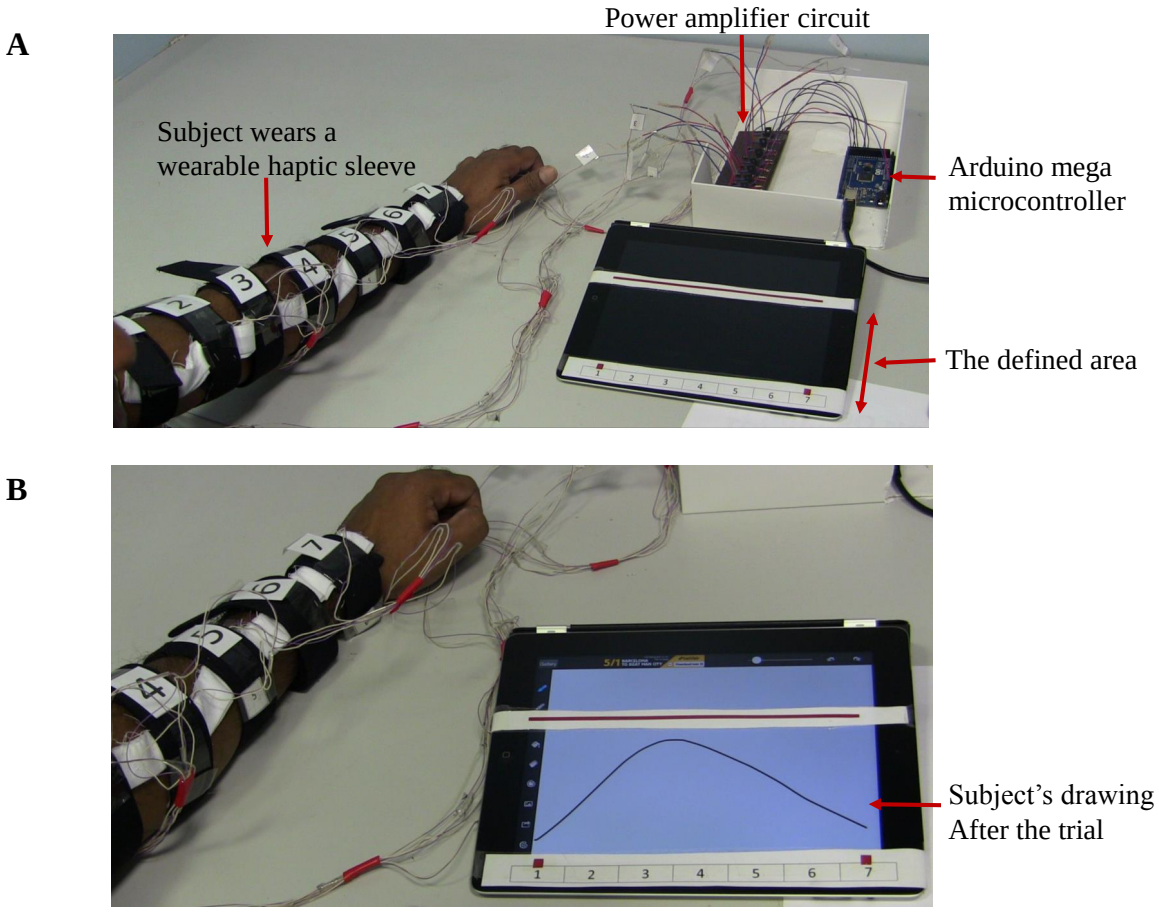

Fig. 6.5 An experimental trial: A) The subjects wears a wearable haptic sleeve with 7 Pico Vibe 10 mm vibration motor. The defined drawing area is shown, and B) Subject's drew what they felt after the trial on an ipad (Draw free app (Apple Inc)).

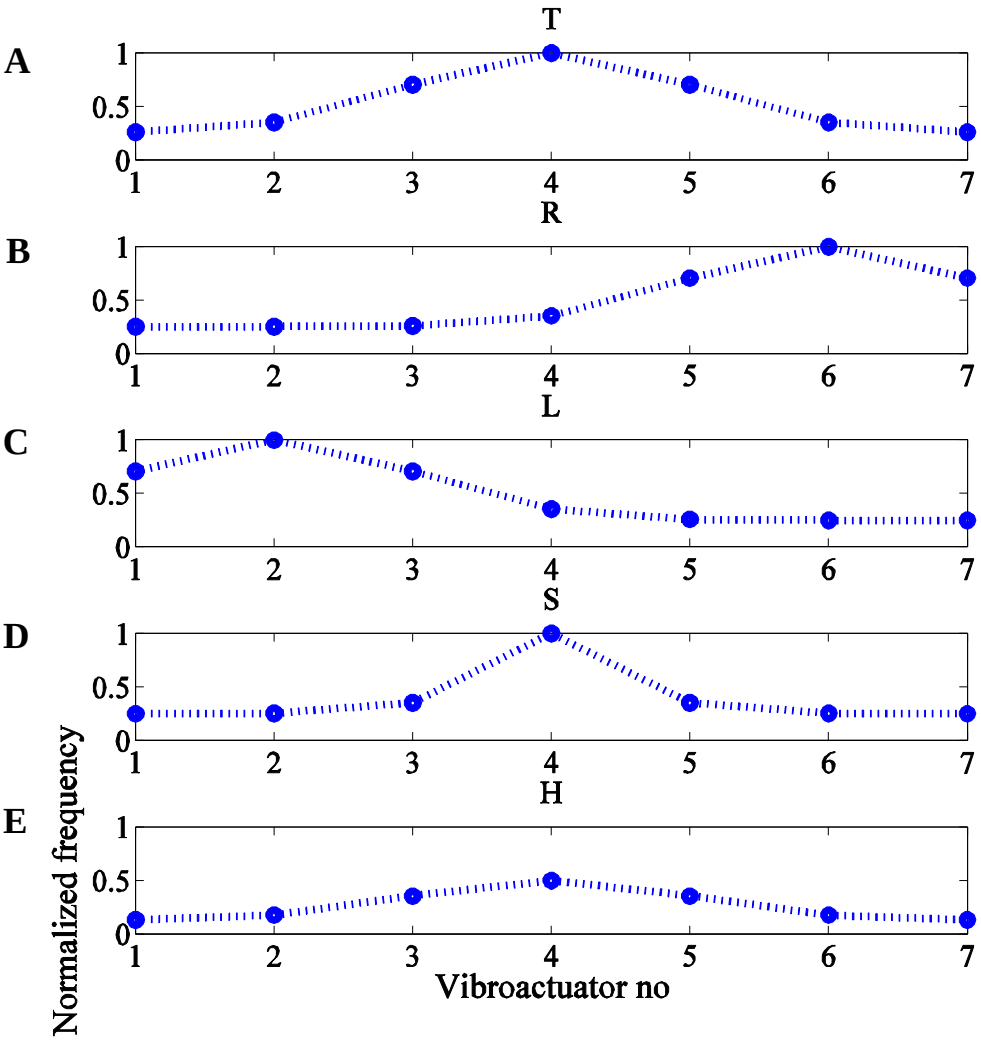

Fig. 6.6 The templates: A) Gaussian Template. The patterns was generated by gaussmf (MATLAB R2012b) with the standard deviation 1 for T, R, L, and H. The standard deviation is 0.5 for S, B) Right shift from the T, C) Left shift from the T, D) Shrink from the T, and E) Half intensity from the T.

the trial, next played the pattern, and finally asked them to draw what ever they felt on the ipad by a smooth curve. After that training session, trained 4 patterns were played randomly. Each primitive shape was played 5 times randomly. Therefore, subjects participated in 44 trials. For more clarity, the order of the trials are shown in Table 6.3. However, the order of the patterns were counter balanced.

Table 6.3 Experiment 2: The pattern order in different trials

Pattern	Trial nos:
T	1-5, 21, 29, 32, 34, 38, 41
R	6-10, 23, 27, 31, 33, 39, 42
L	16-20, 22, 26, 28, 35, 37, 44
H	11-15, 24, 25, 30, 36, 40, 43

6.2.4 Experiment 3: How humans can recognize random linear combinations of trained primitive patterns given by a set of discrete vibroactuators on the forearm

The Experiment 3 was designed to understand how humans recognize linear random combinations of trained primitive patterns given by set of vibroactuators on the forearm. The same group of subjects in Experiment 2 participated in to the Experiment 3. The patterns were selected as linear combinations of T + L, T + R, and L + R as shown in Fig. 6.7A, Fig. 6.7B, and Fig. 6.7C respectively. Moreover, the frequencies of the combined patterns are shown in Table 6.4 and order of the played patterns are shown in Table 6.5. However, the frequencies of combination of two primitive patterns were normalized to bring the maximum frequency to 400Hz as shown in Table 6.4.

Table 6.4 Intensities table for combined primitive patterns

Intensities (Hz):	Vib. 1	Vib. 2	Vib. 3	Vib. 4	Vib. 5	Vib. 6	Vib. 7
T+L	203.66	374.37	400.00	374.37	203.66	44.73	3.66
T+R	3.66	44.73	203.66	374.37	400.00	374.37	203.66
L+R	242.53	400.00	246.97	108.23	246.97	400.00	242.53

Table 6.5 Experiment 3: The pattern order in different trials

Pattern	Trial nos:
T+L	1, 5, 7, 12, 15
T+R	3, 6, 8, 10, 14
L+R	3, 6, 8, 10, 14

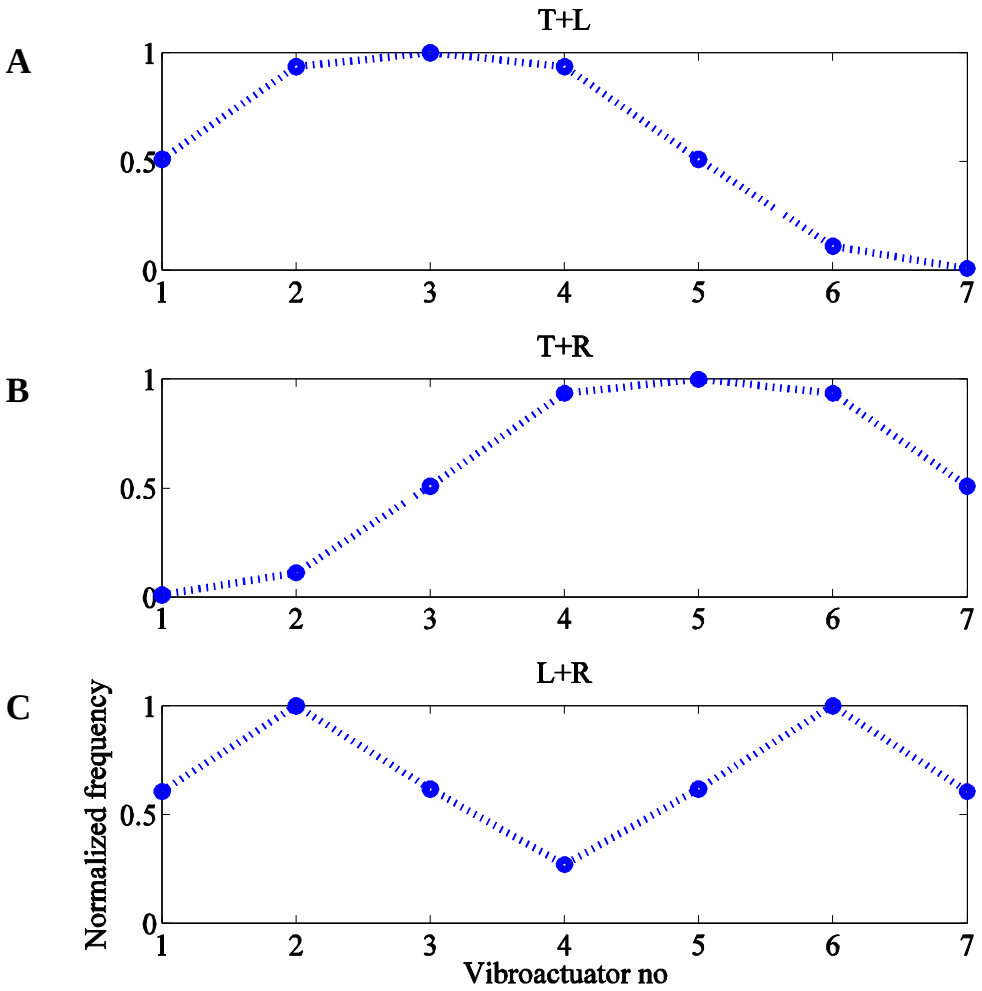

Fig. 6.7 Linear combination of two primitive patterns: A) The combination of T + L, B) The combination of T + R, and C) The combination of L + R.

6.3 Results

6.3.1 Experiment 1

The human sketched raw data for the pattern T, L, R, S, and H in Experiment 1 are shown in Fig. 6.8. The template patterns are shown by black dashed line. The human sketched data in Fig. 6.8 were regressed by respective templates. The regression coefficients are shown in Fig. 6.9 when the human sketched data were regressed with the respective templates in Fig. 6.6 in Experiment 1. The results in Fig. 6.9A show that high correlationship between

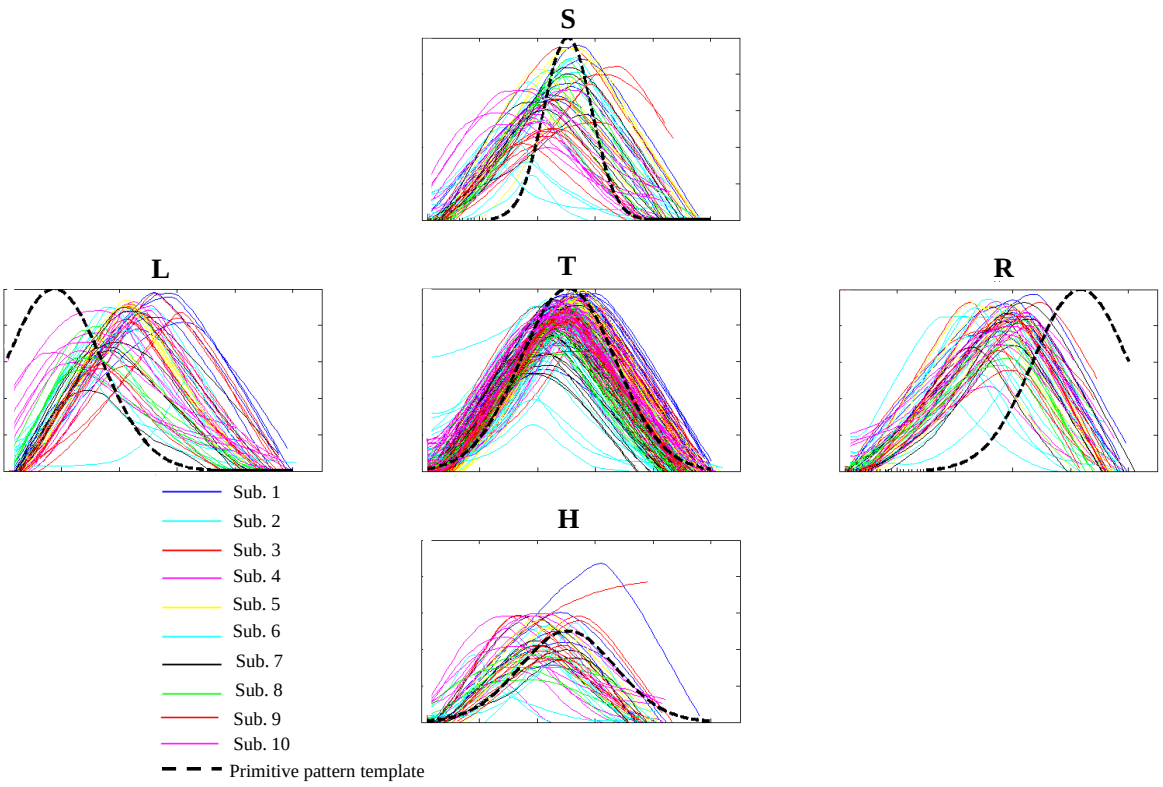

Fig. 6.8 Experiment1: The human sketched data for pattern T, L, R, S, and H for all trials. The templates are shown by black color.

the data and template only when the template T was played. Other intensity patterns show relatively low regression coefficients values as shown in Fig. 6.9B. Moreover, it is noticed that some regression values < 0. The low and negative regression coefficients and higher variability values suggest that subjects were not able to scale and shift the pattern they are trained in. This might come from the fact that the memory of the pattern T interferes with subjects' perception as shown in Fig. 6.8. For example, L and R in Fig. 6.8. For more clarity, the data were regressed only with template T (shown in Fig. 6.6A) as shown in Fig. 6.10 (Note that Fig. 6.9B the regression was done actual pattern that was played).

Fig. 6.10 shows the improvement of the regression coefficients for the patterns when the data are regressed with template T, with respect to Fig. 6.9B for pattern L and R. The improvement of regression coefficient might come from the interference of trained pattern T. Moreover, none of the regression coefficients is < 0 in Fig. 6.10 as noticed in Fig. 6.9B.

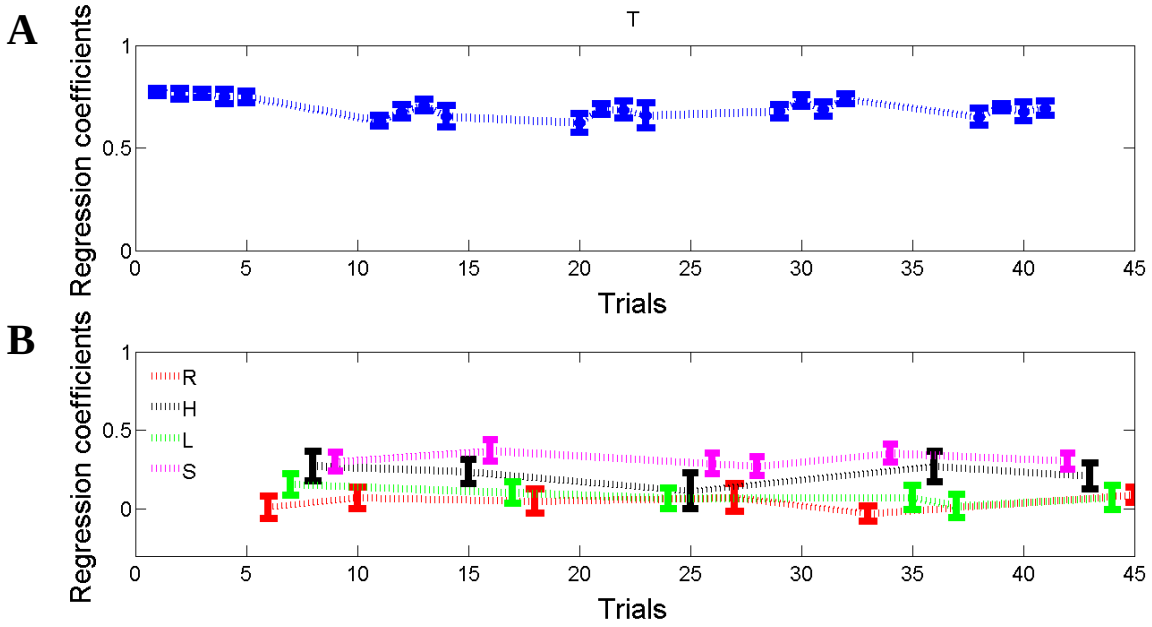

Fig. 6.9 Experiment 1: Regression coefficients when human sketched data regressed with respective templates in Fig. 6.6.

This again suggests interference of the trained pattern T in subject's memory in shifting and scaling as noticed in Fig. 6.8. Therefore, Experiment 2 was conducted to train not only the template T but also all primitive patterns. For more clarity, Mann-Whitney U test ($\alpha = 0.05$) was conducted to test significance difference in regression coefficients in Fig. 6.9B and Fig. 6.10 in all patterns (Since data were not normally distributed, non-parametric Mann-Whitney U test was used to test the significance). It is shown that regression coefficients for pattern R ($p = 0.002$), L ($p = 0.002$), and H ($p = 0.055$) are significantly low. However, it was noted that the regression coefficients for pattern S ($p = 0.132$) was not improved. This again suggests that the pattern S is statistically independent. Moreover, the raw data in Fig. 6.8 also show that subjects were not able to generalize the pattern S. Therefore, the pattern S was dropped in Experiment 2.

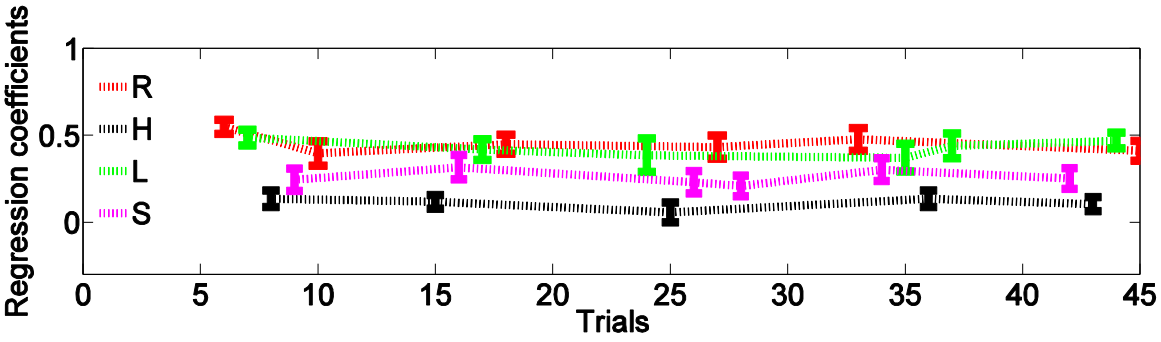

Fig. 6.10 Experiment 1: Regression coefficients when data are regressed only with template T.

Table 6.6 Trained subjects' average percentage improvement of regression coefficients.

Pattern	% improvement
R	43.20
L	29.28
H	45.88

6.3.2 Experiment 2

The human sketched raw data for the pattern T, L, R, and H in Experiment 2 are shown in Fig. 6.11. The template patterns are shown by black dashed line. The human sketched data in Fig. 6.11 were regressed by respective templates. The regression coefficients are shown

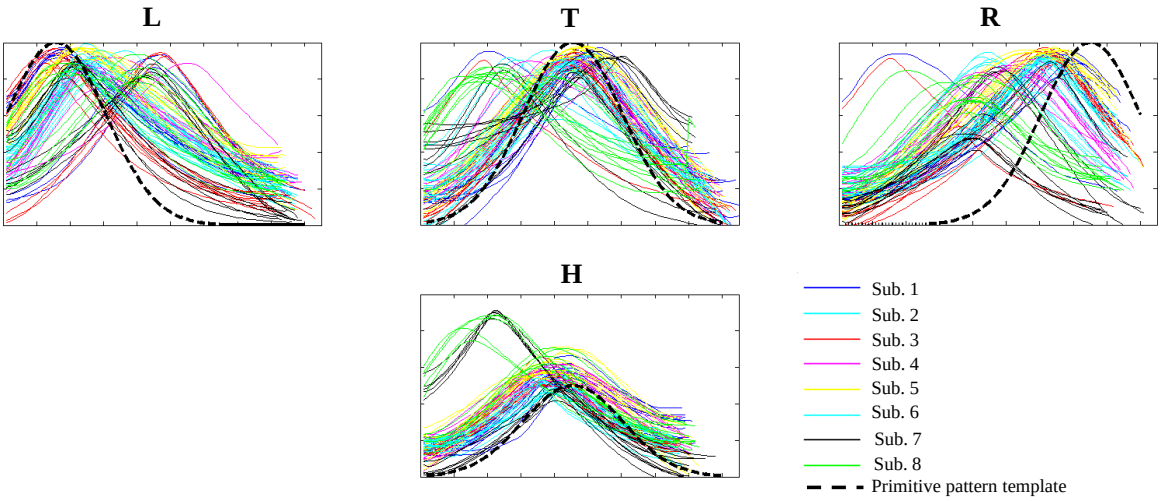

Fig. 6.11 Experiment 2: The human sketched data for pattern T, L, R, and H for all trials. The templates are shown by black dashed line.

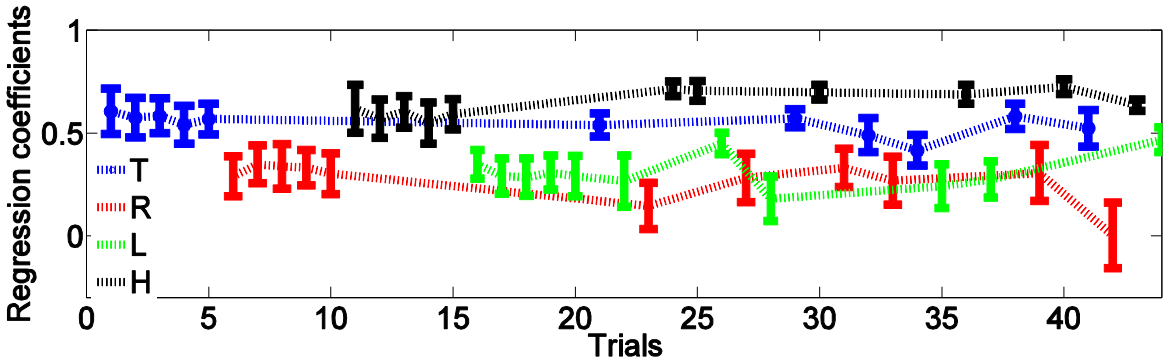

Fig. 6.12 Experiment 2: Regression coefficients when data regressed with respective template in Fig. 6.6.

in Fig. 6.12 when subjects were trained and tested in a random order for patterns T, H, L, and R in Experiment 2. In general, in Fig. 6.12 all regression coefficients are improved with respect to Fig. 6.9 for all primitive patterns. For clarity, trained subject's percentage improvement of regression coefficients with respect to untrained subjects in Experiment 1 is shown in Table 6.6. The regression coefficients of training session are higher for T and H with respect to L and R as shown in Fig. 6.12. It implies that subjects have a better ability to recognize scaled template than shifted ones. Moreover, it can be seen in humans' sketched data in Fig. 6.11. However, the regression coefficients of L is improved across the experimental trails. The results suggest that when subjects are trained for all primitive patterns, they can recognize, scale and shift the patterns more accurately than Experiment 1. Therefore, those results shed light that humans can recognize trained primitive patterns when vibroactuator array generates different stimulation on the forearm. Therefore, wearable haptic based pattern feedback sleeve would be used to convey the shape or stiffness of the obstacle guiding a human in low visibility conditions in human-robot interactions. Moreover, Experiment 3 was conducted to understand how humans recognize the combination of two trained primitive patterns.

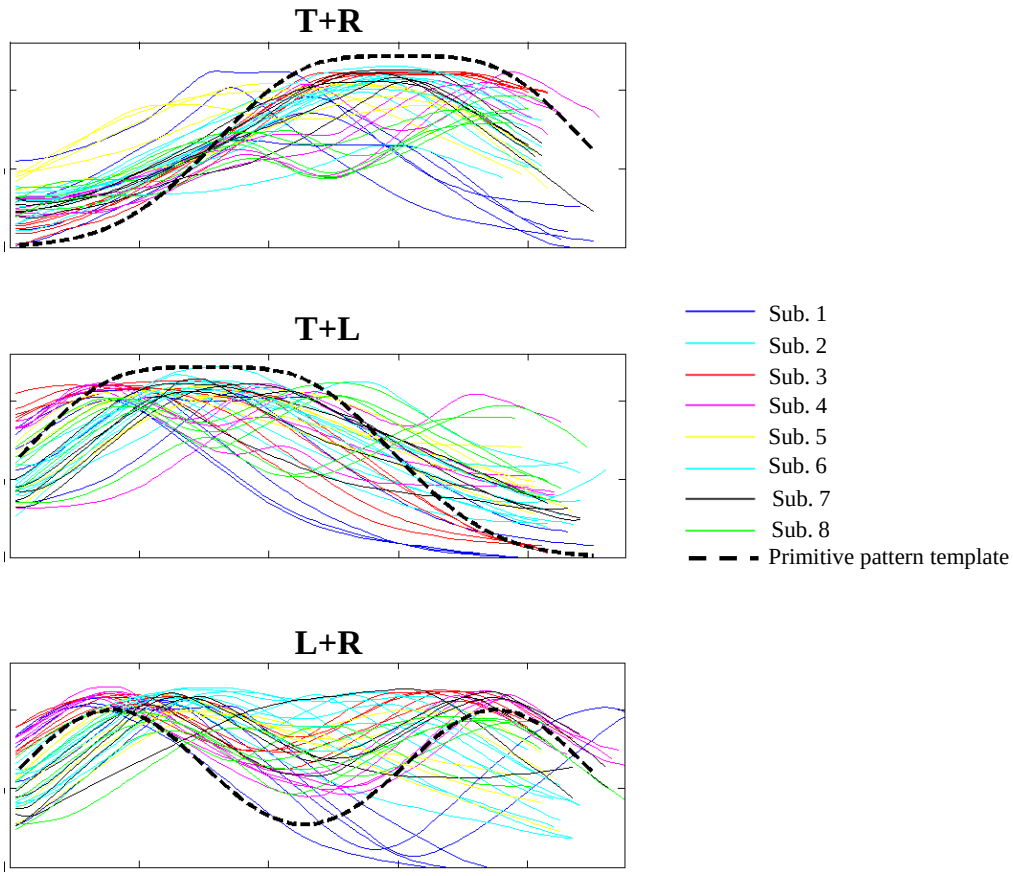

Fig. 6.13 Experiment 3: The human sketched data for pattern T+L, T+R, and L+R for all trials. The templates are shown by black dashed line.

6.3.3 Experiment 3

The human sketched raw data for the pattern T+L, T+R, and L+R in Experiment 3 are shown in Fig. 6.13. The templates are shown by black dashed line. The human sketched data in Fig. 6.11 were regressed by respective templates. The results of Experiment 3 are shown in Fig. 6.14 when the human sketched data were regressed with the respective templates in Fig. 6.7. The regression coefficient values are higher for T+L and T+R as shown in Fig. 6.14. This might come from the frequency values of T+L and T+R patterns as shown in Table 6.4. In Table 6.4, five adjacent vibroactuators are in humans' threshold frequency range (Humans' threshold frequency range is 200 to 400 Hz [69]). Humans were not able to recognize when not enough vibroactuators fall within the most sensitive frequency range [69] as noticed in

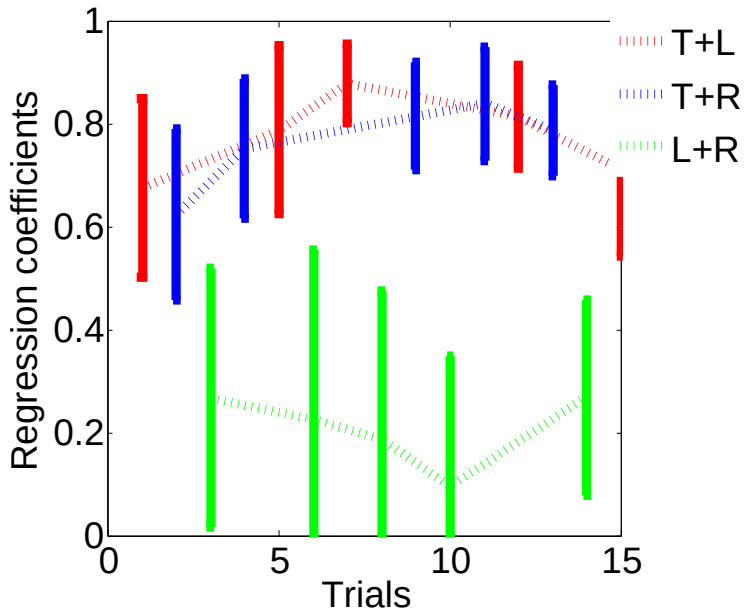

Fig. 6.14 Experiment 3: Regression coefficients when data regressed with respective template in Fig. 6.4.

L+R. The low regression coefficients and higher variability values suggest that activating sufficient adjacent vibroactuators together within the threshold frequency range is more appropriate to convey spatial information. Moreover, humans might be able to recognize uni model than bi model as shown in Fig. 6.13. These results suggest that vibroactuator array is a good alternative to convey spatial information to the humans by activating more vibroactuators simultaneously in low visibility conditions. Moreover, the other advantage is that humans' hands are free to explore the environment while wearing the vibroactuator haptic sleeve in search and rescue in haptic based guiding.

6.3.4 Discussion

Cutaneous perception and haptics are used to enhance skill learning in many virtual environments like Telesurgery [114]. A deeper understanding of how humans generalize and combined trained primitive haptic patterns will help to design wearable haptic feedback system to guide them in low visibility conditions. From Experiment 1, it can be concluded

that the humans find it difficult to scale and shift the pattern they felt with respect to the trained pattern. Even if they were able to scale or shift, the original pattern interferes with the shifted and scaled patterns. Results in Experiment 2 show that trained humans' regression coefficients are improved by 43.20%, 29.28%, and 45.88% for R, L, and H respectively. Those improvements show that humans have a general ability to recognize trained patterns even when they are played in a random order. Moreover, higher regression coefficients for combined primitive patterns in Experiment 3 show that humans can recognize linear combinations of patterns T+L and T+R. In T+L and T+R, five adjacent vibroactuators are in humans' threshold frequency range (Humans' threshold frequency range is 200 to 400 Hz [69]). Humans were not able to recognize when not enough vibroactuators fall within the most sensitive frequency range [69] as noticed in L+R. Furthermore, these results show that humans are able to shift and scale uni model than bi model. Furthermore, the results in Experiment 3 show that humans can recognize, scale, and shift more accurately when enough adjacent vibroactuators are activated in the threshold frequency range simultaneously.

The results of this chapter would give an idea as to how humans mentally construct the cutaneous feedback in different scenarios such as shifting and scaling with respect to trained patterns, recognize all trained patterns even if the patterns were played randomly, and linearly combine primitive patterns. The results explain how to use cutaneous feedback to the blindfolded followers to help them mentally construct the shape and stiffness of obstacles that come into contact with a guider robot. These spatial and temporal qualities of haptic exploration can make the follower aware of a number of physical qualities of an obstacle or environment conditions such as stiffness, force, and friction in guiding. The results give guidelines to design haptic sleeve to guide humans in low visibility conditions.

CHAPTER 7

DISCUSSION AND CONCLUSIONS

7.1 Discussion and conclusions

Abstract

This chapter presents discussion, conclusions of this thesis and future research work. The conclusions derived from identified guiding and following control policies in human demonstration experiments are discussed. Moreover, discussion and conclusions of follower's movements in response to tug forces generated by the guider modeled using a virtual damped inertial model are presented. Furthermore, the conclusions made from human-robot interaction experiments when the control policy identified from human guiders was implemented on a planar 1-DoF robotic arm to perturb the blindfolded subjects' most dominant arm to guide them to a desired position in leftward/rightward directions are discussed. Finally, this chapter discusses the conclusions made from wearable haptic sleeve when humans are trained to scale, shift, and linearly combine trained primitive patterns. Moreover, future possible research directions of the study are discussed. The discussion, conclusions, and future research directions will give an insight as to some fact to take into account in designing guidelines when the human is guided by an intelligent agent via a hard rein in low visibility

conditions.

7.2 Summary of results

Haptic based guidance is a natural solution when a human has to work in low visibility conditions like in indoor fire-fighting, disaster responders, and search and rescue. An intelligent agent (man/machine) with full environment perceptual capabilities is an alternative to enhance navigation in such unfavorable environments. Since haptic communication is the least affected mode of communication in such cases, the thesis's approach is to understand how to extract guiding/following control policies between the duo where one has environment perception capabilities (An intelligent agent: man/machine) while the other one has limited perceptions of the environment (impaired human) via a hard rein. The results would give an insight into the computational structure of motor controllers used by human participants to guide a blindfolded counterpart.

Chapter 2 presents the background and related work of human guidance when the vision is impaired in different environments. None of the those studies focused on how to extract guiding/following control policies to guide a human in low visibility conditions. This thesis shows how to extract guiding/following control policies from human demonstration experiments when a visually impaired human is guided by another human. Trust is one of the most critical factors in urban search and rescue missions because it can impact the decisions human make in uncertain conditions [55]. There have been some attempts to quantify the trust of a human with limited perception of the environment [10], [48] in different environmental conditions. However, this thesis not only quantifies the human trust but also models it in real time. Moreover, the chapter discusses previous studies on proprioceptive and cutaneous feedback in haptic based guidance. However, this thesis contributed to understand how proprioceptive and cutaneous feedback effectively used in haptic based guidance. The more detailed discussion on each chapter is presented below.

Chapter 3 presents the salient features of an optimal state dependent control policy

found in human participants to guide a person with limited visual and auditory perception (follower) in low visibility conditions. If an intelligent agent (man/machine) is given the task to guide such a follower using only a hard rein, the guiding agent should learn a control policy that can effectively manage the variability of follower's behavior [94]. Human demonstration experiments were conducted to understand how two human participants interact with each other using haptic signals through a hard rein to achieve a path tracking goal when one partner was cut off from auditory and visual feedback from the environment (the follower), while the other (the person with environmental perception) gets full state feedback of the follower to find variability of movement and uncertainty of the behavior.

Given the commonly used options to develop a control policy for a robot to guide a human in a low visibility environment such as reinforcement based learning and learning based on demonstrations, learning based on demonstrations was chosen to identify the parameters of an auto-regressive control policy in human demonstration experiments. It is easy to understand the structure of the control policy. The identified controller can be tested for optimality and stability using simple numerical simulations, before testing online using a robotic hardware platform. The proposed control policy derived based on human-human demonstrations is mainly intended to be used in a robot to guide people with good vision working in low visibility environments like in indoor fire-fighting or in other disaster response scenarios.

The predictive and reactive policies of the guider and the follower showed that the R^2 values of the guider's predictive and follower's reactive behavioral policies increased over trials. The Mann-Whitney U test results among different orders of auto-regressive policies confirm that the guider's policy is best approximated by a 3^{rd} order predictive model while the follower's state transition policy is best approximated by a 2^{nd} order reactive model. Therefore, it is possible to state that the guider and the follower give more emphasis on predictive and reactive models respectively. This also accords with previous findings which

showed that subjects learn both predictive and reactive models during different movements [115]. The different orders of the guider's predictive ($N = 3$) and the follower reactive ($N = 2$) policies suggest that in general, the guider depends on more historical information to generate an action, while the follower depends on less. Therefore, interpretations as to why the follower's auto-regressive reactive policy is a 2^{nd} one, whereas the guider's auto-regressive predictive policy in a 3^{rd} or higher order is that a reactive behavior does not need as many past states as in a predictive behavior to take action.

Variability is an indispensable feature in human behavior [116]. Therefore, variation of polynomial coefficients of guider's and follower's control policies suggest the stochastic human behavior in this particular task. These results are consistent with those of previous studies on stochastic human behavior [117], [118], [116] in similar contexts.

Previous work has proved that the total muscle activation for a single task decreased over their learning trials [119]. From the 2^{nd} order best fit curve for the quadratic sum of EMG J for all muscles for the guider, it was observed that J increases to a maximum around the first half of the trials and then decreases in last half of the trials. This suggests that effort optimization is a non-monotonic process. During the first half of the trials, subjects may have given priority to order selection than optimization in the muscle activation space, which is also reflected in the behavior of R^2 values of the guider's order selection. Once the optimal order is selected, subjects exhibit monotonic optimization in the muscle activation space with a corresponding increase of R^2 values. However, the main observation on the guider's muscle activation gradually progresses from an initial muscle co-contraction based command generation strategy to a low energy policy with minimum muscle co-contraction. Therefore, this is in agreement with other studies that show a similar pattern of reduction in muscle co-contraction when motor learning progresses [92], [93]. This phenomenon can come from the fact that the guiding agent builds internal models [120] of hand and task dynamics to guide the blindfolded follower.

Previous studies on human trust on a guiding agent have shown that humans tend to depend entirely on the guiding agent when they are in hazardous environments [10] until sudden a change occurs [96]. This implies that the degree of compliance in a follower should drop if the follower loses trust in the guiding agent.

Therefore, in **Chapter 4**, the follower was modeled as a virtual damped inertial system. Then the virtual mass, virtual damping coefficients, and virtual stiffness were considered as the variability of the follower's impedance parameters at different turn angles. The studies from the three types of paths, the blindfolded subjects who played the role of the follower confirmed that their trust in following the guider was highest in the straight path and it dropped in the other paths. Therefore, the trust was medium in the path with a 60° turn, and least in that with a 90° turn. Experimental results of human subjects show that the variability of the virtual damping coefficients correlates more with the complexity of the path - reflecting the trust level of the follower - than that of the virtual mass or stiffness coefficients. The results imply that the increased impedance comes from the drop in the degree of voluntary following in the follower. It is more of pulling by the follower than an increased pull by the guider.

When the follower's movements in response to tug forces generated by the guider is modeled using a virtual damped inertial model (virtual model because, followers movements largely comes from voluntary forces than due to tug forces of the guider), the variability of the damping coefficient reliably reflects the variability of the follower's trust in the guider. These experimental insights to derive a novel controller that integrates an optimal order control policy with a push/pull force modulator in response to the trust level of the follower monitored using a time varying virtual damped inertial model.

Humans' current movement is a combination of the way of perceiving the perturbation and the human action. Therefore, **Chapter 5** focuses on robot's and humans' behavior, and humans' perception when guider's control policy identified from human demonstration

experiments in Chapter 3 was implemented on a planar 1-DoF robotic arm. In this scenario, humans' behavioral metrics such as rise time (RT), best fit model order of the polynomial fitted to the instantaneous error of the human's position for a given desired angle (N), steady state variability (SSV), and steady state error (SSE) are presented to discuss the human's interaction behavior with robot. The human-robot interaction experiments were conducted with trained and naive subjects.

It was shown that the closed loop controller minimizes the error of following to bring the subject into the desired angular positions. Moreover, less oscillation in model order N (on average the model order $= 2$), low variability in steady state, and less number of commands to reach its rise time confirm the stability of the controller.

Since the haptic perturbation was given in leftward/rightward directions, direction can be a possible cause for behavior and perception in haptic based guidance in low visibility conditions via a hard rein. Therefore, behavior of robot and human are presented in moving leftward/rightward directions. Robot's leftward/rightward movements are symmetric when the robot interacts with both naive/trained subjects. Transient and steady state response behavioral metrics for naive subjects show asymmetry in moving leftward/rightward directions in N and SSV. However, after the training, trained subjects were able to move leftward/rightward directions symmetrically. Again it was found on average naive subjects give more emphasis on 2^{nd} order reactive model as noticed in human demonstration experiment in Chapter 3. However, after training phase trained subjects give more emphasis on 2^{nd} order predictive model. The possible cause could be any internal model in the brain to compensate their perception differently after the training phase.

EMG recording across the arm muscles of Anterior Deltoid (AD), Posterior Deltoid (PD), Biceps (Bc), Median Triceps (MT), Brachioradialis (Br), Flexor Carpi Radialis (FCR), Extensor Carpi Ulnaris (ECU), and Extensor Carpi Radialis (ECR) shows that both naive and trained subjects perceive differently when the arm is perturbed in leftward/rightward

directions. The way of perceiving the perturbation and the human action give an idea of Humans' current movement. It was found that naive and trained subjects' proprioceptive sensors in the muscles are contracted differently when the arm is perturbed from leftward/rightward directions. The human behavior metrics in trained subjects show that even humans perceive differently in leftward/rightward perturbations, they can train to move symmetrically. That might be the reason to change their behavior to predictive nature. Therefore, trained subjects might predict the next action to make a current movement in order to move desired direction accurately.

The experiments with naive and trained subjects show how humans perceive the same perturbation differently depending on the direction and how the training could effect them to move symmetrically. Therefore, these spontaneous reactions in muscle contraction give designing guidelines as to how to train humans to follow a guiding robot when the human is guided via a hard rein in low visibility conditions. Moreover, these findings will be useful to design robots or even to train animals to guide visually impaired people as well as people with good vision in low visibility environments. Therefore, this study shows how to combine some extracted behavioral matrices and humans' perceptions in guiding a human in low visibility conditions.

To make a complete picture of haptic perceptions, not only the proprioceptive but also cutaneous feedback was studied in **Chapter 6** to understand how humans trained in primitive haptic patterns given using a wearable sleeve, can recognize their shifts and linear combinations. The results would give an idea as to how humans mentally construct the cutaneous feedback in different scenarios such as shifting and scaling with respect to trained patterns, how they recognize all trained patterns when played randomly, and how they can recognize linear combination of primitive patterns. The combination of proprioceptive and cutaneous feedback will give a good intuition about human responses towards the haptic perceptions in low visibility conditions.

It was found that the humans find it difficult to scale and shift the pattern they felt with respect to the trained pattern when they were trained for only T. Even if they were able to scale or shift, the the original pattern interferes with the shifted and scaled patterns. When the significance was tested between sketched data were regressed with trained pattern T and sketched data were regressed with actual pattern that was played, pattern R ($p = 0.002$), L ($p = 0.002$), and H ($p = 0.055$) are significantly low. However, it was noted that the regression coefficients for pattern S ($p = 0.132$) was not improved. therefore, the results give some clues about the basic shapes of the primitive patterns could be used to train humans.

After training subjects for all primitive patterns, regression coefficients improved by 43.20%, 29.28%, and 45.88% for pattern R, L, and H respectively. The results suggest that humans have a general ability to recognize trained patterns even when they are played in a random order. Moreover, the results of the linear combinations of primitive patterns show that humans were able to recognize uni model patterns than bi model patterns. For example, it shows higher regression coefficients for T+L and T+R than L+R. Moreover, results imply that humans can recognize, scale, and shift more accurately when enough adjacent vibroactuators are activated in the threshold frequency range simultaneously. The results give an idea as to what kind of shapes could be used to train the humans and their ability to scale, shift, and recognize those primitive patterns. Therefore, this results would be used to convey a message to the human to give an idea of the shape and stiffness of obstacles that come into contact with the robot during guiding in low visibility conditions in future.

7.2.1 Future work

Based on experimental systems identification and numerical simulations on human demonstrations, the guiding agent and the follower experience learning for a optimal stable state-

dependent novel 3rd and 2nd order auto-regressive predictive and reactive control policies respectively. These findings provide a novel theoretical basis to design advanced human-robot interaction algorithms in a variety of cases where a human requires the assistance of a robot to perceive or improve his perception of the surrounding environment. Moreover, by modeling the two party voluntary movement dynamics using a virtual damped inertial model, the ability of modeling the mutual trust between two parties was shown. In the future, the novel controller extracted based on human demonstrations would be used on a human-robot interaction scenario to guide a visually impaired person in various applications like in indoor fire-fighting, search and rescue, medical surgery, etc.

Moreover, the results from human-human demonstrations provide useful design guidelines to human-robot interaction that should account for the real time trust level of the human counterpart. In a human-robot interaction scenario such as in indoor fire-fighter being guided by a robot through thick smoke, the estimate of the followers' trust using the above method could be used to change acceleration/deceleration of the intelligent agent. Moreover, human-robot interaction algorithm that combines a robotic estimate of the following human's trust state with the existing 3rd order predictive guiding algorithm in structured and unstructured environments.

The guiding control policy in Eqs. 3.1 and 3.2 together with the virtual inertial damping model to estimate the trust level of the follower opens up the opportunity to develop an integrated controller that treats the trust level of the follower. That will enable the controller to adjust to the changes of the behavioral dynamics of the follower in varying distraction and stress conditions.

In this thesis the strong evidence of a forward model that predicts the future states of the follower would be used in a predictive control policy. This forward model may contain some approximation of the follower's reactive behavior. It will be interesting to understand detailed computational nature of this prediction used by the guider. Moreover, it was found

that follower's reactive nature was changed to predictive after training phase. Furthermore, the training phase would help to the follower to move symmetrically in leftward/rightward directions as noticed in human-robot interactions when the control policy identified from human guiders was implemented on a planar 1-DoF robotic arm to perturb the blindfolded subjects' most dominant arm to guide them to a desired position in leftward/rightward directions. These limitations will enable the intelligent agent to adjust to the changes of the behavioral dynamics of the human follower in varying distraction and stress conditions.

In the future, it would be useful to study the cost functions that are minimized by the duo, during learning to track a path. This would help to develop a reward based learning algorithm to enable a mobile robot to continuously improve the controller while interacting with a human follower. Moreover, having a closer look at how the guider maybe adaptively combining a reactive controller with a predictive one as some of the individual followers, in order to stabilize learning also would be helpful. It will also be interesting to explore for broader factors affecting the mutual trust, so that predictive action can be taken to maintain a good mutual trust level within the follower in the context of guiding.

Moreover, it would be helpful to test the implemented guider's control policy on the mobile robotic platform in different terrain and cluttered/uncluttered environments when the guider and follower use other possible modes of haptic feedback such as cutaneous feedback through a wireless link, and haptic feedback through a soft rein. This scenario uses existing wearable haptic based vibroactuator array to add cutaneous feedback to the blindfolded followers to help them mentally construct the shape and stiffness of obstacles that come into contact with the robot. Adding vibroactuator haptic sleeve will provide spatial information of the surrounding environment and help to formulate several new hypotheses about on the abilities of the human brain to use a reduced number of sensory modalities to accomplish tasks that they used to do without any sensory deprivation. Furthermore, wearable haptic based vibroactuator array would be expanded for both arms to convey complete spatial

information while the user's arm is free to explore the immediate environment.

In addition to applications in robotic guidance of a person in a low visibility environment, the findings shed light on human-robot interaction applications in other areas like robot-assisted minimally invasive surgery (RMIS). Surgical tele-manipulation robot could use better predictive algorithms to estimate the parameters of remote environment for the surgeon with more accurate adaption of control parameters by constructing internal models of interaction dynamics between tools and tissues in order to improve clinical outcomes [121]. Therefore, research can continue to discover a generic robotic learning strategy/algorithm that can be generalized across RMIS as well as robotic assisted guidance in low visibility environments.

BIBLIOGRAPHY

[1] C. P. Jackson, R. C. Miall, and D. Balslev, "Spatially valid proprioceptive cues improve the detection of a visual stimulus," *Experimental brain research*, vol. 205, no. 1, pp. 31–40, 2010.

[2] J. R. Marston, J. M. Loomis, R. L. Klatzky, and R. G. Golledge, "Nonvisual route following with guidance from a simple haptic or auditory display.," *Journal of Visual Impairment & Blindness*, vol. 101, no. 4, pp. 203–211, 2007.

[3] J. M. Loomis, R. G. Golledge, and R. L. Klatzky, "Navigation system for the blind: Auditory display modes and guidance," *Presence: Teleoperators and Virtual Environments*, vol. 7, no. 2, pp. 193–203, 1998.

[4] A. Allan Melvin, B. Prabu, R. Nagarajan, and I. Bukhari, "Rovi: a robot for visually impaired for collision-free navigation," 2009.

[5] J. Penders, L. Alboul, U. Witkowski, A. Naghsh, J. Saez-Pons, S. Herbrechtsmeier, and M. El-Habbal, "A robot swarm assisting a human fire-fighter," *Advanced Robotics*, vol. 25, no. 1-2, pp. 93–117, 2011.

[6] P. A. Hancock, D. R. Billings, K. E. Schaefer, J. Y. Chen, E. J. De Visser, and R. Parasuraman, "A meta-analysis of factors affecting trust in human-robot interaction," *Human Factors: The Journal of the Human Factors and Ergonomics Society*, vol. 53, no. 5, pp. 517–527, 2011.

[7] D. R. Billings, K. E. Schaefer, J. Y. Chen, and P. A. Hancock, "Human-robot interaction: developing trust in robots," in *Proceedings of the seventh annual ACM/IEEE international conference on Human-Robot Interaction*, pp. 109–110, ACM, 2012.

[8] E. Park, Q. Jenkins, and X. Jiang, "Measuring trust of human operators in new generation rescue robots," in *Proceedings of the JFPS International Symposium on Fluid Power*, vol. 2008, pp. 489–492, , 2008.

[9] R. Yagoda, "What! you want me to trust a robot? the development of a human robot interaction (hri) trust scale.," 2011.

[10] D. P. Stormont, "Analyzing human trust of autonomous systems in hazardous environments," in *Proceedings of the Human Implications of Human-Robot Interaction workshop at AAAI*, vol. 2008, 2008.

[11] F. Gemperle, T. Hirsch, A. Goode, J. Pearce, D. Siewiorek, and A. Smailigic, "Wearable vibro-tactile display," 2003.

[12] Oxford, "Sense," 2014. [Online; accessed 31-October-2014].

[13] L. Ramirez, S. Denef, and T. Dyrks, "Towards human-centered support for indoor navigation," in *Proceedings of the SIGCHI Conference on Human Factors in Computing Systems*, pp. 1279–1282, ACM, 2009.

[14] Google, "Guide dog," 2014. [Online; accessed 01-August-2014].

[15] Google, "Horse riding," 2014. [Online; accessed 01-August-2014].

[16] J. J. Gibson, "The senses considered as perceptual systems.," 1966.

[17] H. H. Clark and D. Wilkes-Gibbs, "Referring as a collaborative process," *Cognition*, vol. 22, no. 1, pp. 1–39, 1986.

[18] J. Moll and E.-L. Sallnäs, "Communicative functions of haptic feedback," in *Haptic and Audio Interaction Design*, pp. 1–10, Springer, 2009.

[19] J. M. Loomis, R. G. Golledge, R. L. Klatzky, and J. R. Marston, "Assisting wayfinding in visually impaired travelers," *Applied spatial cognition: From research to cognitive technology*, pp. 179–202, 2007.

[20] R. G. Golledge, *Wayfinding behavior: Cognitive mapping and other spatial processes*. JHU Press, 1999.

[21] J. J. Rieser, D. Guth, and E. Hill, "Mental processes mediating independent travel: Implications for orientation and mobility," *Journal of Visual Impairment and Blindness*, 1982.

[22] W. R. Wiener, R. L. Welsh, and B. B. Blasch, *Foundations of orientation and mobility*, vol. 1. American Foundation for the Blind, 2010.

[23] S. Shoval, I. Ulrich, and J. Borenstein, "Navbelt and the guide-cane [obstacle-avoidance systems for the blind and visually impaired]," *Robotics & Automation Magazine, IEEE*, vol. 10, no. 1, pp. 9–20, 2003.

[24] V. Kulyukin, C. Gharpure, J. Nicholson, and S. Pavithran, "Rfid in robot-assisted indoor navigation for the visually impaired," in *Intelligent Robots and Systems, 2004.(IROS 2004). Proceedings. 2004 IEEE/RSJ International Conference on*, vol. 2, pp. 1979–1984, IEEE, 2004.

[25] Q. Ladetto and B. Merminod, "An alternative approach to vision techniques: Pedestrian navigation system based on digital magnetic compass and gyroscope integration," *Cybernetics and Information*, 2002.

[26] D. Titterton and J. L. Weston, *Strapdown inertial navigation technology*, vol. 17. IET, 2004.

[27] J. M. Loomis, R. L. Klatzky, R. G. Golledge, *et al.*, "Navigating without vision: basic and applied research," *Optometry & Vision Science*, vol. 78, no. 5, pp. 282–289, 2001.

[28] J. Campbell, R. Sukthankar, and I. Nourbakhsh, "Techniques for evaluating optical flow for visual odometry in extreme terrain," in *Intelligent Robots and Systems, 2004.(IROS 2004). Proceedings. 2004 IEEE/RSJ International Conference on*, vol. 4, pp. 3704–3711, IEEE, 2004.

[29] D. H. Warren and E. R. Strelow, *Electronic Spatial Sensing for the Blind: Contributions from Perception, Rehabilitation, and Computer Vision*. No. 99, Springer, 1985.

[30] J. Fruchterman, "Talking maps and gps systems," in *Rank Prize Funds Symposium on Technology to Assist the Blind and Visually Impaired (Grasmere, Cumbria, England*, 1996.

[31] A. Helal, S. E. Moore, and B. Ramachandran, "Drishti: An integrated navigation system for visually impaired and disabled," in *Wearable Computers, 2001. Proceedings. Fifth International Symposium on*, pp. 149–156, IEEE, 2001.

[32] S. Holland, D. R. Morse, and H. Gedenryd, "Audiogps: Spatial audio navigation with a minimal attention interface," *Personal and Ubiquitous Computing*, vol. 6, no. 4, pp. 253–259, 2002.

[33] I. Ulrich and J. Borenstein, "The guidecane-applying mobile robot technologies to assist the visually impaired," *Systems, Man and Cybernetics, Part A: Systems and Humans, IEEE Transactions on*, vol. 31, no. 2, pp. 131–136, 2001.

[34] J. M. Loomis, R. L. Klatzky, R. G. Golledge, *et al.*, "Navigating without vision: basic and applied research," *Optometry & Vision Science*, vol. 78, no. 5, pp. 282–289, 2001.

[35] S. Tachi, K. Tanie, K. Komoriya, and M. Abe, "Electrocutaneous communication in a guide dog robot (meldog)," 1985.

[36] R. Golledge, R. Klatzky, J. Loomis, and J. Marston, "Stated preferences for components of a personal guidance system for nonvisual navigation," *Journal of Visual Impairment & Blindness (JVIB)*, vol. 98, no. 03, 2004.

[37] J. M. Loomis, R. G. Golledge, R. L. Klatzky, J. M. Speigle, and J. Tietz, "Personal guidance system for the visually impaired," in *Proceedings of the first annual ACM conference on Assistive technologies*, pp. 85–91, ACM, 1994.

[38] J. M. Loomis, R. G. Golledge, and R. L. Klatzky, "Navigation system for the blind: Auditory display modes and guidance," *Presence: Teleoperators and Virtual Environments*, vol. 7, no. 2, pp. 193–203, 1998.

[39] R. G. Golledge, J. M. Loomis, R. L. Klatzky, A. Flury, and X. L. YANG, "Designing a personal guidance system to aid navigation without sight: Progress on the gis component," *International Journal of Geographical Information System*, vol. 5, no. 4, pp. 373–395, 1991.

[40] M. A. Goodrich and A. C. Schultz, "Human-robot interaction: a survey," *Foundations and trends in human-computer interaction*, vol. 1, no. 3, pp. 203–275, 2007.

[41] J. Casper and R. R. Murphy, "Human-robot interactions during the robot-assisted urban search and rescue response at the world trade center," *Systems, Man, and Cybernetics, Part B: Cybernetics, IEEE Transactions on*, vol. 33, no. 3, pp. 367–385, 2003.

[42] A. Finzi and A. Orlandini, "A mixed-initiative approach to human-robot interaction in rescue scenarios," *American Association for Artificial Intelligence (www. aaai. org)*, 2005.

[43] R. R. Murphy, "Human-robot interaction in rescue robotics," *Systems, Man, and Cy-*

bernetics, Part C: Applications and Reviews, IEEE Transactions on, vol. 34, no. 2, pp. 138–153, 2004.

[44] J. L. Casper and R. R. Murphy, "Workflow study on human-robot interaction in usar," in *Robotics and Automation, 2002. Proceedings. ICRA'02. IEEE International Conference on*, vol. 2, pp. 1997–2003, IEEE, 2002.

[45] J. Casper and R. R. Murphy, "Human-robot interactions during the robot-assisted urban search and rescue response at the world trade center," *Systems, Man, and Cybernetics, Part B: Cybernetics, IEEE Transactions on*, vol. 33, no. 3, pp. 367–385, 2003.

[46] J. PENDERS, P. JONES, A. RANASINGHE, and T. NANAYAKARA, "Enhancing trust and confidence in human robot interaction," *UKRE, Sheffield*, pp. 25–3, 2013.

[47] P. de Vries, C. Midden, and D. Bouwhuis, "The effects of errors on system trust, self-confidence, and the allocation of control in route planning," *International Journal of Human-Computer Studies*, vol. 58, no. 6, pp. 719–735, 2003.

[48] E. Freedy, E. DeVisser, G. Weltman, and N. Coeyman, "Measurement of trust in human-robot collaboration," in *Collaborative Technologies and Systems, 2007. CTS 2007. International Symposium on*, pp. 106–114, IEEE, 2007.

[49] J. D. Lee and N. Moray, "Trust, self-confidence, and operators' adaptation to automation," *International Journal of Human-Computer Studies*, vol. 40, no. 1, pp. 153–184, 1994.

[50] M. T. Dzindolet, S. A. Peterson, R. A. Pomranky, L. G. Pierce, and H. P. Beck, "The role of trust in automation reliance," *International Journal of Human-Computer Studies*, vol. 58, no. 6, pp. 697–718, 2003.

[51] X. Jiang, M. T. Khasawneh, R. Master, S. R. Bowling, A. K. Gramopadhye, B. J. Melloy, and L. Grimes, "Measurement of human trust in a hybrid inspection system based on signal detection theory measures," *International journal of industrial ergonomics*, vol. 34, no. 5, pp. 407–419, 2004.

[52] J. D. Lee and K. A. See, "Trust in automation: Designing for appropriate reliance," *Human Factors: The Journal of the Human Factors and Ergonomics Society*, vol. 46, no. 1, pp. 50–80, 2004.

[53] B. M. Muir, "Trust between humans and machines, and the design of decision aids," *International Journal of Man-Machine Studies*, vol. 27, no. 5, pp. 527–539, 1987.

[54] J. A. Colquitt, J. A. LePine, R. F. Piccolo, C. P. Zapata, and B. L. Rich, "Explaining the justice–performance relationship: Trust as exchange deepener or trust as uncertainty reducer?," *Journal of Applied Psychology*, vol. 97, no. 1, p. 1, 2012.

[55] E. Park, Q. Jenkins, and X. Jiang, "Measuring trust of human operators in new generation rescue robots," in *Proceedings of the JFPS International Symposium on Fluid Power*, vol. 2008, pp. 489–492, 2008.

[56] J. A. Colquitt, J. A. LePine, C. P. Zapata, and R. E. Wild, "Trust in typical and high-reliability contexts: building and reacting to trust among firefighters," *Academy of Management Journal*, vol. 54, no. 5, pp. 999–1015, 2011.

[57] A. Mörtl, M. Lawitzky, A. Kucukyilmaz, M. Sezgin, C. Basdogan, and S. Hirche, "The role of roles: Physical cooperation between humans and robots," *The International Journal of Robotics Research*, vol. 31, no. 13, pp. 1656–1674, 2012.

[58] P. A. Hancock, D. R. Billings, K. E. Schaefer, J. Y. Chen, E. J. De Visser, and R. Parasuraman, "A meta-analysis of factors affecting trust in human-robot interaction," *Hu-*

man Factors: The Journal of the Human Factors and Ergonomics Society, vol. 53, no. 5, pp. 517–527, 2011.

[59] C. T. Fuentes and A. J. Bastian, "Where is your arm? variations in proprioception across space and tasks," *Journal of Neurophysiology*, vol. 103, no. 1, pp. 164–171, 2010.

[60] C. M. Harris and D. M. Wolpert, "Signal-dependent noise determines motor planning," *Nature*, vol. 394, no. 6695, pp. 780–784, 1998.

[61] R. A. Scheidt, M. A. Conditt, E. L. Secco, and F. A. Mussa-Ivaldi, "Interaction of visual and proprioceptive feedback during adaptation of human reaching movements," *Journal of Neurophysiology*, vol. 93, no. 6, pp. 3200–3213, 2005.

[62] D. W. Franklin, U. So, E. Burdet, and M. Kawato, "Visual feedback is not necessary for the learning of novel dynamics," *PloS one*, vol. 2, no. 12, pp. e1336–e1336, 2007.

[63] J. Colebatch and D. McCloskey, "Maintenance of constant arm position or force: reflex and volitional components in man.," *The Journal of physiology*, vol. 386, no. 1, pp. 247–261, 1987.

[64] M. O. Ernst and M. S. Banks, "Humans integrate visual and haptic information in a statistically optimal fashion," *Nature*, vol. 415, no. 6870, pp. 429–433, 2002.

[65] P. DIZIO and J. R. LACKNER, "Motor adaptation to coriolis force perturbations of reaching movements: endpoint but not trajectory adaptation transfers to the nonexposed arm," *Trial*, vol. 1, no. 41, p. 81, 1995.

[66] C. Tong, D. M. Wolpert, and J. R. Flanagan, "Kinematics and dynamics are not represented independently in motor working memory: evidence from an interference study," *The Journal of neuroscience*, vol. 22, no. 3, pp. 1108–1113, 2002.

[67] A. Ranasinghe, J. Penders, P. Dasgupta, K. Althoefer, and T. Nanayakkara, "A two party haptic guidance controller via a hard rein," in *Intelligent Robots and Systems (IROS), 2013 IEEE/RSJ International Conference on*, pp. 116–122, IEEE, 2013.

[68] A. Ranasinghe, K. Althoefer, T. Nanayakkara, J. Penders, and P. Dasgupta, "An optimal state dependent haptic guidance controller via a hard rein," in *Systems, Man, and Cybernetics (SMC), 2013 IEEE International Conference on*, pp. 2322–2327, IEEE, 2013.

[69] F. Gemperle, T. Hirsch, A. Goode, J. Pearce, D. Siewiorek, and A. Smailigic, "Wearable vibro-tactile display," tech. rep., Technical report, Carnegie Mellon University, 2003.

[70] L. A. Jones, "Kinesthetic sensing," in *in Human and Machine Haptics*, Citeseer, 2000.

[71] L. Post, I. Zompa, and C. Chapman, "Perception of vibrotactile stimuli during motor activity in human subjects," *Experimental brain research*, vol. 100, no. 1, pp. 107–120, 1994.

[72] J. B. Van Erp, H. A. Van Veen, C. Jansen, and T. Dobbins, "Waypoint navigation with a vibrotactile waist belt," *ACM Transactions on Applied Perception (TAP)*, vol. 2, no. 2, pp. 106–117, 2005.

[73] R. W. Cholewiak and A. A. Collins, "Vibrotactile localization on the arm: Effects of place, space, and age," *Perception & psychophysics*, vol. 65, no. 7, pp. 1058–1077, 2003.

[74] K. Tsukada and M. Yasumura, "Activebelt: Belt-type wearable tactile display for directional navigation," in *UbiComp 2004: Ubiquitous Computing*, pp. 384–399, Springer, 2004.

[75] M. Pielot, B. Poppinga, W. Heuten, and S. Boll, "A tactile compass for eyes-free pedestrian navigation," in *Human-Computer Interaction–INTERACT 2011*, pp. 640–656, Springer, 2011.

[76] L. A. Jones and N. B. Sarter, "Tactile displays: Guidance for their design and application," *Human Factors: The Journal of the Human Factors and Ergonomics Society*, vol. 50, no. 1, pp. 90–111, 2008.

[77] J. C. Bliss, M. H. Katcher, C. H. Rogers, and R. P. Shepard, "Optical-to-tactile image conversion for the blind," *Man-Machine Systems, IEEE Transactions on*, vol. 11, no. 1, pp. 58–65, 1970.

[78] C. Wall, M. S. Weinberg, P. B. Schmidt, and D. E. Krebs, "Balance prosthesis based on micromechanical sensors using vibrotactile feedback of tilt," *Biomedical Engineering, IEEE Transactions on*, vol. 48, no. 10, pp. 1153–1161, 2001.

[79] A. A. Priplata, J. B. Niemi, J. D. Harry, L. A. Lipsitz, and J. J. Collins, "Vibrating insoles and balance control in elderly people," *The Lancet*, vol. 362, no. 9390, pp. 1123–1124, 2003.

[80] A. H. Rupert, "An instrumentation solution for reducing spatial disorientation mishaps," *Engineering in Medicine and Biology Magazine, IEEE*, vol. 19, no. 2, pp. 71–80, 2000.

[81] M. Pielot, B. Poppinga, and S. Boll, "Pocketnavigator: vibro-tactile waypoint navigation for everyday mobile devices," in *Proceedings of the 12th international conference on Human computer interaction with mobile devices and services*, pp. 423–426, ACM, 2010.

[82] R. Velazquez, E. Fontaine, and E. Pissaloux, "Coding the environment in tactile maps

for real-time guidance of the visually impaired," in *Micro-NanoMechatronics and Human Science, 2006 International Symposium on*, pp. 1–6, IEEE, 2006.

[83] D. Dakopoulos and N. Bourbakis, "Towards a 2d tactile vocabulary for navigation of blind and visually impaired," in *Systems, Man and Cybernetics, 2009. SMC 2009. IEEE International Conference on*, pp. 45–51, IEEE, 2009.

[84] S. Scheggi, M. Aggravi, F. Morbidi, and D. Prattichizzo, "Cooperative human-robot haptic navigation," in *Robotics and Automation (ICRA), 2014 IEEE International Conference on*, pp. 2693–2698, IEEE, 2014.

[85] K. O. Sofia and L. Jones, "Mechanical and psychophysical studies of surface wave propagation during vibrotactile stimulation," *Haptics, IEEE Transactions on*, vol. 6, no. 3, pp. 320–329, 2013.

[86] L. A. Jones, J. Kunkel, and E. Piateski, "Vibrotactile pattern recognition on the arm and back," *Perception*, vol. 38, no. 1, p. 52, 2009.

[87] Wikipedia, "autoregressive (AR) model," 2014. [Online; accessed 14-September-2014].

[88] M. Flanders, "Choosing a wavelet for single-trial emg," *Journal of neuroscience methods*, vol. 116, no. 2, pp. 165–177, 2002.

[89] M. J. Richardson and T. Flash, "Comparing smooth arm movements with the two-thirds power law and the related segmented-control hypothesis," *The Journal of Neuroscience*, vol. 22, no. 18, pp. 8201–8211, 2002.

[90] A. Ranasinghe, J. Penders, P. Dasgupta, K. Althoefer, and T. Nanayakkara, "A two party haptic guidance controller via a hard rein," in *Intelligent Robots and Systems (IROS), 2013 IEEE/RSJ International Conference on*, pp. 116–122, IEEE, 2013.

[91] A. Ranasinghe, K. Althoefer, T. Nanayakkara, J. Penders, and P. Dasgupta, "An optimal state dependent haptic guidance controller via a hard rein," in *Systems, Man, and Cybernetics (SMC), 2013 IEEE International Conference on*, pp. 2322–2327, IEEE, 2013.

[92] N. Bhushan and R. Shadmehr, "Computational nature of human adaptive control during learning of reaching movements in force fields," *Biological cybernetics*, vol. 81, no. 1, pp. 39–60, 1999.

[93] S. Saeb, C. Weber, and J. Triesch, "Learning the optimal control of coordinated eye and head movements," *PLoS computational biology*, vol. 7, no. 11, p. e1002253, 2011.

[94] V. Duchaine and C. Gosselin, "Safe, stable and intuitive control for physical human-robot interaction," in *Robotics and Automation, 2009. ICRA'09. IEEE International Conference on*, pp. 3383–3388, IEEE, 2009.

[95] Oxford, "Confidence," 2014. [Online; accessed 18-November-2014].

[96] G. Johannsen and W. B. Rouse, "Mathematical concepts for modeling human behavior in complex man-machine systems," *Human Factors: The Journal of the Human Factors and Ergonomics Society*, vol. 21, no. 6, pp. 733–747, 1979.

[97] R. C. Oldfield, "The assessment and analysis of handedness: the edinburgh inventory," *Neuropsychologia*, vol. 9, no. 1, pp. 97–113, 1971.

[98] H. Akaike, "A new look at the statistical model identification," *Automatic Control, IEEE Transactions on*, vol. 19, no. 6, pp. 716–723, 1974.

[99] Wikipedia, "Muscle tendon," 2015. [Online; accessed 12-April-2015].

[100] Wikipedia, "Spindle muscle," 2015. [Online; accessed 13-April-2015].

[101] Googler, "Tendon," 2015. [Online; accessed 11-April-2015].

[102] Wikipedia, "Electromyography," 2015. [Online; accessed 25-January-2015].

[103] R. G. Mello, L. F. Oliveira, and J. Nadal, "Digital butterworth filter for subtracting noise from low magnitude surface electromyogram," *Computer methods and programs in biomedicine*, vol. 87, no. 1, pp. 28–35, 2007.

[104] P. L. Gribble, D. J. Ostry, V. Sanguineti, and R. Laboissière, "Are complex control signals required for human arm movement?," *Journal of Neurophysiology*, vol. 79, no. 3, pp. 1409–1424, 1998.

[105] R. Pfeifer, M. Lungarella, and F. Iida, "Self-organization, embodiment, and biologically inspired robotics," *science*, vol. 318, no. 5853, pp. 1088–1093, 2007.

[106] K. Aizawa, "Understanding the embodiment of perception," *The Journal of philosophy*, vol. 104, no. 1, pp. 5–25, 2007.

[107] K. S. Hale and K. M. Stanney, "Deriving haptic design guidelines from human physiological, psychophysical, and neurological foundations," *Computer Graphics and Applications, IEEE*, vol. 24, no. 2, pp. 33–39, 2004.

[108] R. D. Gilson, E. S. Redden, and L. R. Elliott, "Remote tactile displays for future soldiers," tech. rep., DTIC Document, 2007.

[109] L. A. Jones and S. J. Lederman, *Human hand function*. Oxford University Press, 2006.

[110] J. Gray and M. Sato, "Properties of the receptor potential in pacinian corpuscles," *The Journal of physiology*, vol. 122, no. 3, pp. 610–636, 1953.

[111] I. Oakley, Y. Kim, J. Lee, and J. Ryu, "Determining the feasibility of forearm mounted vibrotactile displays," in *Haptic Interfaces for Virtual Environment and Teleoperator Systems, 2006 14th Symposium on*, pp. 27–34, IEEE, 2006.

[112] I. R. Summers, J. J. Whybrow, D. A. Gratton, P. Milnes, B. H. Brown, and J. C. Stevens, "Tactile information transfer: A comparison of two stimulation sites," *The Journal of the Acoustical Society of America*, vol. 118, no. 4, pp. 2527–2534, 2005.

[113] T. Kaaresoja and J. Linjama, "Perception of short tactile pulses generated by a vibration motor in a mobile phone," in *Eurohaptics Conference, 2005 and Symposium on Haptic Interfaces for Virtual Environment and Teleoperator Systems, 2005. World Haptics 2005. First Joint*, pp. 471–472, IEEE, 2005.

[114] S. A. C. Roger W, Cholewiak, "Cutaneous feedback,"

[115] D. A. Nowak and J. Hermsdörfer, "Predictive and reactive control of grasping forces: on the role of the basal ganglia and sensory feedback," *Experimental Brain Research*, vol. 173, no. 4, pp. 650–660, 2006.

[116] N. Mitsunaga, C. Smith, T. Kanda, H. Ishiguro, and N. Hagita, "Robot behavior adaptation for human-robot interaction based on policy gradient reinforcement learning," in *Intelligent Robots and Systems, 2005.(IROS 2005). 2005 IEEE/RSJ International Conference on*, pp. 218–225, IEEE, 2005.

[117] J. D. Sterman, "Deterministic chaos in models of human behavior: Methodological issues and experimental results," *System Dynamics Review*, vol. 4, no. 1-2, pp. 148–178, 1988.

[118] A. M. van Mourik, A. Daffertshofer, and P. J. Beek, "Deterministic and stochastic features of rhythmic human movement," *Biological cybernetics*, vol. 94, no. 3, pp. 233–244, 2006.

[119] I. A. Stokes and M. Gardner-Morse, "Lumbar spinal muscle activation synergies predicted by multi-criteria cost function," *Journal of Biomechanics*, vol. 34, no. 6, pp. 733–740, 2001.

[120] K. A. Thoroughman and R. Shadmehr, "Learning of action through adaptive combination of motor primitives," *Nature*, vol. 407, no. 6805, pp. 742–747, 2000.

[121] C. Preusche, T. Ortmaier, and G. Hirzinger, "Teleoperation concepts in minimal invasive surgery," *Control engineering practice*, vol. 10, no. 11, pp. 1245–1250, 2002.

APPENDIX A

APPENDIX 1

A.1 Ethical statement

This study was approved by King's College London Bio medical Sciences, Medicine, Dentistry and Natural and Mathematical Sciences research ethics committee (REC Reference number BDM/11/12-20).

A.2 Information sheet and consent form

The information sheet and consent form to recruit the subjects are as follows

INFORMATION SHEET FOR PARTICIPANTS

KING'S College LONDON

REC Reference Number: **BDM/11/12-20**

YOU WILL BE GIVEN A COPY OF THIS INFORMATION SHEET

REINS : Human-robot communication through tactile feedback

We would like to invite you to participate in this original research project if you are more than 18 years old, and do not suffer from any motor diseases (ex. Parkinson's). Priority is given to visually impaired people and those who have prior training in fire fighting in low visibility conditions. You will be given a trial with auditory noise to decide whether to continue or not. You should only continue to participate if you want to; choosing not to take part will not disadvantage you in any way. Before you decide whether you want to take part, it is important for you to understand why the research is being done and what your participation will involve. Please take time to read the following information carefully and discuss it with others if you wish. Ask us if there is anything that is not clear or if you would like more information.

The main objective of the study is to understand how humans can develop a language to communicate with a robot through reins. Three types of reins will be studied: a soft rein (rope), a hard rein (stick), and a wireless rein (Wii mote). You will hold one end of a rein. The other end will be held by a robot. The robot will encode a message out of a bank of possible messages in waves transferred to the human's end through the rein and wait for 5 seconds before sending it again if a response wave from you is not received within 5 seconds. You will be informed of the possible list of messages the robot will encode prior to the experiment. You will also be shown demonstrations of how to encode a list of commands. You will wear four hand bands containing passive markers to record arm movements, electromyography (EMG) sensors, and a pair of earphones that will give a background noise of 70dB (Cocktail party, restaurant noise).

- The experiment will be conducted in (room number to be decided). ***An experiment will last for a maximum of two hours.***
- Instructions to wait for a message from the robot and to generate a command will be given to you via the earphones. In all other times, the earphones will generate a maximum of 70dB background noise you will typically find in a cocktail party or restaurant.
- Movement data will be collected by a 3D motion capturing system while ***you*** interact with the robot. Sensors to measure acceleration and electromyography (EMG) maybe pasted on the skin of the upper and lower arm. ***To minimize fatigue you will receive a 1-minute break every 5 minutes. However, you can also request for breaks more often if you feel any discomfort.***
- **EMG sensors will be attached to muscles in the shoulder as well as lower arm. Your skin will have to be cleaned with alcohol before attaching sensors. If your skin is allergic to alcohol, the experiment will not proceed. There are no known after-effects of attaching EMG sensors to the skin.**
- **Please wear loose clothing so that your skin can be easily cleaned and above mentioned sensors can be easily attached to the skin. We will take adequate precautions to cover your clothes to prevent any stains due to alcohol. You will also be given the option to wear a dress made available during the experiment.**
- You have to wear earphones to receive auditory distraction of 70dB. **This is the typical noise level in a restaurant. Therefore any risk beyond distraction at a restaurant by other conversations will not be expected.** However, you will experience a trial distraction to decide if you wish to continue participating in the experiment, and you can quit the experiment at any time.
- ***You*** will be compensated @ £6 per hour, and get a free copy of the final report of the study. **Full payment will be made upon completion of the study. If you withdraw from the study before completing the experiment in its entirety, you will be reimbursed for your travel expenses only.**

- **You can withdraw the data up to one week from completion of the study.** ***If you have any queries, please directly contact the principal investigator***: Dr. Thrishantha Nanayakkara, Email: thrish.antha@kcl.ac.uk
- We will strictly follow the provisions of the Data Protection Act 1998, whereby, we will retain only the anonymised data such as handedness, sex, age for official records. ***They will be shared only among the researchers involved in this study.***

Are you are happy to be contacted about participation in future studies? Yes ☐ ***No*** ☐

Your participation in this study will not be affected should you choose not to be re-contacted.

If you would like more information, please contact **Dr. Thrishantha Nanayakkara**
Email: thrish.antha@kcl.ac.uk
Telephone: 020-7848-2256,
Postal address: Room 1.23, Strand Building
Division of Engineering
King's College, University of London
Strand
London WC2R 2LS

[redacted]

Please complete this form after you have read the Information Sheet and/or listened to an explanation about the research.

KING'S College LONDON

Title of Study: REINS : Human-robot communication through tactile feedback

King's College Research Ethics Committee Ref: BDM/11/12-20

- **Thank you for considering taking part in this research. The person organising the research must explain the project to you before you agree to take part.**
- **If you have any questions arising from the Information Sheet or explanation already given to you, please ask the researcher before you decide whether to join in. You will be given a copy of this Consent Form to keep and refer to at any time.**
- **You can withdraw your data within one week from completion of the study.**
- **I understand that if I decide at any time during the research that I no longer wish to participate in this project, I can notify the researchers involved and withdraw from it immediately without giving any reason. *Yes* ☐ *No* ☐**
- **I consent to the processing of my personal information for the purposes explained to me. I understand that such information will be handled in accordance with the terms of the Data Protection Act 1998. *Yes* ☐ *No* ☐**
- ***Are you are happy to be contacted about participation in future studies? Yes* ☐ *No* ☐**

Participant's Statement:

I _____

agree that the research project named above has been explained to me to my satisfaction and I agree to take part in the study. I have read both the notes written above and the Information Sheet about the project, and understand what the research study involves.

Signed **Date**

***Are you are happy to be contacted about participation in future studies? Yes* ☐ *No* ☐**

RESEARCHER

I undertake to abide by accepted ethical principles and appropriate code(s) of practice in carrying out this study. The information supplied above is to the best of my knowledge accurate. I have read the Application Guidelines and clearly understand my obligations and the rights of participants, particularly in so far as to obtaining valid consent. I understand that I must not commence research with human participants until I have received full approval from the ethics committee.

Signature …… **Date**…….

STUDENT PROJECTS (including PhD) – SUPERVISOR AUTHORISATION

I confirm that I have read this application and will be acting as the student researcher's supervisor for this project. The proposal is viable and the student has appropriate skills to undertake the research. The Information Sheet and recruitment procedures for obtaining informed consent are appropriate and the ethical issues arising from the project have been addressed in the application. I understand that research with human participants must not commence without full approval from the ethics committee.

Name of Supervisor:

Signature ……
Date……

MEDICAL SUPERVISION (if appropriate)

Name of Medical Supervisor:

Medical Supervisor's MDU/MPS (or other insurance provider) number:

……

Signature of Medical Supervisor:

……
Date……..

CONTACT DETAILS Give the details of the individual who should receive all correspondence concerning the application. Correspondence will normally be sent for the attention of the researcher. It is the responsibility of the researcher (and contact if different) to forward all copies of correspondence to the appropriate parties as required. Students should ensure that their supervisor is provided with copies of all correspondence.

Name: Thrishantha Nanayakkara

Full postal address:
Room 1.23, Strand Building
Division of Engineering
King's College, University of London
Strand
London WC2R 2LS

Telephone number: Tel: 020 7 848 2256

Email: thrish.antha@kcl.ac.uk